Chemical, multispectral, and textural constraints on the composition and origin of rocks at the Mars Pathfinder lading site

H. Y. McSween, Jr.[1], S. L. Murchie[2], J. A. Crisp[3], N. T. Bridges[3], R. C. Anderson[3], J. F. Bell III[4], D. T. Britt[5], J. Brückner[6], G. Dreibus[6], T. Economou[7], A. Ghosh[1], M. P. Golombek[3], J. P. Greenwood[1], J. R. Johnson[8], H. J. Moore[9], R. V. Morris[10], T. J. Parker[3], R. Rieder[6], R. Singer[11], and H. Wänke[6]

[1]Department of Geological Sciences, University of Tennessee, Knoxville

[2]Applied Physics Laboratory, Johns Hopkins University, Baltimore, Maryland

[3]Jet Propulsion Laboratory, California Institute of Technology, Pasadena

[4]Center for Radiophysics and Space Research, Cornell University, Ithaca, New York

[5]Lunar and Planetary Laboratory, University of Arizona, Tucson

[6]Max-Planck-Institut für Chemie, Mainz, Germany

[7]Enrico Fermi Institute, University of Chicago, Illinois

[8]U. S. Geological Survey, Flagstaff, Arizona

[9]U. S. Geological Survey, Menlo Park, California

[10]NASA Johnson Space Center, Houston, Texas

[11]Catalina Technologies, Tucson, Arizona

Revised version submitted to
Journal of Geophysical Research
June 1998

Abstract. Rocks at the Mars Pathfinder landing site are probably locally derived materials, reworked and deposited by catastrophic floods and possibly excavated as ejecta from a nearby crater. Observed textures on rock surfaces include pitted, knobby, smooth, lineated, and bumpy. Uncertainties in the nature of these surface textures, plus overprinting by aeolian abrasion, weathering, and dust coatings, prevent unambiguous interpretation. One rock exhibits a structure resembling exfoliation, and some others have oriented faces that may suggest columnar jointing. All these features may indicate the presence of volcanic, sedimentary, or impact-generated rocks or perhaps some limited combination of rocks with varying origins. Multispectral imaging has resolved four spectral classes of rock surfaces: gray and red, which commonly occur on different surfaces of the same rocks; pink, which is probably soil crusts; and maroon, which occurs as large rounded boulders, mostly in the far field. These rocks can be assigned to two spectral trends based on the position of their peak reflectance: the primary spectral trend contains gray, red, and pink rocks, as well as bright red soils, and constitutes most of the optical surface; maroon rocks and some spectrally similar brown soils constitute the secondary spectral trend. The spatial pattern of spectral variations observed in most rocks is apparently oriented along the prevailing wind direction. The primary spectral trend arises from thin ferric coatings of aeolian dust on darker rocks. The secondary spectral trend is apparently due to coating by a different ferric mineral, probably maghemite or ferrihydrite. A chronology based on rock spectral attributes suggests that the large rounded boulders of the maroon spectral class may constitute the oldest petrologic unit (a flood deposit) at the site, succeeded by smaller cobbles possibly deposited in an impact event, and followed by aeolian erosion and deposition. Nearly linear chemical trends in APXS rock compositions are interpreted as mixing lines between the compositions of rock and adhering dust, a conclusion also supported by a strong correlation between the abundance of sulfur and red/blue (670/440 nm) spectral ratio. Because most magmas at reasonable oxidation states contain little dissolved sulfur, extrapolations of regression lines of elements versus sulfur to zero sulfur give the composition of a presumed igneous rock. The chemistry and calculated normative mineralogy of the sulfur-free rock are similar to those of common terrestrial volcanic rocks, and its classification corresponds to andesite. Igneous rocks of this composition may occur in combination with coarse clastic sedimentary rocks or impact melts and breccias derived from an igneous parent. However, the spectral mottling expected on multi-lithologic conglomerates or breccias is not observed in any APXS-analyzed rocks, although mottling does occur on several small cobbles. Interpretation of the rocks as andesites is complicated by the

absence of a "1 μm" pyroxene absorption band in the spectra of even the cleanest rocks. Plausible explanations include abundant impact glass, masking of the pyroxene band by magnetite, or the existence of calcium- and iron-rich pyroxenes and olivine (inferred from normative pyroxene compositions in the sulfur-free rock and the likely breakdown of ferroan pigeonite to fayalite plus silica) which have pushed the absorption band minimum past the imager's spectral range. The inferred andesitic composition is most similar to terrestrial anorogenic icelandites, formed by fractionation of basaltic magmas following a tholeiitic differentiation trend, rather than to orogenic andesites. It does not lie along a calculated liquid line of descent for shergottite melts at shallow depth, but instead may require a parental magma with higher alumina content. Early melting of a relatively primitive Martian mantle could produce such an aluminous parent magma, supporting the ancient age of Pathfinder rocks inferred from their incorporation in Hesperian flood deposits. Although rocks of andesitic composition at the Pathfinder site may represent samples of ancient Martian crust, inferences drawn about a necessary role for water or plate tectonics in their petrogenesis are probably unwarranted. Even though such rocks might have formed by repeated crustal melting, fractional crystallization of basaltic magma is a simpler explanation.

1. Introduction

The Mars Pathfinder landing site is strewn with semi-rounded pebbles, cobbles, and boulders that comprise 16% of the surface area [*Smith et al.,* 1997a]. The remainder of the site consists of fines, partly as windblown "drift" forming various aeolian bedforms, and partly as deposits typically strewn with small pebbles. The measured rock abundance is similar to an estimate for the entire Pathfinder landing ellipse (18-25%) based on thermal emissivity results [*Christensen,* 1986]. The characteristics of this rocky landscape are consistent with deposition by the Ares and Tiu catastrophic floods, possibly overprinted by ejecta from a nearby impact crater [*Golombek et al.*, 1997a; *Parker and Rice*, 1997]. The Pathfinder location was originally selected, in part, on the premise that it might be a "grab bag" site containing rocks carried by floods from the ancient southern highlands [*Golombek et al.*, 1997b]. However, the 800-km distance to the southern highlands boundary, the recognition that terrestrial floods do not carry large rocks great distances, and the angularity of many blocks all suggest that rocks at the Pathfinder site may be locally derived [*Malin et al.*, 1997]. Some rocks might be related to domes, interpreted to be volcanic [*Greeley et al.*, 1977] or sedimentary [*Parker and Rice*, 1997], located approximately 100 km east of the site and asso-

ciated with a dark mottled unit that extends into the western part of the Pathfinder landing ellipse. More likely, the rocks are samples of a ridged plains unit [*Britt et al.*, 1998] or of older crust that may constitute the local bedrock and exposed, streamlined islands. Rocks at the Pathfinder site itself are Hesperian-age materials interpreted to be the lowermost floors of the outflow channel system [*Rotto and Tanaka*, 1995; *Tanaka*, 1997]. It is likely that the bedrock beneath this unit is Lower Hesperian but it could be partly Upper Noachian, or both, depending on local stratigraphy.

The relative locations of rocks described or alluded to in this paper, as well as the rover traverse, are shown in Figure 1. This map can be cross-referenced with a previously published panoramic view of the landing site showing rock names and locations (Plate 6 of *Mars Pathfinder*, 1997).

The nature of the Pathfinder site rocks is somewhat uncertain because of conflicting or ambiguous observations and measurements. Preliminary imaging results [*Rover Team*, 1997; *Smith et al.*, 1997a] suggested that a diverse assortment of rocks is present, an inference that appears to be inconsistent with available rock chemistry [*Rieder et al.*, 1997a]. Here we describe chemical compositions measured by the rover-mounted Alpha Proton X-ray Spectrometer (APXS), multispectral imaging by the Imager for Mars Pathfinder (IMP), and observations of structures and surface textures by the IMP and by rover cameras. These data allow new inferences to be drawn concerning the mineralogy, petrology, and origin of these rocks. Our interpretations are guided, to some extent, by the geologic context of the Pathfinder site, by previous observations at Viking sites, and by the petrogenesis of SNC meteorites which are commonly thought to be Martian rocks [*McSween*, 1994, and references therein]. The integrated chemical, multispectral, and textural data suggest that the Pathfinder site is apparently dominated by a distinctive, perhaps unusual lithology.

2. Rock Structures and Textures

2.1. Nature of the Observations

Observations were made using cameras on both the lander and rover that permit interpretations of rock textures. The front camera on the rover provided close-up images of rocks at a spatial resolution of 0.7-1 mm per pixel at closest range. For rocks farther than 1.3 m from the IMP lander camera yet within 40 cm of rover cameras, the spatial resolution of the uncompressed rover camera images is better than that for lossless IMP images. However, "super-resolution" images pre-

pared by coregistering and co-adding multiple single-frame IMP images [*Parker*, 1998] can improve the resolution of IMP images by factors of 2 to 3. The option to compress rover images at 4.9:1 was selected only for a few rover frames, used primarily for navigation. Many compression options were available for IMP, and most of the images were in the range 1.3:1 lossless to 12:1 lossy. More description of these cameras was provided by *Smith et al.* [1997b] and *Rover Team* [1997]. The IMP and rover front cameras each provide stereoscopic pairs; stereo calibration images were available for the rover cameras but no flat-field images. Images from the rover rear color camera did not prove as useful, due to the different focal lengths of the red, green, and infrared pixels and the small dynamic range of the infrared pixels.

2.2. Results

A variety of surface textures and structures are seen on the rocks at the landing site, including pitted, knobby, smooth, lineated, and bumpy textures, and exfoliation structures. For each type, we provide a description and discuss the possible genetic implications, with emphasis placed on rocks analyzed by APXS (Table 1). These textures may be indicative of a number of processes, but they are not diagnostic of a particular type of rock.

Pits in the 0.1 to 1 cm size range are found on many rock surfaces, typically occupying areas of 5-10 volume %. The pitted textures resemble those of some rocks at the Viking Lander 1 site rather than the spongy-looking rocks common at the Viking Lander 2 site. On some rocks, such as Souffle' and the Dice, the pits could be volcanic vesicles, although aeolian processes probably have enlarged the original vesicles and changed their shapes [*Greeley and Iverson*, 1985]. A possible alternative to vesicles is chemically etched pits, such as those formed in Antarctica during brief periods when rock surfaces have thin films of snow melt; this mechanism has been proposed as an explanation for the pits in rocks at Viking landing sites [*Allen and Conca*, 1991]. Other possibilities include etching of softer minerals in a matrix of harder minerals [*Carr*, 1981] or wind blasting to carve ventifact pits. It is unclear whether vesicles on the surface of Stimpy (Figure 2) might have exerted control on wind abrasion or whether all of the pits could be due to weathering. The difference between the deep pits covering most of Stimpy's surface and the curved slotted grooves at the top of the rock may reflect a relationship between the impact angle of saltating particles and susceptibility to abrasion (*Greeley et al.*, 1982). A surface of Moe that has suffered strong wind abrasion shows only a few small pits, suggesting either that this rock is not vesicu-

lar or that the pits were filled by dust. Yogi is another rock that appears to have only a few pits.

One rock, Squash, exhibits an unusual knobby shape with lobes and a protrusion roughly 10 cm in size (Figure 3). No other rocks at the site have similar protrusions. This texture could indicate that the rock is an autobrecciated lava, a pillow basalt, a sediment containing rounded cobbles, a volcanic rock with lithic fragments, or an impact breccia. The protrusions have lower albedo than the rest of the rock, much of which appears to be coated with dust or has a matrix that mineralogically resembles the dust. The other side of Squash facing the IMP does not have as many protrusions, and has a near-vertical, fairly dust-free face and a dust-covered top.

Linear features, typically appearing as repeating subtle light-dark bands spaced 3-5 mm apart, are seen on many Pathfinder rocks. The most striking examples are Chimp (Figure 4) and Zebra. The boundaries of the bands cannot be resolved well enough to describe the sharpness of the transition, but they do not appear to pinch out or thicken. In some places lineations may be bands defined by thin subtle topographic ridges, but most appear to be flush with the rock surface. Other rocks with these linear features include Mini-Matterhorn, Yogi (lower east face), Half Dome, Ender, Squid, Flat Top, and Booboo. The lineation is not a camera or image-processing artifact (e.g., the same lineation seen on the front face of Flat Top in rover images also appears in super-resolution IMP images, at an orientation of about 40° to its top surface). Sometimes the lineation is more easily seen in a super-resolution composite image or an anaglyph (requiring 3-D red/blue glasses) than in a single-frame image, but the features are also found in single-frame images. In some rocks, such as Barnacle Bill, multiple orientations of apparent lineations are faint and nonpervasive. In any case, similarly oriented linear features might reflect any of the following: orientation of stresses the rock has experienced; sedimentary or igneous layering; wind-carved rilles; metamorphic foliation; or internal alignments of bubbles, minerals, or zones of weakness. Alignment of cm-size vesicles in rocks at the Viking landing sites [*McCauley et al.*, 1979); *Carr*, 1981] imparts a layered texture to some of those rocks. Alignment of pits of this size range is uncommon in Pathfinder rocks, although Chimp (Figure 4) is an exception. However, it is possible that lineations on other Pathfinder rocks are expressions of smaller (subpixel scale) aligned vesicles. A terrestrial analog might be the horizontal zones rich in vesicles found in inflated basaltic lava flows, although the scale of these layers is 10-300 cm [*Thordarson and Self*, 1996; *Cashman and Kauahikaua*, 1997; *Self et al.*, 1997]. Inflated flows also exhibit banding on vertical uplift scarps and cracks due to align-

ment of vesicles and changes in vesicularity, but this banding does not pervade rocks deeply [*Hon et al.*, 1994]. If the Pathfinder lineations originated in this manner, all surfaces exhibiting lineations would have to be expansion cracks formed during lava emplacement. This is unlikely, considering their probable abrasion during transport. Yet another form of vesicle layering, on the 10-50 cm scale, has been described in intrusive rocks [*Toramaru et al.*, 1996]. The physics of vesicle layering in igneous rocks is not well understood, so the scale of such layering on Mars could be different.

Only one rock at the landing site, Chimp, has a structure that strongly resembles exfoliation (top left side of rock in Figure 4), where an outer, possibly more highly weathered portion of the rock appears to have spalled off. The rock surface beneath the spall either has a higher albedo or perhaps is rougher and has collected dust more efficiently than the smoother outer surfaces of the rock. A large crack runs from top to bottom (39 cm). Exfoliation results from rock expansion and fracturing due to temperature changes, mineral expansion due to chemical weathering, or release of internal stresses when overburden is removed. If exfoliation was a predominant weathering style at the landing site in the past, some rounded boulders may owe their shapes to spheroidal weathering. Another example of mechanical breakdown of rocks is provided by Barnacle Bill, which has small rock fragments with similar pitted textures in front of it that appear to have broken off the rock.

Rounded bumps on a scale of several mm are common on some Pathfinder rocks such as Wedge, Barnacle Bill, and Shark (Figures 5, 6, 7). Bumps could be surface expressions of crystals, pebbles, cobbles, or rock fragments more resistent to erosion, or they might have formed by aeolian abrasion (*Whitney and Dietrich*, 1973) or chemical etching. If the bumps are weathering features, Wedge's bumpy texture is the most intensely altered surface of this type. Larger (2-4 cm) rounded lumps, like those seen on the base of Barnacle Bill (Figure 6) and Bambam, could be rounded cobbles in a conglomerate, rounded lithic fragments in a volcanic rock, or concretions.

Prince Charming and Shark (Figure 7) are examples of rocks that have bumpy textures accompanied by rounded pits, mostly in the 0.5 to 3 cm size range. These rocks have been suggested to be conglomerates, with some pebbles still embedded and others plucked out to produce sockets [*Rover Team*, 1997]. Such rocks might be the source for the rounded pebbles and cobbles seen in the soil, which are similar in size to the bumps. Analogous features were not observed in Viking soils, nor were rocks with similar bumps and pits. Although these curious surface textures may be suggestive of conglomerates, they are not diagnostic and

could occur in other rock types such as weathered volcanic rocks.

Stimpy and Hassock each have three rock faces oriented in such a fashion to suggest that they are polygonal prisms [*Rover Team*, 1997]. The implication is that the rocks may exhibit columnar jointing, a structure common in volcanic flows. Stereometric measurements of Stimpy indicate that the angles between the three faces are $120^{o} \pm 15^{o}$ and the angles of the faces on Hassock are $135\text{-}140^{o} \pm 15^{o}$. These two rocks could be columnar lavas, but other interpretations are possible. For instance, they might be cracked rock faces developed during dehydration or freeze-thaw cycles.

Because of the equivocal nature of the structures and textures observed in Pathfinder rocks, these observations cannot be used to specify uniquely whether the rocks are volcanic, sedimentary, metamorphic, impactites, or some assortment of rocks with varying origins. However, some rock types, such as highly stratified sediments, appear to be ruled out. The textural interpretations are complicated by the likelihood that multiple processes were responsible, and the original rock textures that carry petrogenetic information have almost certainly been overprinted by aeolian abrasion, chemical weathering, and coatings of dust. These issues might be resolved in the future, if diagnostic textures are revealed in newly generated super-resolution IMP images.

3. Multispectral Imaging of Rocks

3.1. Overview and Analytical Methods

A description of the design and operation of the IMP was given by *Smith et al.* [1997b]. IMP is an electronically shuttered, multispectral binocular imager, in which light from each eye is diverted by a mirror through a spectral filter and to a separate half of a CCD. The filters are located in a 24-position filter wheel, designed so that each eye looks through a filter at opposite positions on the wheel. Three filters (445, 671, and 967 nm) are duplicated at opposite positions for color stereo imaging. The remaining filters are intended for atmospheric opacity measurements or for discrimination of iron minerals, principally low-calcium pyroxenes and ferric phases that are actually found in Martian meteorites or whose existence on Mars is suggested on thermodynamic grounds. For the mineralogic filters, additional spectral bandpasses are viewed either by the right eye (480, 531, 600, 752 nm) or the left eye (802, 858, 898, 931, 1003 nm). Spectral measurements are reconstructed from the images by coregistration of images

through different bandpasses; the spectrum is "handed off" from one eye to the other between 752 and 802 nm. Figure 8 shows a representative IMP spectrum of a soil near the rock Mint Julep. IMP spectra of rocks and soils share the basic characteristics of a ferric absorption edge extending from 440 nm (the shortest wavelength filter) to a reflectivity maximum at 750 or 800 nm, and gradually decreasing reflectivity from the maximum to the longest wavelength filter at 1000 nm. Differences among the spectra may be quantified using several parameters.

The reflectance (designated R^*) is measured relative to the reflectance of the onboard calibration target which was characterized in detail during laboratory studies [*Reid et al.*, 1997]. Reflectance at a red (670 or 750 nm) wavelength is representative of the intrinsic brightness of rock and soil materials, plus photometric effects. Reflectance at a blue (440 nm) wavelength is in general much less variable between Martian rocks and soils [*Soderblom*, 1992], but certain rocks at the Pathfinder site are characterized by atypically high or low blue reflectance. The red/blue reflectance ratio indicates the magnitude of the red slope in the region of strong ferric electronic absorptions by many ferric-bearing minerals [*Sherman et al.*, 1982; *Morris et al.*, 1985; *Bishop*, 1995]. Variations in the red/blue ratio are functions of the concentration and mineralogy of the ferric-bearing phases, particle size of both composite polymineraloic aggregates and the included particles of ferric minerals, and the mineralogy and structure of the composite particles [*Wendlandt and Hecht*, 1966; *Kortum*, 1969; *Sherman et al.*, 1982; *Morris et al.*, 1985; *Morris and Lauer*, 1990]. *Morris et al.* [1998] show there is a general correlation between the red/blue ratio and iron oxidation state in natural composite particles (oxidatively altered volcanic tephra). The peak reflectance of typical Martian spectra [*Mustard and Bell*, 1994], as well as the spectra of most ferric minerals [*Sherman et al.*, 1982; *Morris et al.*, 1985; *Bishop*, 1995], occurs near 750 nm. However, in a few minerals (most notably ferrihydrite and maghemite), the peak occurs instead at or near 800 nm (Figure 9). A subset of rocks and soils at the Pathfinder landing site, including the Mint Julep soil shown in Figure 8, exhibits the longer-wavelength reflectance peak. Two crystal-field absorption bands are observed at the wavelengths of IMP at the landing site. The stronger one, centered around 530 nm, is manifested as an inflection or "kink" in the strongly red-sloped spectrum. A weak kink is characteristic of many ferric minerals, but among those either found in Martian meteorites or predicted to have formed under plausible conditions at the Martian surface [*Gooding*, 1978, 1992; *Burns*, 1992, 1994], only ferrihydrite, maghemite, and especially hematite have a strong kink (Figure 9). Depth of the kink is characterized here relative to a continuum between 440 and 670 nm. The other absorption, which is present only in a

subset of the observed rocks and soils, is centered at 900-930 nm. The depth of this "900 nm" band is characterized here relative to a continuum between 800 and 1000 nm. Most plausible ferric minerals have a band center at or beyond 900 nm, whereas hematite has a band center near 860 nm. Some ferrous minerals, most notably low-calcium and high-calcium pyroxenes, also exhbit a diagnostic band centered near 900-930 nm [*Cloutis and Gaffey*, 1991].

Three main techniques were used to assess spectral variations in rocks at the Pathfinder landing site. First, spectral parameter images were calculated from calibrated mosaics. Those shown in Figure 10 are produced from the "gallery panorama" (2:1 compression) because of its continuous spatial coverage and the large amount of spectral variance that can be represented using its 440 nm, 530 nm, and 670 nm channels. Second, using the parameterized images as a guide to spectral heterogeneities at the site, representative spectra were extracted from various rocks and associated soils to characterize spectral properties in greater detail. To highlight the differences between spectra, they are shown ratioed to an average of typical bright red drifts at the site. Spectral variations were explored in detail using these type spectra, utilizing various methods such as scatterplots of spectral parameters and various multivariate techniques. We used spectra taken from both "multispectral spots" (no compression) and the "superpanorama" (2:1 compression) [*Smith et al.*, 1997a]. For consistency, only those from the super-panorama are shown here. Finally, based on the results of analysis of the type spectra, unit classification maps were derived based on thresholding of spectral parameter values. Such maps are only a tool for understanding variations at the site; their boundaries are abrupt, in contrast to the typically gradational spatial variations in spectral properties. Superpanorama data were used for this purpose, because they are the only data covering substantial swaths of the landing site simultaneously in all of the visible and near-infrared image channels which we found necessary to discriminate rock and soil units. All data used were calibrated using CCD corrections and measurements of the IMP calibration targets as described by *Reid et al.* [1997].

3.2. Spatial Variations in Rock Spectral Properties

The spectral properties of rock surfaces facing the Pathfinder lander show strong variations azimuthally. Southwest of the lander, facing the prevailing northeast wind direction [*Smith et al.*, 1997a], rock surfaces are generally similar spectrally. Compared to drift they exhibit a similar low blue reflectance but a lower reflectance at longer wavelengths, a lower red/blue ratio, and a weaker kink.

Northeast of the lander, on rock faces away from the prevailing wind direction, a greater degree of heterogeneity is observed (Figure 10). First, *gray* portions of many cobbles and small boulders, having a variety of shapes, resemble spectrally rocks on the southwest side of the lander (blue arrows). Second, *red* portions of cobbles and small boulders exhibit elevated red/blue ratios and a stonger kink (bright red arrows). Commonly, both kinds of surfaces occur on the same rocks, with gray portions concentrated at edges or on the vertices between facet-like faces. Third, a few tabular, *pink* rock-like masses have red/blue ratios nearly as high as in drift, but exceed drift in brightness, especially at shorter wavelengths (pink arrows). Fourth, large, typically rounded boulders in the far field (dark red arrows) have as high a red/blue ratio and as strong a kink as drift, but are darker at all wavelengths. These *maroon* boulders also have facets which exhibit the gray reflectance properties typical of upwind rock faces. Yogi is one of the best examples: the upwind side of the rock is relatively gray, whereas its downwind side is redder and similar to large, red rocks in the far field. There are also rare examples of rocks with dominantly red upwind faces to the south of the lander, and spectrally analogous soils (discussed below and by *Bell et al.* [1998]) occur at all azimuths.

Illumination geometry does cause temporal variations in the measured properties of rock surfaces, but on well illuminated rock surfaces these changes are smaller than the variation between spectral classes. Large degrees of reddening due to sky radiance are observed only on highly shaded rock faces. For example, the superpanorama image of Yogi shows a small "bluer," well illuminated face on the left side of the rock; this same area appears redder in the gallery panaorama when that portion of the rock surface is relatively shaded.

The azimuthal variation in rock spectral properties is important evidence for understanding heterogeneity. The relative homogeneity and gray color of upwind rock faces, the redder color (approaching the color of drift) of the downwind faces of large boulders, the presence of gray portions on generally red rocks, and the concentration of such gray surfaces at edges and vertices all evoke preferential removal or lack of deposition of thin, oxidized coatings from those faces most exposed to prevailing winds. Consequently, much of the spectral heterogeneity of the rocks is apparently only "skin deep." This interpretation is consistent with many similar results from imaging studies of rock surfaces at the Viking Lander sites [*Evans and Adams*, 1979; *Sharp and Malin*, 1984; *Guinness et al.*, 1987], including longer-term observations of changes in dust coatings on many rock facets [*Guinness et al.*, 1982].

Although the upwind/downwind dichotomy in rock spectral properties is the

most obvious source of spectral heterogeneity, at least three other types of spectral heterogeneities are observed. Most common is a brightening and reddening of tabular or downwind surfaces of relatively gray blocks, such as Flat Top (Figure 11a). In some rocks such as Barnacle Bill, the brightening and reddening is concentrated in pits on rock surfaces. On Barnacle Bill and a number of other rocks at the north end of the Rock Garden, the brighter, redder top surfaces thicken in the downwind direction into wind tails, indicating that either airfall drift accumulated on the rock or was preserved as an erosional remnant of a pre-exisiting thicker drift layer [*Smith et al.*, 1997a]. Several gray boulders to the southwest of the lander in the Rock Garden also exhibit a redder horizontal band along the lowermost several centimeters of the rock (Figure 11a). This banding is interpreted as a thin remnant of a pre-existing drift layer that has been nearly removed by aeolian erosion [*Smith et al.*, 1997a].

The least common type of spectral heterogeneity is mottling of the northeast-facing, typically scoured sides of cobbles. Despite surface textures suggestive of layering or included fragments, described above, very few rocks exhibit color variations thought to correspond to compositional differences within unweathered rock, such as parallel banding or mottling. (Because of the necessity for registration of images acquired through different filters, color heterogeneities in rocks are less resolvable spatially than are morphologic features.) This is true even of rocks suggested to have "sockets" formed by loss of pebbles from a conglomerate [*Rover Team*, 1997]. However, two rocks to the south of the lander exhibit mottled spectral properties absent from other rocks in the near field. Ginger, a lobate cobble approximately 15 cm in diameter, exhibits rounded, gray lobes a few centimeters in size separated by a dark, very red groundmass (Figure 11b). Boris, a subangular rock-like mass about 20 cm in size, exhibits subangular patches ~5 cm in size of differing spectral classes (brighter and redder through darker and grayer), separated by a gray groundmass (Figure 11c).

3.3. Rock Spectral Classes

Each of the four major spectral classes of rock surfaces is distinguished by characteristic properties and modes of occurrence, as described below. Parameterized spectral properties for each class are summarized in Table 2.

Gray rock surfaces (Figures 12a,b) are observed on rocks of all sizes. Relative to drift, gray rocks are comparable in reflectance at short wavelengths but are darker at long wavelengths. The type specimen, Shark, is in the Rock Garden (Figure 1). Peak reflectance occurs at 750 nm; at longer wavelengths, no well-

defined absorption band minimum is observed. The low reflectance, low red/blue ratio, and weak or absent kink in gray rock surfaces are consistent with weakly weathered Fe^{2+}-containing rocks. The lack of a well-defined absorption contrasts with most comparably colored (dark) regions of Mars, which exhibit a "1- m" absorption band several percent in depth, centered at 950-980 nm [*Mustard et al.*, 1993, 1997; *Bell et al.*, 1997]. The same Martian dark regions typically also exhibit an absorption band near 2100 nm [*Mustard et al.*, 1993, 1997]. The positions, centers, and relative depths of the two absorption bands in such regions are diagnostic of pyroxenes with variable calcium and moderate iron contents, such as those in basaltic shergottites [*Singer and McSween*, 1993; *Mustard et al.*,1993, 1997].

Red rock surfaces (Figure 12a,b) also occur on rocks of all sizes, typically on those that exhibit gray surfaces on other faces. Compared to drift, red rocks are higher in reflectance at short wavelengths but are comparable in reflectance at long wavelengths. The type specimen, Broken Wall, is at the north end of the Rock Garden (Figure 1). As with gray rocks the reflectance peak is at 750 nm, and there is no evidence of a near-infrared absorption band.

Compared to gray rocks, the higher reflectance, higher red/blue ratio, and stronger kink in red rock surfaces all suggest the presence of greater amounts of ferric minerals. However, the lack of a well-defined near-infrared absorption implies that such minerals must be extremely fine-grained or poorly crystalline. On the same rocks, the gray properties of surfaces more exposed to abrasion suggest that the brightening, reddening ferric component occurs as a very thin coating or rind either of drift or of an oxidized weathering product.

Pink rock surfaces (Figure 12a,b) occur on several tabular rock-like masses partially buried by drift, as crusts in the soil east of Yogi, and on a number of pebbles between the lander and Yogi. The type specimen, Scooby Doo, is north-northeast of the lander (Figure 1) nearby to similar occurrences. Relative to drift, pink rocks are higher in reflectance at all wavelengths, especially short wavelengths – hence the designation "pink." They are readily distinguished from background materials in blue (440 nm) images, in which they are anomalously bright (Figure 10d). The reflectance peak is at 750-800 nm. Scooby Doo was a site of rover soil mechanics tests [*Rover Team*, 1997], and no abrasion of the surface was observed when the rover's right rear wheel was placed on the rock and turned in place. This result is consistent with a material at least as indurated as a hardpan soil. The similarity of pink rock to typical drift, both in its spectral properties and elemental abundances [*Rieder et al.*, 1997a], and its mechanical strength suggest that the surfaces of rocks of this group are encrusted drift. They are con-

sidered further in a companion paper on Pathfinder soils [*Bell et al.*, 1998].

Maroon rock surfaces (Figure 13a,b) occur mostly on large, rounded boulders including Yogi and comparable boulders in the far field. The type specimen, Seal, is a large boulder in the far field on the left side of Figure 10. In addition, maroon surfaces occur on portions of two smaller rocks in the near field, Ginger and Lamb. Relative to drift, maroon rocks are darker at all wavelengths. Spectral shape is very similar to that of pink rocks, the main difference being in reflectance. Compared with the more common red rocks, maroon rocks are darker at short wavelengths but of comparable infrared reflectance (Figure 9a,b). Maroon rocks are readily distinguished from background materials in blue (440 nm) images, in which they appear anomalously dark (Figure 10d). In the near-infrared, many maroon rocks are distinct from other rocks at the Pathfinder site: the reflectance peak is at 800 nm rather than 750 nm, and there is a weak ferric absorption band at 900-930 nm. Lamb shows the most pronounced development of the absorption band and the shift in peak reflectance toward longer wavelengths. Many rocks with maroon faces, such as Yogi and Booboo, also exhibit gray faces on their upwind surfaces.

The high red/blue ratio and strong kink of maroon rocks and the presence of gray surfaces on the rocks' upwind sides all suggest that the maroon spectral properties originate in a ferric-rich coating, as in the case of red rocks. The development of an infrared absorption in some maroon rocks could, by itself, be taken to indicate simply a larger particle size or greater crystallinity of the ferric mineral than in the drift or on the surfaces of red and pink rocks. However, the magnitude in shift in the wavelength of the reflectance peak is not an expected effect of textural variations, and it is not an observed effect of variations in ferric mineral crystallinity or particle size [*Bell et al.*, 1990]. Rather, the wavelength shift may indicate a mineralogic difference between maroon surfaces and the majority of other red materials, which have their reflectance peak at 750 nm (c.f. Figure 9).

3.4. Relationship of Rock Spectral Classes and Drifts

The pervasiveness of drift at the landing site, the occurrence of different spectral classes on the same rocks, and the evidence for rock spectral variations arising from thin surface coatings or rinds all suggest relationships of rock spectral classes with each other and with drift. Such relationships were explored at the Viking Lander sites by *Adams et al.* [1986] and *Guinness et al.* [1987, 1997], who found similar evidence for strong spectral effects of surface coatings or rinds on rocks, as well as evidence for certain locally derived dark soils that were inter-

preted as abrasion or spallation products from adjacent rocks [*Sharp and Malin*, 1984].

In characterizing these types of relationships at the Pathfinder landing site, it is critical to recognize subtle but important near-infrared spectral differences within drift (Figure 14) [*Bell et al.*, 1998]. Most drift at the site, which we call "bright red drift," has a reflectance maximum at 750 nm and lacks an infrared absorption. However, there are restricted locations at which drift has its reflectance peak at 800 nm and exhibits a weak infrared absorption at 900-930 nm. These attributes are analogous to those of many maroon rocks. These brown soils occur in the lee of Yogi, in association with Lamb, and north of the lander surrounding the partially buried boulder Mint Julep. An exposure of a soil unit with a similarly strong visible-wavelength spectral curvature was detected at the Viking Lander 2 site [*Guinness et al.*, 1987], and was interpreted as evidence for hematitically altered volcanic tephra.

Key spectral parameters indicating the relationships between rock groupings and drifts are reflectance and the strengths of absorptions. Figure 15a shows that red/blue ratio and strength of the 530 nm absorption are highly correlated, indicating that the ferric phase responsible for reddening rocks also accounts for the 530 nm absorption. This relationship does not uniquely indicate the identity of the dominant ferric mineral(s), but it does favor phases with strong kinks (ferrihydrite, maghemite, and especially hematite) and preclude those lacking a significant kink (especially goethite).

Figure 15b shows the relationship between reflectance and red/blue ratio. Most rocks, which belong to the gray, red, and pink classes, exhibit an increase in red/blue ratio (and kink) with increasing reflectance, indicating that they are brightened by a ferric component. Among maroon rocks and both kinds of drift, there is a distinctly different relationship between reflectance and spectral shape: both the red/blue ratio and kink are largely independent of reflectance, which varies by a factor of $\geq$2 with little variation in spectral shape (hence, spectra of maroon rocks ratioed to drift are nearly horizontal lines as in Figures 13b).

Figure 15c shows the relationship between calculated strengths of the crystal field absorptions at 530 nm and 900 nm. Among gray, red, and pink rocks and much bright red drift, nominal strengths of the two absorptions are inversely related. This result indicates greater concavity in the near-infrared portions of spectra of grayer, less altered rock surfaces, as expected from a pyroxene-like absorption, even though a band minimum is not resolved. This curvature was confirmed by fitting the near-infrared ($\geq$750 nm) reflectances of rocks using a second-order polynomial. All except the reddest of the gray rocks, Wedge, exhibit a

consistent upward curvature and several approach zero slope at 1000 nm. This curvature could result from a pyroxene, olivine, or glass absorption even though a band minimum is not resolved, but it could not result from spectral continuum effects of a ferric coating [*Singer and Roush*, 1993; *Fischer and Pieters*, 1993] because the correlation with red/blue ratio is of the opposite sense to that predicted for a ferric coating. Figure 15d shows the relationship between red/blue ratio and 900 nm band depth. Due to the high correlation between kink and red/blue ratio, essentially the same relationships are observed as in Figure 15c.

The correlated spectral parameters among gray, red, pink rocks and bright red drift and their predominance at the site leads us to associate them into a "primary spectral trend." Examination of the spectra in Figure 12a shows that rocks and drift in the primary trend also have in common a reflectance peak at or near 750 nm. Among maroon rocks, brown soil, and some bright red drift, a second trend is evident in Figures 15c,d, in which kink and red/blue ratio are nearly invariant but 900 nm absorption strength increases to as much as several percent. These materials we associate into a "secondary" spectral trend. Further from the intersection of the two trends, the maroon rocks and brown soils exhibit a reflectance peak at 800 nm rather than 750 nm (Figure 13). At the intersection of the two trends, maroon rocks grade into pink rocks, consistent with the similarity in their spectral shapes despite reflectance differences.

The association of the two trends with different local environments was explored in detail in the quadrant northwest of the lander, containing Yogi and several other large boulders (Figure 16a). The superpanorama of this area was used to map the four major spectral units, based on the two spectral trends shown in Figures 15c,d and the ranges of parameter values for each class summarized in Table 2. We classified the units based on the relationship between red/blue ratio and 900 nm band depth shown in Figure 15d, because these parameters can both be calculated from left-eye channels, avoiding problems with parallax difference and calibration uncertainty. Rocks on the primary spectral trend can be separated based on thresholding of the red/blue ratio. Separating maroon rocks is less straightforward; although they lie on a distinct trend, their red/blue ratios overlap those of pink rocks and drift and their nominal 900 nm band depths overlap the range in gray rocks. We therefore defined a "residual 900 nm band depth," which characterizes how far a given spectrum lies from the average relationship in primary trend rocks between the band depth and red/blue ratio. Residuals are shown in Figure 16c. Low residuals (shown in blue to green hues) characterize the primary spectral trend. Higher residuals (red hues) characterize the unusually strong 900 nm absorptions in the secondary spectral trend. On rocks, high resid-

uals occur on surfaces of large, round boulders, covering parts of Booboo (right edge of image) and Valentine (far left of Yogi) but only recessed parts of Yogi. High residuals are also found in some brown soils, in small deposits of drift in the lee of Yogi, and in subsurface soils exposed by rover wheel tracks.

The unit classification map is shown in Figure 16d. Because the classification scheme is blind to differences in reflectance between rocks and soils, bright red drift classifies as pink rock, brown soil classifies as maroon rock, and there may be crossovers of maroon rocks into the pink category. Four important conclusions arise from this exercise: First, rocks and soils forming the primary spectral trend (gray, red, and pink rocks, some bright red drift) dominate the scene. They are the primary constituent of the optical surface, and materials forming the secondary trend (maroon rocks and brown soils, some bright red drift) are uncommon. Second, red and pink surfaces or accumulations of bright red drift are common on rocks of all sizes, shapes, and presumably ages. In other words, whatever processes formed the primary spectral trend have acted upon all materials in the scene. Third, maroon rock surfaces are nearly restricted to large, typically rounded boulders interpreted previously [*Smith et al.*, 1997a] to be the older of two generations of rocks at the site. In other words, processes forming the secondary spectral trend seem to have had little effect on younger pebbles and cobbles throughout the scene. Fourth, disturbed soils exposed in the rover tracks share spectral affinities with maroon rocks. The spectral difference between the uppermost drift and the subsurface is concordant with soil mechanics results [*Rover Team*, 1997] indicating a lesser cohesion and finer grain size in the uppermost ~1 cm of drift overlying a poorly sorted, cloddy material.

The primary and secondary spectral trends have fundamentally different attributes: the relationship of spectral properties with reflectance; the relationship between strength of the two observed absorptions; their spatial association with rocks of different size, shape, and probably age; and the wavelength of the reflectance peak. These differences indicate that the two trends originate from different physical processes and suggest that they may involve different ferric mineral compositions. These possibilities are explored in greater detail below.

3.5. Drift Coatings: An Explanation for Spectral Variations

The spatial pattern of spectral variations on rocks and their relationship to wind direction strongly suggest that the major source of spectral heterogeneity is thin ferric coatings. The spectral effects of such coatings has been investigated in the laboratory by *Fischer and Pieters* [1993] and *Shelfer and Morris* [1998], in the

context of Viking Lander multispectral imaging by *Adams et al.* [1986] and *Guinness et al.* [1987, 1997], and using telescopic observations by *Singer* [1980]. Viking analyses indicated that most rock surfaces appeared to be relatively unweathered and simply covered or coated to varying thicknesses with somewhat amorphous, oxidized material. The darkest block surface analyzed by *Guinness et al.* [1987], for example, was well matched spectrally by an unoxidized Hawaiian basaltic andesite naturally coated with about 30 μm of exogenic palagonite. The laboratory studies [*Fischer and Pieters*, 1993; *Shelfer and Morris*, 1998] reveal that on a dark, spectrally neutral substrate, including but not limited to basalt, increasing thickness of an optically thin, smooth ferric coating causes an increase in reflectance at all wavelengths, an increase in red/blue ratio, and an increase in strength of ferric absorptions. A coating only several microns thick drastically alters the spectral signature of the substrate, and a coating thickness of only several tens of microns causes the spectral properties of the rock to approach those of the coating phase [*Fischer and Pieters*, 1993]. However, ferric coatings exhibit three major differences from uncompacted ferric powder: they are brighter, ferric absorptions are weaker, and they have lesser red/blue ratios. These differences can arise from wavelength-dependent transparency of the coating or wavelength-dependent scattering effects. The effects of increasing coating thickness follow quite closely the primary spectral trend characterizing gray, red, and pink rocks. As rocks become redder they become as bright as drift or brighter, especially at short wavelengths, but at comparable reflectances the ferric absorptions are weaker in primary trend rocks than in drift (Figure 15b).

The primary trend is unlikely to be the result of weathering rinds formed by chemical alteration of the local rocks. As described below and by *Bell et al.* [1998], the soils at the Pathfinder site cannot be formed by alteration of local rocks via any single mechanism we have considered, and the reddening agent on main trend rocks exhibits a clear chemical signature of soils at the site. Hence, the same evidence argues against ferric coatings on primary trend rocks occurring predominantly as weathering rinds. Instead, the primary trend results from different thicknesses of a continuous, optically thin coating of drift on dark rocks, or it results from different areal coverages of dark rock by a thicker (tens of microns), smooth coating of drift. Figure 17 compares type spectra of main trend rocks with laboratory data, with both sets of spectra ratioed to the uncompacted ferric material (bright red drift or ferric powder) to isolate the spectral effects of coatings. An increasing thickness of a very thin, continuous ferric coating closely mimics the shift in spectral properties from gray to red to pink rocks (Figure 17a). In reality, a coating may be spatially discontinuous and concentrated in the recesses between

surface irregularities on a rock. To simulate such a configuration, different areal coverages of a discontinuous coating were modeled as linear (areal) mixtures of dark rock and an optically relatively thick (38 μm) coating [e.g. *Singer and McCord*, 1979]. Again, increasing coverage by the coating mimics the shift in spectral properties from gray to red to pink rocks (Figure 17b). Either hypothesis makes two predictions which are testable with APXS elemental abundance measurements: progressively redder rocks should exhibit a progressively more drift-like composition, and the reddest primary trend rocks should most closely approach the composition of drift. Both predictions are confirmed by analyses as described below.

Based on this analysis, our working hypothesis for the origin of the primary spectral trend is variations in the thickness and/or coverage of coatings of drift on gray rocks. Red rocks may be partially covered with coatings tens of microns thick, or they may have a continuous coating only several microns thick. Pink rocks may simply be gray rocks with a coating of drift as thin as several tens of microns; spectrally, there is little difference between such a coating and cemented drift.

The different spectral systematics of the secondary spectral trend are inconsistent with it having the same physical origin as the primary trend. A simple textural difference in coatings is insufficient to explain the differences in the near-infrared spectra of rocks in the two trends. The simplest explanation for the difference between the two trends is a different ferric mineral coating on the secondary trend rocks, which assumes more of the properties of primary trend rocks as an additional coating of bright red drift is added. To maintain the drift-like redness, the coating on maroon rocks must be optically thick (50 μm or more) and rough at the scale of a wavelength of light [*Fischer and Pieters*, 1993].

The ferric mineralogy of primary trend materials cannot be determined definitively. The presence of a strong kink does implicate hematite, ferrihydrite, or maghemite, but none of these can be confirmed because of the lack of a well defined infrared absorption. The best spectral analog to bright Martian soils is a mixture of phases, with poorly crystalline, nanometer-sized particles of ferric oxide dispersed in an aluminosilicate matrix [*Morris et al.*, 1993]. These mixtures occur naturally in certain palagonitic tephras from Hawaii [*Singer*, 1982; *Morris et al.*, 1990, 1993; *Bell et al.*, 1993]. The nanophase ferric material in palagonite may lie along a continuum in composition between hematite and ferrihydrite; either constituent is consistent with the presence of the strong kink [*Morris et al.*, 1998]. Telescopic measurements of regions covered by bright red drift reveal an infrared absorption centered near 860 nm of low but variable depth, consistent with a few

percent or less of crystalline hematite [*Bell et al.*, 1990]. The primary trend materials at the Pathfinder site are probably part of this globally distributed material, but on the low end of crystalline hematite abundance.

At least three explanations for the secondary spectral trend appear plausible. First, secondary trend rocks and soils may contain ferrihydrite, which exhibits a consistent wavelength position of the 900 nm band as well as an 800 nm reflectance peak. Ferrihydrite is predicted to have formed under a variety of plausible Martian liquid water environments [*Burns*, 1992, 1994], and the requisite liquid water environment is supported by landforms at the Pathfinder site. Second, secondary trend materials may contain maghemite, which has many of the same spectral attributes. Maghemite could have formed in weathering rinds on mafic rocks and in soil particles by oxidation of magnetite, without invoking a necessarily "wet" environment, and its occurrence at the landing site would be consistent with results of the magnetic properties experiment [*Hviid et al.* [1997]. Third, secondary trend materials may contain more than one iron-bearing mineral, yielding composite properties similar to those of ferrihydrite or maghemite. For instance, certain impact melt rocks from Manicouagan Crater containing mixtures of hematite and pyroxene have reflectivity maxima near 800 nm and a weak absorption near 900 nm [*Morris et al.*, 1995].

4. Rock Chemistry

4.1 APXS Analyses

Detailed descriptions of the APXS instrument design and operation were provided by *Rieder et al.* [1997b], and a typical Martian rock X-ray spectrum (Barnacle Bill) was illustrated by *Rieder et al.* [1997a]. Five preliminary rock analyses (X-ray mode only), previously published by *Rieder et al.* [1997a], are reproduced in Table 3. Although the composition of one pink rock (Scooby Doo) is available [*Rieder et al.*, 1997a], this analysis is not reported here because it is more appropriately considered in a discussion of Pathfinder soil compositions. Because atmospheric CO_2 between the APXS sensor head and the sample significantly impacted the alpha mode spectra, the abundances of light elements will not be available until the instrument is recalibrated under Martian conditions of CO_2 pressure and temperature. Proton spectra are unaffected by CO_2, but they can only be interpreted along with the alpha data. Alpha and proton mode analyses should allow determination of oxygen, i.e. determination of the approximate redox state of

the rocks, as well as more precise analyses of Na_2O and other oxides with overlapping spectral lines (MgO, Al_2O_3, and SiO_2). A second measurement of Half Dome and measurements of three additional rocks (Chimp, Moe, and Stimpy) were obtained after the rover battery had expired, resulting in measurements with high thermal noise taken during the Martian day; these analyses have not yet been deconvolved.

Rock analyses have been normalized to 98% oxides to correct for unreported P_2O_5, MnO, and Cr_2O_3, which have large errors because their peaks are buried within other spectral lines. Further calibration for these components is ongoing. All iron is reported as FeO (henceforth called FeO^*). Analytical uncertainties reported in Table 3 were derived from the range in differences found between certified and measured values for eight reference standards. *Rieder et al.* [1997a] also reported APXS analyses of two meteorites, including the SNC meteorite Zagami, to demonstrate the accuracy of the instrument.

The performance of the APXS instrument was excellent throughout the entire period of operation on the Martian surface. Especially good was its electronics gain stability over the entire temperature range from -87°C to about -20°C. The total energy deviation for a particular energy was less than 0.2 channels (12 eV). This excellent stability contributed to a better than expected peak resolution in Martian spectra. In order to test the overall precision of the X-ray mode, 10 laboratory measurements of the same sample have been performed with different accumulation times ranging from 1 hour to >24 hours. The results of the 10 analyses were statistically identical for all the major elements in the sample. This high precision allows the interpretation of relatively small differences in the compositions of rocks (see below).

In some of the following figures, analyses of Pathfinder and Viking soils are plotted to illustrate their chemical relationships to the rocks. Like the rocks, the Pathfinder soils [*Rieder et al.*, 1997a] are normalized to 98% total oxides. For comparison purposes, XRF analyses of Viking soils [*Clark et al.*, 1982] have been normalized to 95.4% total oxides (98% minus the average Pathfinder soil value of $Na_2O + K_2O = 2.6\%$, oxides which were below detection limits in the Viking data set).

4.2 Rock Compositions and Mixing Lines

Table 4 summarizes coefficients for all possible correlations between oxide abundances in the five analyzed rocks. Rock compositions, when plotted on two-

component diagrams (Figure 18), form roughly linear arrays with soil analyses falling consistently at one end of the array [*Rieder et al.*, 1997a]. The most straighfoward interpretation of these arrays is that they are mixing lines, with end members defined by a single rock composition and the average soil composition (the latter presumably in the form of adhering dust). Differences in the compositions of Pathfinder and Viking soils [*Bell et al.*, 1998] indicate that the admixed component more closely resembles the local soil than the more sulfur-rich soils at the Viking sites (e.g. Figures 18a, 19b). The APXS only determines elemental abundances to depths of a few tens of microns, so any surficial dust or weathering rind would greatly affect the rock analyses. In addition, the percentage of dust component in a bulk APXS analysis of the rock with a thin (<100 μm) dust coating is higher for lighter elements like sodium than for heavier elements like iron because the X-rays for elements with lower atomic weights are absorbed more by the sample [*Crisp*, 1998].

If we assume that the rocks are igneous, the rock composition can be retrieved from plots of sulfur (which is enriched in Pathfinder soils) versus other oxides. The solubility of sulfur in magmas at reasonable oxidation states is small, normally no more than a few tenths of a percent by weight [*Carroll and Webster*, 1994; *Jambon*, 1994]. Accepting that the sulfur contents of typical igneous rocks are in the 0-0.2 weight % range, we can extrapolate linear regression lines through the data to zero sulfur and thereby estimate the composition of the rock end member, as illustrated in Figure 19. Linear regression coefficients for all oxides versus SO_3 are given in Table 4. For a sample size of five rocks, the correlations that are statistically significant at the 90% confidence level are those >0.80: SiO_2-TiO_2, FeO^*-TiO_2, MgO-SO_3, and Cl-SO_3. However, the regression coefficients for seven additional pairs are >0.70. The effects of closure (the constant sum problem for compositional data [*Aitchison*, 1986]) reduce the significance of the negative correlations in Table 4.

The sulfur-free rock composition determined in this way is given in Table 3. This composition exhibits some of the same chemical peculiarities that are found in SNC meteorites. The Pathfinder rocks' high Fe/Mg and low Al/Si are characteristic of shergottites, nakhlites, Chassigny, and ALH84001 [*Wänke and Dreibus*, 1988; *Rieder et al.*, 1997b], and the sulfur-free rock plots along the Mars mantle-crust fractionation line (defined by the compositions of SNC meteorites and Martian soils) in a diagram of Mg/Si versus Al/Si (see Figure 4 of *Rieder et al.* [1997a]). The sulfur-free rock's high Fe/Mg probably reflects the FeO abundance of the Martian mantle [*Wänke and Dreibus*, 1988], but its low Al/Si might be an

artifact of normalization to a high silicon content (explained more fully below). The sulfur-free rock has significantly higher SiO_2 than SNC meteorites, and its relatively high K_2O content (and apparently high P_2O_5 content, as judged from raw spectra) imply that it is more highly differentiated and richer in incompatible elements than are basaltic shergottites.

4.3. Rock Norm and Classification

The chemical composition of the sulfur-free rock has been recast into mineralogy using the C.I.P.W. norm formulation (Table 3). This calculation is based on idealized, anhydrous minerals that crystallize under equilibrium conditions in igneous rocks. In the norm calculation, we have assumed that the Fe_2O_3/FeO molar ratio is the same as that measured in basaltic shergottites (0.026) [*McSween and Jarosewich*, 1983]. The norm for the sulfur-free rock is dominated by feldspars (albite, anorthite, and orthoclase), pyroxenes (hypersthene and diopside), and quartz. We emphasize that this norm is only provisional, because changes in the abundances of alkalis and other light element oxides and/or redox state (which may occur when alpha-proton data are available) would affect the proportion of feldspar and other phases. Inclusion of P_2O_5 would produce normative apatite at the expense of diopside. The normative calculation is intended to emphasize differences between rocks, so small changes in chemical composition may result in more dramatic distinctions in the norm.

Of course, we do not know if the rocks at the Pathfinder site are igneous and, as already discussed, certain textural features in some rocks may suggest a sedimentary origin [*Rover Team*, 1997]. The composition of the sulfur-free rock, however, is similar to those of some igneous rocks. Figure 20 shows plots of normative feldspar compositions and normative "color index" (defined as the sum of hypersthene + diopside + iron-titanium-chromium oxides), with the shaded areas representing the fields of common terrestrial volcanic rocks [adapted from *Irvine and Baragar*, 1971]. The sulfur-free rock plots within the shaded areas in each case; there is no reason *a priori* why sedimentary rocks should do so. Although the normative feldspar compositions for the average Pathfinder soil [*Rieder et al.*, 1997] and the sulfur-free rock are similar (Figure 20a), their normative color indices are not (Figure 20b). This comparison suggests that even if the Pathfinder rocks are sedimentary, they are likely to be clastic rocks comprised mostly of volcanic fragments.

Based on its chemistry and normative mineralogy, the sulfur-free rock has an

andesitic composition. On a silica versus alkalis diagram commonly used for classification of volcanic rocks [*Le Bas et al.*, 1986], the sulfur-free rock plots within the field of andesite and the individual (dust-contaminated) rock compositions fall mostly in the basaltic andesite field (Figure 21). Andesites are hypersthene-normative volcanic rocks with 57-62 weight % SiO_2 (calculated on an anhydrous basis), TiO_2 < 1.75%, and K_2O < (0.145 x SiO_2 - 5.135) [*Gill*, 1981]. The abundances of TiO_2 (0.7%) and K_2O (0.7% < 3.86% for this silica content) in the sulfur-free rock composition support the classification.

Geochemical classification is also sometimes used for sedimentary rocks, although determinations based on grain size and mineralogy are preferred. Using the scheme of *Herron* [1988], which distinguishes sandstones based on log Na_2O/K_2O versus log SiO_2/Al_2O_3, the sulfur-free rock plots in the field of graywackes. On a plot of log $Fe_2O_3^*/K_2O$ versus log SiO_2/Al_2O_3 used for classifying sandstones and shales, the sulfur-free rock would be termed an iron-sand.

5. Comparison of Chemical and Multispectral Data

5.1. Spectral and Chemical Analyses of the Same Spots

It was recognized early in the development of the Pathfinder mission that correlating APXS and IMP data might provide important information on the nature of the rocks and insights into the processes that formed them [*Golombek*, 1997; *Smith et al.*, 1997b]. Chemical evidence for variable soil coatings on the rocks, already discussed, can only be compared with spectral data if IMP and APXS measurements are taken from precisely the same locations. IMP images documenting each APXS deployment on rocks are shown in Figure 22. The exact position of each APXS spot was determined through careful analyses of rover camera and IMP images. In cases where the location was especially difficult to estimate, JPL rover engineering software was used to measure accurately the rover and APXS positions. The number of pixels subtended by the APXS spot in IMP images was assumed to be a linear function of distance from the IMP. For each spot, spectra were generated using calibrated data [*Reid et al.*, 1997] from all IMP geology filters in the superpanorama and multispectral-spot sequences. For most APXS sites two or more spectra, each taken at a different time of day and under varying lighting conditions, were available (Table 5). Some APXS soil spots were either disturbed by the rover or contained compacted soils. In these cases, spectra were measured from areas near the spot locations. Except in

cases where spots were heavily shadowed, all spectra were used. The reflectances at each wavelength were adjusted slightly to account for small differences between the left and right eyes of the IMP caused by calibration errors. Redness of each spot was measured by taking the ratio of reflectances at 750 nm (near-infrared) and 440 nm (blue). In most cases, reflectances from the IMP right eye were used. The Yogi right-eye 440 nm image had missing packets in the area of the APXS spot, so left-eye data were used in this one case. The left-eye image contained a minor degree of pixel saturation due to overexposure. Under optimal lighting conditions at slightly different times of day, ratios varied by no more than 0.4. for rocks and 0.1 for soils (except Mermaid Dune, which varied by 0.5). Because of the minor differences, these points were averaged.

5.2. Results

The interpretation of rock compositions at the Pathfinder site as mixtures of rock plus adhering dust is strongly supported by a correlation between rock composition and spectral features [*Bridges et al.*, 1997]. The red (750 nm)/blue (440 nm) ratio (Table 5) measures the spectral similarity of individual rocks to soil, with the reddest rocks being most similar. The red/blue ratios are plotted against SO_3 because Martian soils are very sulfur-rich and red relative to the rocks. Figure 23 demonstrates that APXS soil sites are generally redder than rock sites; the only exception is the soil at Mermaid Dune, which has a slightly lower red/blue ratio than Yogi. The red/blue ratios for the entire data set and for the rocks alone correlate very well with SO_3 (Figure 23). Correlations of red/blue ratio with other chemical components in the rock analyses (e.g. Cl and FeO^*) are less significant.

These observations imply that a dust or soil covering is present on all the rocks, even in apparently clean areas selected for APXS measurements. As noted previously, spectra of rocks at the Viking Lander 1 site have also been interpreted to reflect mixtures of rock and soil [*Adams et al.*, 1986], although no chemical data for those rocks exists. The sulfur detected in APXS rock measurements is strongly affected by superficial coatings of dust or soil and is therefore not representative of the rock chemistry.

The smaller range of Cl and FeO^* concentrations in rocks and soils relative to SO_3 is probably one reason for their poor correlations with red/blue ratios. The lack of correlation of red/blue ratio with FeO^* in rocks suggests that the abundances of spectrally active ferric components in the dust and rock do not affect the spectral properties as much as the thickness and areal distribution of dust on rock

surfaces, consistent with our previous results.

6. Interpretations and Discussion

6.1. Igneous, Sedimentary, Impact, or Alteration?

One of the most basic questions about rocks at the Pathfinder landing site is how they formed. The andesite-like composition of the sulfur-free rock shares geochemical characteristics with some common terrestrial volcanic rocks and with SNC meteorites of undisputed igneous origin. This strongly suggests, but does not mandate, an igneous origin for at least the subset of rocks for which APXS analyses have been reported. Pits interpreted as vesicles and facets possibly caused by columnar jointing also imply a volcanic origin for some rocks at the landing site. Physical rheology models applied to the morphology of lava flows on Martian shield volcanoes are consistent with viscosities appropriate for magma compositions ranging from ultramafic to andesitic [*Hulme*, 1976; *Moore et al.*, 1978; *Zimbelman*, 1985; *Cattermole*, 1987; *Lopes and Kilburn*, 1990]. However, landforms suggestive of silicic volcanism, such as resurgent domes and festooned flows in the Martian highlands, are uncommon [*Hodges and Moore*, 1994]. Calculation of the viscosity of an andesitic magma having the composition of the sulfur-free rock, using the method of *Shaw* [1972], gives a minimum value of 4.5×10^3 Pa·s at 1100°C, similar to the lower end of the viscosity range estimated for Martian magmas. Finally, the observation that all analyzed rocks at the site have similar compositions and spectral properties mitigates against non-igneous rocks that have considerable variability, such as layered sediments. We believe that a plausible, perhaps compelling case has been made that many Pathfinder rocks are volcanic in origin, but we must also consider other possibilities.

For most rocks, spatial variations in spectral properties provide little evidence with which to distinguish igneous, sedimentary, or impact-generated origins. Nearly all spectral heterogeneity results from coverings of drift, or variations in spectral shape and reflectance easily reconciled with ferric mineral coatings. Apparently scoured gray rock surfaces exhibit little in the way of organized spatial variations in color. The two significant exceptions are the cobbles discussed earlier, Ginger and Boris. Ginger's dark gray lobes separated by a maroon groundmass could be interpreted as a ferric-cemented conglomerate; alternatively, a small, dark red patch behind Ginger may indicate that the rock was overturned by airbag retraction, so that the red material on Ginger could be adhering disturbed

soil. Also, the color variations could originate from remnant maroon material preserved between eroded, dark gray protuberances. Boris' varicolored, subangular blotches separated by a dark gray groundmass could similarly be interpreted as a breccia cemented by a ferric-poor material, possibly "dark soil" [*Bell et al.*, 1998] or tephra. Spectral data for a few rocks provide tantalizing but ambiguous evidence for limited lithologic variations at the site, but they do not support a particular origin for most rocks.

As previously noted, textural observations may suggest that some rocks at the Pathfinder site are conglomerates. Coarse clastic rocks have chemical compositions that mimic the compositions of the rocks that were disaggregated to form them. For example, the Poway conglomerate in California contains virtually identical minor and trace element abundances to the volcanic rocks from which its gravel fragments were derived [*Abbott and Smith*, 1989]. Even finer-grained sandstones dominated by rock fragments (i.e. wackes) can retain the chemistry of their source rocks, as indicated by the diagnostic trace element patterns in wackes from different tectonic settings [*Bhatia*, 1985]. Consequently, inferences drawn from such sedimentary rocks about the petrogenesis of their igneous protoliths may still be valid.

It is also possible that Pathfinder rocks are impact melts or impact breccias. Their high normative feldspar contents, relative to SNC meteorites, might support the hypothesis that they experienced impact melting. Shock-loaded feldspars are more readily melted than most rock-forming minerals, and small-scale shock melted veins in shergottites are commonly enriched in a feldspathic component [*McSween and Jarosewich*, 1983]. However, melt rocks from large-scale impacts on the Earth and Moon typically show little differentiation from the bulk target materials [*Warren et al.*, 1996]. Samples of the oldest Martian stratigraphic units would be more likely to have experienced pervasive shock metamorphism and melting as part of the late heavy bombardment [*Ash et al.*, 1996], and the only ancient Martian meteorite has been multiply shocked and partly melted [*Treiman*, 1995].

Another possibility is that the rocks are shock-melted dust deposits [*Schultz and Mustard*, 1998]. Impact-melting of terrestrial loess produces glassy, vesicular rocks of variable composition which have spectra similar to Pathfinder rocks. However, the compositions of soils at the Pathfinder site [*Rieder et al.*, 1997] are distinct from the sulfur-free rock composition, so fractionation during shock melting would be required.

Although a significant amount of ejecta could have been deposited at the Pathfinder site from the large crater to the south, estimates based on the crater's size

and distance from the site suggest that most of its ejecta would be significantly smaller (< 20 cm diameter) than any of the rocks analyzed by APXS [*Smith et al.*, 1997a]. The ejecta model of *McGetchin et al.* [1973] predicts that the thickness of a uniform ejecta deposit from this crater should be 0.3 m, but new crater morphology data from Mars Global Surveyor suggest that ejecta blanket thickness based on this paradigm is overestimated [*Garvin and Frawley*, 1998]. The limit of continous ejecta [*Moore et al.*, 1974] is only about 1.75 km from the crater center, well short of its 2.95-km distance from the landing site. Consequently, it seems unlikely that any large Pathfinder rocks, of sizes like those analyzed by APXS, are ejecta from this crater.

Finally, we acknowledge the possibility that the rocks may be coated with siliceous weathering rinds, even after removal of adhering dust. Hawaiian basalts exposed to semi-arid weathering develop hydrous silica coatings that thicken and incorporate detrital material with age [*Farr and Adams*, 1984; *Crisp et al.*, 1990]. These coatings tend to be discontinuous and variable in thickness, up to tens of microns, and may be underlain by thinner zones of iron oxides. Nearly pure silica coatings are colorless, but weathered basaltic detritus incorporated into older coatings produces colors ranging from brown to red. Measured SiO_2 contents for these rinds are higher (>66 weight %, and commonly >80%) than that estimated for the Pathfinder sulfur-free rock, and analyzed oxide sums are lower (<90%, as appropriate for opal or hydrated silica glass) than some Pathfinder rocks (low sums in some APXS analyses are thought to result from variations in the measurement geometry; *Rieder et al.* [1997a]). However, the discontinuous and thin character of siliceous rinds might allow lower measured bulk silica contents and higher totals on APXS-sized spots. Under ordinary terrestrial weathering conditions silica is leached from basalt, but acid conditions or cyclic wetting and drying can concentrate silica [*Farr and Adams*, 1984] or a silica glaze can form as a reaction product on the rock surface in the presence of dew or light rain [*Casey et al.*, 1993; *Dorn and Meek*, 1995]. Formation of siliceous coatings on Martian rocks by an analogous process, however, might require intermittent rainfall on Mars, which seems unlikely in the past billion years or so. If coatings formed in the Noachian, rainfall might have been an agent, but then transportation of rocks by floods would likely have removed the coatings. The observation that Pathfinder rocks with the highest silica contents are least spectrally reddened is opposite the trend expected if siliceous coatings incorporated detritus (as do Hawaiian basalt rinds), but could be rationalized if detritus-free coatings are covered by a veneer of less siliceous dust.

6.2. Stratigraphic Implications of Rock Spectral Features

A key implication of the spatial associations of primary and secondary trend spectral attributes with rocks of different morphologic classes is a stratigraphy of rock spectral features, provided that the large, rounded boulders predate smaller rocks as interpreted by *Smith et al.* [1997a]. Figure 24 shows a three-stage sequence of events that can explain these spatial associations. In stage 1, large rounded boulders and their maroon coatings were emplaced. The same material forming the coatings may have been emplaced elsewhere, perhaps as brown soils exposed in the subsurface by rover tracks. In stage 2, the small cobbles were emplaced. Some small rocks may have retained a maroon coating due to an origin by fragmentation of large, old boulders. Concurrently or later, a layer of bright red drift at least several centimeters thick was emplaced. In stage 3, emplacement of rocks has largely ceased. Aeolian erosion has partially removed the maroon coatings from old rocks, and it has redistributed the bright red drift leaving the red band at the base of many rocks. Brown soil may be exposed in the subsurface or by spallation from maroon rocks. Emplacement of very small amounts of bright red drift on gray rocks has produced coated red and pink rocks. Some pink materials may also originate from exposure of preexisting, cemented brown soil or drift.

In terms of geologic events, stage 1 may include deposition of flood materials, stage 2 a second flood event of lesser magnitude or emplacement of impact crater ejecta and airfall drift, and stage 3 subsequent aeolian erosion and redeposition. If this sequence is correct, then the different ferric phases proposed to occur on primary trend and secondary trend rocks originated in two different periods, and perhaps two different paleoenvironements. If the ferric phase occuring in redder trend rocks is maghemite or ferrihydrite as proposed above, it may be a mineralogic signature of the wetter flood environment in which large, rounded boulders were emplaced.

6.3. Absence of a Pyroxene Absorption Band

Basalts similar in mineralogy to some SNC meteorites (specifically basaltic shergottites) are commonly thought to represent large portions of the Martian surface. The marked compositional similarity between these meteorites and Martian soils [*Baird and Clark*, 1981] suggests a pervasive basaltic source for weathered materials [*McSween*, 1994]. Near-infrared spectral similarities between shergottites and dark regions of the Martian crust, interpreted as relatively rocky regions,

buttress this conclusion [*Soderblom*, 1992; *Mustard et al.*, 1993; *Singer and McSween*, 1993; *Mustard and Sunshine*, 1995]. The Martian remote-sensing spectra contain two absorption bands that indicate the presence of pyroxenes with variable calcium and iron contents. Deconvolution of the spectra reveal overlapping absorption bands for both pigeonite and augite [*Mustard and Sunshine*, 1995; *Mustard et al.*, 1997], with iron-rich compositions similar to those in shergottites. Although these spectral observations are commonly cited as evidence for a predominantly basaltic Martian surface, it might be impossible to distinguish pyroxene-bearing andesites. The calculated norm for the sulfur-free rock at the Pathfinder landing site contains both hypersthene and diopside (Table 3), which would presumably be represented in a volcanic rock by pigeonite and augite, respectively. *Adams et al.* [1986] found that the best spectral match for rocks at the Viking 1 Lander site was a mixture of gray andesite with palagonite dust and a coarse rock-like soil. However, they cautioned that the rather featureless, three-band spectra did not warrant assignment of a specific rock type.

The inability to discern a pyroxene absorption band near 1000 nm in IMP spectra of any Pathfinder rocks is disconcerting, given that this band commonly appears in spectra of dark regions observed telescopically and from orbit. Analysis of the continuum effects of atmospheric aerosols on the remote data shows that, at the surface, the typical "1 μm" band in dark regions should exhibit a minimum within the wavelength range covered by IMP [*Erard et al.*, 1994]. Although adhering dust is very effective in hiding the spectral signatures of underlying rocks [*Fischer and Pieters*, 1993], it is still surprising that no pyroxene band is observed in gray rocks with the least dust coating.

A number of hypotheses have been conceived to explain the absence of the band minimum. Lack of a band minimum due to gross calibration error is refuted by the resolution of a band minimum in some ferric materials at the site. More significantly, absorption bands are accurately resolved in IMP spectra of different ferric minerals embedded in color chips on the IMP calibration targets [*Reid et al.*, 1997]. A band could be present but extremely weak and not resolved above noise in the data, due to a very fine-grained rock texture. However, available image resolution (1-5 mm per pixel) could resolve mineral grains only as coarse as those in medium- to coarse-grained igneous rock, so the failure of images to resolve mineral grains may not necessarily indicate a very fine-grained texture, e.g. <50 μm [*Mustard and Hays*, 1997]. Alternatively, relatively "clean" gray rock surfaces may contain a silica coating which masks spectral properties of pyroxene in the rock interior. However, the existence of such coatings is inconsistent with the lesser abundance or absence of ferric-rich coatings on the same rock faces, unless silica

coatings are significantly harder to remove than ferric coatings.

We favor three hypotheses for the apparent absence of a pyroxene band. First, the rocks may be volcanic or impact glasses; the "1 m" band in Fe^{2+}-containing glasses is centered near 1100 nm. The IMP spectral range is insufficient to resolve a band minimum in glasses but could detect the infrared curvature like that observed in gray rocks. However, glasses in very old rocks might be expected to have devitrified, especially in the presence of water. Second, a masking phase dispersed throughout the rocks may obscure an absorption. Magnetite is common in terrestrial volcanic rocks and some SNC meteorites [*McSween*, 1994], and laboratory spectra show that its presence can drastically weaken the absorption due to pyroxene [*Hunt et al.*, 1974; *Cloutis et al.*, 1990]. Third, the pyroxene compositions in these rocks could be significantly higher in iron and/or calcium than are typical for Mars. Such a composition could push the center of the band to or beyond 1000 nm so that it would not be resolvable by IMP, but would produce the observed infrared spectral curvature. Figure 25 illustrates zoned pyroxene compositions in the Nakhla and Shergotty meteorites, with superimposed contours of the "1 μm" band minima for pyroxenes of various compositions [*Cloutis and Gaffey*, 1991]. Augite compositions in Nakhla are rich in calcium (Wo component), and the absorption band minimum (illustrated as a shaded box) lies beyond 1000 nm. Basaltic shergottites contain both high-calcium (augite) and low-calcium (pigeonite) pyroxenes. The absorption bands for pigeonite and augite overlap, so that the band positions of bulk basaltic shergottites (illustrated as a second shaded box) fall between the actual pyroxene compositions at band positions less than 1000 nm. However, the compositions of normative pyroxenes in the Pathfinder sulfur-free rock are significantly richer in iron (Fs component) than are Shergotty pyroxenes. Very iron-rich pigeonite is metastable and tends to breakdown into fayalite plus silica [*Lindsley and Anderson*, 1983], so the actual assemblage in the rock may be ferroaugite plus fayalitic olivine. The positions of the band minima for ferroaugite [*Cloutis and Gaffey*, 1991] and iron-rich olivine [*King and Ridley*, 1987] lie beyond 1000 nm and thus would not be seen in IMP spectra. The tendency for the pyroxene band minima contours to bend downward towards the iron-rich side of the quadrilateral (Figure 25) suggests that even a composite pyroxene band minimum for augite and pigeonite might occur beyond 1000 nm.

6.4. Andesite Petrogenesis

On Earth, andesites are the second most abundant lava type, occurring mostly at destructive plate margins. The direct production of andesitic magma has sometimes been attributed to melting of mantle peridotite under hydrous conditions, fluxed by metamorphic dehydration of the subducted slab. However, high-pressure experiments [*Nicholls and Ringwood*, 1973; *Mysen et al.*, 1974] have demonstrated the difficulty (or, in some cases, the impossibility) of forming primary andesitic melts under such conditions. The consensus now is that andesites form primarily by fractional crystallization of basaltic magmas, a conclusion reached by *Gill* [1981] after an extensive review of the published evidence. Lesser amounts of andesitic magmas result from other processes, such as magma mixing, crustal assimilation, and partial melting [e.g. *DePaolo*, 1981; *Hildreth and Moorbath*, 1988; *Foden and Green*, 1992].

Magmas erupted at subduction zones (andesites in this setting are sometimes called "orogenic andesites") follow one of two differentiation paths, depending on whether they exhibit significant iron-enrichment with increasing fractionation. Figures 26 and 27 compare the tholeiitic and calc-alkaline differentiation trends, which are controlled by fractionation at low pressures under anhydrous conditions or at higher (crustal) pressures with water present, respectively [*Grove and Baker*, 1984; *Sisson and Grove*, 1993]. In Figure 26 (adapted from *Gill* [1981]), the liquid lines of descent are reflected in increasing SiO_2, and orogenic suites fall on both sides of the boundary separating tholeiitic and calc-alkaline rocks. Also shown in this figure is a liquid line of descent leading to anorogenic "icelandites," which are andesitic rocks formed by fractional crystallization of basaltic magmas in other tectonic settings such as spreading centers and intraplate hot spots [e.g. *Carmichael*, 1964; *Ashley et al.*, 1995]; icelandites invariably exhibit tholeiitic trends. The Pathfinder sulfur-free rock composition, as well as all the individual rock analyses (which are adulterated by adhering dust), clearly fall within the tholeiite field, as do the compositions of melts for SNC meteorites. Figure 27 (adapted from *Grove and Kinzler* [1986]) illustrates tholeiitic iron enrichment in terms of MgO, FeO^*, and alkalis; again, the Pathfinder rocks and SNC melts are clearly tholeiitic.

The most obvious chemical differences between orogenic andesites and anorogenic icelandites is that icelandites have higher FeO^* and lower Al_2O_3 abundances at a given SiO_2 content [*Gill*, 1981]. These are the same geochemical properties that make the Pathfinder sulfur-free rock (and SNC meteorites) distinctive. In fact, anorogenic icelandites provide the closest terrestrial analogy for the

sulfur-free rock composition. Figure 28 compares the abundances of SiO_2, Al_2O_3, TiO_2, FeO^*, and MgO in the sulfur-free rock with those of fractionated lavas from the Galapagos Spreading Center at 85°W and the experimentally determined Galapagos liquid line of descent [*Juster et al.*, 1989]. Only the TiO_2 content differs appreciably from the icelandites in this differentiation sequence.

Because the compositions of basaltic shergottite liquids seem to plot at plausible positions for a parental magma that might generate the sulfur-free rock (Figures 26 and 27), we have also plotted the QUE94201 bulk composition (the only shergottite thought to represent a liquid [*McSween et al.*, 1997]) and the Shergotty intercumulus melt composition in Figure 28. Like the shergottites and the norm of the sulfur-free rock, icelandites commonly contain both high-calcium and low-calcium pyroxenes [e.g. *Carmichael*, 1964]. Normative Fs contents of diopside (Fs_{31}) and hypersthene (Fs_{61}) in icelandites [*Carmichael*, 1964] are only slightly less iron-rich than normative pyroxenes in the sulfur-free rock (Fs_{37} and Fs_{75}, respectively). Given the young crystallization ages of shergottites [summarized by *McSween*, 1994] and old ages of Pathfinder rocks as inferred from their mobilization by ancient floods, it is unrealistic to expect that shergottite magmas could actually have given rise to the sulfur-free rock composition. However, some geochemical characteristics of the Martian mantle, such as Al_2O_3 depletion and FeO^* enrichment [*Wänke and Dreibus*, 1988], might be imprinted on magmas of any age. The shergottite liquid lines of descent, calculated using the MELTS program [*Ghiorso and Sack*, 1995] at low pressure and appropriate oxygen fugacities, deviate significantly from that of Galapagos magmas (Figure 28) and do not pass through or near the composition of the sulfur-free rock. Thus, it is difficult to relate the Pathfinder rocks directly to shergottites by fractionation processes at shallow depth, although they clearly share some distinctive geochemical properties [*Rieder et al.*, 1997a]. We note, however, that the MELTS program does not always correctly predict the crystallization behavior of highly evolved magmas [*Yang et al.*, 1996].

The chemical similarities between the sulfur-free rock and terrestrial anorogenic icelandites imply that any attempts to interpret the andesitic compositions of these rocks as requiring a significant role for water in their petrogenesis, or even the existence of Martian plate tectonics, are probably unwarranted. The small amounts of water that may have existed in the lithosphere of Mars were probably too small to generate much silica-rich magma [*Campbell and Taylor*, 1983]. A more plausible explanation for these rocks is that they formed by fractional crystal-

lization of basaltic magmas, possibly represented by some rocks of the Hesperian ridged plains unit that outcrops near the Pathfinder site [*Britt et al.*, 1998]. *Rutherford and Hess* [1981] discussed the likelihood that melting and fractionation processes might generate siliceous magmas on Mars, concluding that it might be appropriate to think of Mars as intermediate between the Moon (where silica-rich lithologies are very uncommon) and Iceland (which has ~10 volume % of exposed icelandite).

Comparison of the alumina contents of fractionating SNC and MORB melts (Figure 28) with the Al_2O_3 abundance of the Pathfinder sulfur-free rock suggests that its parent basaltic magma was more aluminous than SNC parent magmas. Such a magma composition may signal melting of a relatively primitive Martian mantle source, one that had not yet been depleted in Al_2O_3 by partial melting [*Longhi et al.*, 1992]. Because differentiation of Mars occurred within the first 100 Ma of solar system history, as inferred from Sm-Nd and Hf-W isotopic systematics in Martian meteorites [*Harper et al.*, 1995; *Lee and Halliday*, 1997], this may imply that the rocks at the Pathfinder landing site are very old. Heavily cratered Noachian crust outcrops near and possibly beneath channel deposits at the Pathfinder landing site, and these rocks could have been sampled by floods or by impact.

The andesitic composition of the Pathfinder sulfur-free rock resembles the average composition of the Earth's crust. *Rieder et al.* [1997a] suggested that Pathfinder rocks might provide a more representative sampling of the ancient Martian crust than does the ALH84001 meteorite, a 4.5 Ga-old orthopyroxenite. The widespread occurrence of rocks with andesitic compositions on Mars was originally suggested based on Mariner 9 thermal emission spectra of suspended dust [*Hanel et al.*, 1972]. Formation of an andesitic crust by simple fractional crystallization would require a huge quantity of basaltic magma, however, so the petrogenetic mechanism inferred to produce the Pathfinder sulfur-free rock would probably be more consistent with a mafic average crustal bulk composition. Production of an andesitic crust on Mars might have been accomplished by repeated periods of partial melting, probably over an extended period of time, as on the Earth. Although such a complex scenario cannot be ruled out, local fractionation of basaltic magma provides a simpler explanation for the Pathfinder rocks.

7. Summary and Conclusions

Chemical, multispectral, and textural studies of rocks at the Mars Pathfinder site allow the following conclusions and interpretations to be drawn:

(1) Rock surfaces exhibit combinations of pitted, knobby, smooth, lineated, and bumpy textures. Original textures have been overprinted by aeolian abrasion, weathering, and dust coatings, complicating their interpretations. One rock has a structure resembling exfoliation, and several others resemble polygonal prisms which may suggest columnar jointing. The equivocal nature of most observed surface textures means that they cannot be used to determine uniquely the origin of the rocks.

(2) Four spectral classes of rock surfaces are identified: Gray and red surfaces commonly occur on the same rocks, with gray portions on the upwind sides or at eroded edges and red portions on downwind surfaces. Several pink rocks occur as tabular rock-like masses, probably soil crusts. Maroon rocks are mostly large, rounded boulders in the far field. Correlated spectral parameters allow the rocks to be assigned to two spectral trends: rocks of the primary spectral trend, which share a reflectance peak at 750 nm, include most materials (both rocks and soils) in the optical surface. Only maroon rocks and spectrally similar brown soils are assigned to the secondary spectral trend, defined by reflectance peaks at longer wavelengths.

(3) The spatial pattern of spectral variations in rocks and their relationship to wind direction suggest that the source of spectral heterogeneity (i.e. the primary spectral trend) is primarily thin ferric coatings of red aeolian dust on dark rocks. The ferric phase in primary trend coatings is ambiguous due to lack of a diagnostic spectral signature. The secondary spectral trend apparently requires coating by a different ferric mineral with distinct spectral properties (possibly maghemite or ferrihydrite).

(4) Preliminary APXS analyses of most elements in rocks plot as nearly linear arrays, interpreted as mixing lines between a single rock composition and adhering dust. This interpretation is supported by a strong correlation between rock sulfur contents and red/blue spectral ratios measured at the same spots. Extrapolations of regression lines to zero sulfur give the approximate composition of a presumed igneous rock. Its chemistry corresponds to that of andesitic volcanic rock.

Further possible interpretations and inferences derived from the above data are as follows:

(5) The normative mineralogy of the sulfur-free rock is consistent with norms of

common terrestrial volcanic rocks, suggesting that the relatively large rocks analyzed by APXS are igneous. The calculated (probably minimum) viscosity of a magma having the composition of the Pathfinder sulfur-free rock overlaps the range of viscosity estimates for Martian lava flows based on models that relate rheology to flow morphology. However, the spectral mottling seen in several rocks (not analyzed by APXS) and the suggestion of rounded clasts and sockets on the surfaces of a few rocks might imply that coarse clastic sedimentary rocks or impact breccias are also present. It is also possible that the analyzed rocks are coated with siliceous weathering rinds, although the requirement for intermittent rainfall or dew, if the process is analogous to that on Earth, makes this less likely.

(6) Large, rounded boulders of the maroon spectral class may predate smaller rocks at the site, and the ferric mineral coating that defines the maroon class may be a mineralogic signature of the flood environment in which the boulders were emplaced. Smaller, more angular rocks may represent deposition from a second flood event or ejecta from a nearby impact crater. The latter event was followed by aeolian erosion and deposition.

(7) The absence of a "1μm" pyroxene absorption band in the spectra of any Pathfinder rocks is perplexing. The presence of some mafic phase is supported by upward curvature in infrared portions of the spectra of gray rock surfaces with less dust cover. One possible explanation for the lack of a resolved band center is that the rocks are volcanic or impact glasses, which have absorption bands centered near 1100 nm (beyond the IMP spectral range). Alternatively, the band may be masked by magnetite in the rock, or the presence of iron-rich augite and fayalitic olivine (the latter formed by breakdown of metastable iron-rich pigeonite) may have pushed the absorption band beyond 1000 nm.

(8) The chemistry of sulfur-free rock, if igneous, is consistent with fractionation along a tholeiitic trend. The rock composition does not lie along calculated liquid lines of descent for shergottite melts at low pressure, but instead may require a more aluminous basaltic parent. Its composition is most similar to terrestrial icelandites (andesites formed by fractional crystallization of basaltic magma in anorogenic settings), rather than like the more common orogenic andesites.

(9) Speculations about possible roles for water and plate tectonics in Martian petrogenesis, based on andesitic rocks at the Pathfinder site, are not justified. Although these rocks may represent ancient crust, as inferred from higher alumina concentrations that might characterize partial melts from a primitive mantle, a complex origin involving repeated crustal melting seems less likely than their derivation by fractional crystallization of basaltic magmas.

Acknowledgements. We appreciate thoughtful reviews by Tim Grove, Vicky Hamilton, and an anonymous reviewer. Tom Daley assisted with image processing and spectral analysis. Support for this research was provided by NASA through contracts to the individual investigators or was carried out at the Jet Propulsion Laboratory, California Institute of Technology, under contract with the National Aeronautics and Space Administration.

References

Abbott, P. L., and T. E. Smith, Sonora, Mexico, source for the Eocene Poway Conglomerate of southern California, *Geology*, 17, 329-332, 1989.

Adams, J. B., M. O. Smith, and P. E. Johnson, Spectral mixture modeling: A new analysis of rock and soil types at the Viking Lander 1 site, *J. Geophys. Res.*, 91, 8098-8112, 1986.

Aitchison, J., *The Statistical Analysis of Compositional Data*, Chapman and Hall, New York, 416 pp., 1986.

Allen, C. C., and J. L. Conca, 1991, Weathering of basaltic rocks under cold, arid conditions: Antarctica and Mars, *Proc. Lunar Planet. Sci. Conf.*, 21, 711-717, 1991.

Ash, R. D., S. F. Knott, and G. Turner, A 4-Gyr shock age for a Martian meteorite and implications for the cratering history of Mars, *Nature*, 380, 57-59.

Ashley, P. M., R. A. Duncan, and C. A. Freebrey, Ebor Volcano and Crescent Complex, Northeastern New South Wales - Age and geological development, *Australian J. Earth Sci.*, 42, 471-480, 1995.

Baird, A. K., and B. C. Clark, On the original igneous source of Martian fines, *Icarus*, 45, 113-123, 1981.

Bell, J. F. III, T. McCord, and P. Owensby, Observational evidence of crystalline iron oxides on Mars, *J. Geophys. Res.*, 95, 14,447-14,461, 1990.

Bell, J. F. III, R. V. Morris, and J. B. Adams, Thermally altered palagonitic tephra: A spectral and process analog to the soil and dust of Mars, *J. Geophys. Res.*, 98, 3373-3385, 1993.

Bell, J. F. III, M. Wolff, P. James, T. Clancy, S. Lee, and L. Martin, Mars surface mineralogy from Hubble Space Telescope imaging during 1994-1995: Observations, calibration, and initial results, *J. Geophys. Res.*, 102, 9109-9123, 1997.

Bell, J. F. III, H. Y. McSween, Jr., S. L. Murchie, J. R. Johson, R. Reid, R. V.

Morris, R. C. Anderson, J. L. Bishop, N. T. Bridges, D. T. Britt, J. A. Crisp, T. Economou, A. Ghosh, J. P. Greenwood, H. P. Gunnlaugsson, R. M. Hargraves, S. Hviid, J. M. Knudsen, M. B. Madsen, H. J. Moore, R. Rieder, and L. Soderblom, Mineralogic and compositional properties of Martian soil and dust: Preliminary results from Mars Pathfinder, *J. Geophys. Res.*, submitted, 1998.

Bhatia, M. R., Rare earth element geochemistry of Australian Paleozoic graywackes and mudrocks, *Sed. Geol.*, 45, 97-113, 1985.

Bishop, J., *Spectroscopic Analyses of Chemically Altered Montmorillonites and Applications to the Soils of Mars*, Ph.D. thesis, Brown University, 1995.

Bridges, N., R. A. Anderson, J. A. Crisp, T. Economou, and R. Reid, Separating dust and rock APXS measurements based on multispectral data at the Pathfinder landing site, *EOS*, 78, F402, 1997.

Britt, D. T., R. Anderson, J. F. Bell III, J. Crisp, T. Economou, K. E. Herkenhoff, M. B. Madsen, H. Y. McSween, S. Murchie, R. Reid, R. Rieder, R. B. Singer, and L. Soderblom, The mineralogy of the Mars Pathfinder landing site, *Lunar Planet. Sci.*, 29, 1776, 1998.

Burns, R., The fate of iron on Mars: Mechanism of oxidation of basaltic minerals to ferric-bearing assemblages, *Workshop on Chemical Weathering on Mars, Lunar Planet. Inst. Tech. Rept.*, 92-04, Part 1, 8-9, 1992.

Burns, R., Schwertmannite on Mars: Deposition of this ferric oxyhydroxysulfate mineral in acidic saline meltwaters, *Lunar Planet. Sci. XXV*, 203-204, 1994.

Campbell, I. H., and S. R. Taylor, No water, no granites - no oceans, no continents, *Geophys. Res. Lett.*, 10, 1061-1064, 1983.

Carmichael, I. S. E., The petrology of Thingmuli, a Tertiary volcano in eastern Iceland, *J. Petrol.*, 5, 435-460, 1964.

Carr, M. H., *The Surface of Mars*, Yale Univ., New Haven, 226 pp., 1981.

Carroll, M. R., and J. D. Webster, Solubilities of sulfur, noble gases, halogens, in *Volatiles in Magmas, Reviews in Mineralogy 30*, edited by M. R. Carroll and J. R. Holloway, pp. 232-279, Mineral. Soc. Am., Washington, 1994.

Casey, W. H., H. R. Westrich, J. F. Banfield, G. Ferruzzi, and G. W. Arnold, Leaching and reconstruction at the surfaces of dissolving chain-silicate minerals, *Nature*, 366, 253-256, 1993.

Cashman, K. V., and J. P. Kauahikaua, Reevaluation of vesicle distributions in basaltic lava flows, *Geology*, 25, 419-422, 1997.

Cattermole, P., Sequence, rheological properties, and effusion rates of volcanic

flows at Alba Patera, Mars, *J. Geophys. Res.*, 92, B4, E553-E560, 1987.

Christensen, P. R., The spatial distribution of rocks on Mars, *Icarus*, 68, 217-238, 1986.

Clark, B. C., A. K. Baird, R. J. Weldon, D. M. Tsusaki, L. Schnabel, and M. P. Candelaria, Chemical composition of Martian fines, *J. Geophys. Res.*, 87, B12, 10,059-10,067, 1982.

Cloutis, E. A., and M. J. Gaffey, Pyroxene spectroscopy revisited: Spectral-compositional correlations and relationship to geothermometry, *J. Geophys. Res.*, 96, E5, 22,809-22826, 1991.

Cloutis, E. A., M. J. Gaffey, D. G. W. Smith, and R. St. J. Lambert, Reflectance spectra of mafic silicate-opaque assemblages with applications to meteorite spectra, *Icarus*, 84, 315-333, 1990.

Crisp, J. A., The effect of thin coatings of dust or soil on the bulk APXS composition of the underlying rocks at the Pathfinder landing site, *Proc. Lunar Planet. Sci. Conf.*, 29, 1962, 1998.

Crisp, J., A. B. Kahle, and E. A. Abbott, Thermal infrared spectral character of Hawaiian basaltic glasses, *J. Geophys. Res.*, 95, B13, 21,657-21,669, 1990.

DePaolo, D. J., Trace element and isotopic effects of combined wall rock assimilation and fractional crystallization, *Earth Planet. Sci. Lett.*, 53, 189-202, 1981.

Dorn, R. I., and N. Meek, Rapid formation of rock varnish and other rock coatings on slag deposits near Fontana, California, *Earth Surf. Proc.*, 20, 547-560,1995.

Erard, S., J. Mustard, S. Murchie, M.-P. Bibring, P. Cerroni, and A. Corodine, Martian aerosols: Near-infrared spectral properties and effects on the observation of the surface, *Icarus*, 111, 317-337, 1994.

Evans, D. L., and J. B. Adams, Comparison of Viking Lander multispectral images and laboratory reflectance spectra of terrestrial samples, *Proc. Lunar Planet. Sci. Conf.*, 10, 1829-1834, 1979.

Farr, T. G., and J. B. Adams, Rock coatings in Hawaii, *Geol. Soc. Amer. Bull.*, 95, 1077-1083, 1984.

Fischer, E., and C. Pieters, The continuum slope of Mars: Bi-directional reflectance investigations and applications to Olympus Mons, *Icarus*, 102, 185-202, 1993.

Foden, J. D., and D. H. Green, Possible role of amphibole in the origin of andesite - some experimental and natural evidence, *Contrib. Mineral. Petrol.*, 109, 479-493, 1992.

Garvin, J. B., and J. J. Frawley, Martian impact crater morphometry: Preliminary results from the Mars Orbiter Laser Altimeter (MOLA) investigation, *Lunar Planet. Sci.*, 29, 1495.

Ghiorso, M. S., and R. O. Sack, Chemical mass transfer in magmatic proceses IV. A revised and internally consistent thermodynamic model for the interpolation and extrapolation of liquid-solid equilibria in magmatic systems at elevated temperatures and pressures, *Contrib. Mineral. Petrol.*, 119, 197-212.

Gill, J., *Orogenic Andesites and Plate Tectonics*, Springer-Verlag, Berlin, 390 pp., 1981.

Golombek, M. P., The Mars Pathfinder mission, *J. Geophys. Res.*, 102, 3953-3965, 1997.

Golombek, M. P., R. A. Cook, T. Economou, W. M. Folkner, A. F. C. Haldemann, P. H. Kallemeyn, J. M. Knudsen, R. M. Manning, H. J. Moore, T. J. Parker, R. Rieder, J. T. Schofield, P. H. Smith, and R. M. Vaughan, Overview of the Mars Pathfinder mission and assessment of landing site predictions, *Science*, 278, 1743-1748, 1997a.

Golombek, M. P., R. A. Cook, H. J. Moore, and T. J. Parker, Selection of the Mars Pathfinder landing site, *J. Geophys. Res.*, 102, E2, 3967-3988, 1997b.

Gooding, J., Chemical weathering on Mars: Thermodynamic stabilities of primary minerals (and their alteration products) from mafic igneous rocks, *Icarus*, 33, 483-513, 1978.

Greeley, R., and J. D. Iverson, *Wind as a Geological Process*, Cambridge University Press, Cambridge, 333 pp, 1985.

Greeley, R., E. Theilig, J. E. Guest, M. H. Carr, H. Masursky, and J. A. Cutts, Geology of Chryse Planitia, *J. Geophys. Res.*, 82, 4093-4109, 1977.

Greeley, R., R. N. Leach, S. H. Williams, B. R. White, J. B. Pollack, D. H. Krinsley, and J. R. Marshall, Rate of wind abrasion on Mars, *J. Geophys. Res.*, 87, 10,009-10,024, 1982.

Grove, T. L., and M. B. Baker, Phase equilibrium controls on the tholeiitic versus calc-alkaline differentiation trends, *J. Geophys. Res.*, 89, B5, 3253-3274, 1984.

Grove, T. L., and R. J. Kinzler, Petrogenesis of andesites, *Ann. Rev. Earth Planet. Sci.*, 14, 417-454, 1986.

Guinness, E. A., C. E. Leff, and R. E. Arvidson, Two Mars years of surface changes seen at the Viking landing sites, *J. Geophys. Res.*, 87, 10,051-10,058, 1982.

Guinness, E. A., R. E. Arvidson, M. A. Dale-Bannister, R. B. Singer, and E. A. Bruckenthal, On the spectral reflectance properties of materials exposed at the Viking landing sites, *J. Geophys. Res.*, 92, E575-E587, 1987.

Guinness, E. A., R. E. Arvidson, I. H. D. Clark, and M. K. Shepard, Optical scattering properties of terrestrial varished basalts compared with rocks and soils at the Viking Lander sites, *J. Geophys. Res.*, 102, E12, 28,687-28,703, 1997.

Hale, V. P. S., H. Y. McSween, Jr., and G. A. McKay, Cumulus pyroxene in Shergotty: The discrepancy between experimental and observational studies, *Lunar Planet. Sci.*, 28, 495-496, 1997.

Hanel, R., B. Conrath, W. Hovis, V. Kunde, P. Lowman, W. Maguire, J. Pearl, J. Pirranglia, C. Prabhakara, B. Schlachmann, G. Levin, P. Straat, and T. Burke, Investigation of the martian environment by infrared spectroscopy on Mariner 9, *Icarus*, 17, 423-442, 1972.

Harper, C. L., L. A. Nyquist, B. Bansal, H. Weismann, and C.-Y. Shih, Rapid accretion and early differentiation of Mars indicated by $^{142}Nd/^{144}Nd$ in SNC meteorites, *Nature*, 267, 213-217, 1995.

Harvey, R. P., and H. Y. McSween, Jr., The petrogenesis of the nakhlites: Evidence form cumulate mineral zoning, *Geochim. Cosmochim. Acta*, 56, 1655-1663, 1992.

Herron, M. M., Geochemical classification of terrigenous sands and shales from core or log data, *J. Sed. Petrol.*, 58, 820-829, 1988.

Hildreth, W., and S. Moorbath, Crustal contributions to arc magmatism in the Andes of central Chile, *Contrib. Mineral. Petrol.*, 98, 455-489, 1988.

Hodges, C. A., and H. J. Moore, *Atlas of Volcanic Landforms on Mars*, U. S. Geol. Surv. Prof. Paper 1534, U. S. Government Printing Office, Washington, DC, 194 pp., 1994.

Hon, K., J. Kauahikaua, R. Denlinger, and K. Mackay, Emplacement and inflation of pahoehoe sheet flows: Observations and measurements of active lava flows on Kilauea Volcano, Hawaii, *Geol. Soc. Am. Bull.*, 106, 351-370, 1994.

Hulme, G., The interpretation of rheological properties and effusion rate of an Olympus Mons lava, *Icarus*, 27, 207-213, 1976.

Hunt, G. R., J. W. Salisbury, and C. J. Lenhoff, Visible and near infrared spectra of minerals and rocks: IX. Basic and ultrabasic igneous rocks, *Modern Geol.*, 5, 15-22, 1974.

Hviid, S. F., M. B. Madsen, H. P. Gunnlaugsson, W. Goetz, J. M. Knudsen, R. B.

Hargraves, P. Smith, D. Britt, A. R. Dinesen, C. T. Morgensen, M. Olsen, C. T. Pedersen, and L. Vistisen, Magnetic properties experiments on the Mars Pathfinder lander: Preliminary results, *Science*, 278, 1768-1770, 1997.

Irvine, T. N., and W. R. A. Baragar, A guide to the chemical classification of the common volcanic rocks, *Can. J. Earth Sci.*, 8, 523-548, 1971.

Jambon, A., Earth degassing and large-scale geochemical cycling of volatile elements, in *Volatiles in Magmas, Reviews in Mineralogy 30*, edited by M. R. Carroll and J. R. Holloway, pp. 479-517, Mineral. Soc. Am., Washington, 1994.

Juster, T. C., T. L. Grove, and M. R. Perfit, Experimental constraints on the generation of FeTi basalts, andesites, and rhyodacites at the Galapagos Spreading Center, 85°W and 95°W, *J. Geophys. Res.*, 94, B7, 9251-9274, 1989.

King, T. V. V., and I. Ridley, Relation of the spectrscopic reflectance of olivine to mineral chemistry and some remote sensing applications, *J. Geophys. Res.*, 92, B11, 11,457, 1987.

Kortum, G., *Reflectance Spectroscopy*, Springer-Verlag, New York, 366 pp, 1969.

Le Bas, M. J., R. W. Le Maitre, A. Streckeisen, and B. Zanettin, A chemical classification of volcanic rocks based on the total alkali-silica diagram, *J. Petrol.*, 27, 745-750, 1986.

Lee, D.-C., and A. N. Halliday, Core formation on Mars and differentiated asteroids, *Nature*, 388, 854-857, 1997.

Lindsley, D. H., and D. J. Andersen, A two-pyroxene thermometer, *J. Geophys. Res.*, 88 Suppl., A887-A906, 1983.

Longhi, J., and V. Pan, The parent magas of the SNC meteorites, *Proc. Lunar Planet. Sci. Conf.*, 19, 695-709, 1989.

Longhi, J., E. Knittle, J. R. Holloway, and H. Wänke, The bulk composition, mineralogy and internal structure of Mars, in *Mars*, edited by H. H. Kieffer, B. M. Jakosky, C. W. Snyder, and M. S. Matthews, pp. 184-208, Univ. of Arizona Press, Tucson, 1992.

Lopes, R. M. C., and C. R. J. Kilburn, Emplacement of lava flow fields: Application of terrestrial studies to Alba Patera, Mars, *J. Geophys. Res.*, 95, B9, 14,383-14,397, 1990.

Malin, M., T. Parker, R. Greeley, R. Jaumann, U. Keller, R. Kirk, L. Matthies, M. Sims, L. Soderblom, C. Stoker, and R. Sullivan, Geology and geomorphology of the Pathfinder landing site, *EOS*, 78, F395, 1997.

Mars Pathfinder, Foldout plates, *Science*, 278, 1734-1742, 1997.

McCauley, J. F., C. S. Breed, F. El-Baz, M. I. Whitney, and M. J. Grolier, Pitted and fluted rocks in the western desert of Egypt: Viking comparisons, *J. Geophys. Res.*, 84, 8222-8232, 1979.

McCoy, T. J., G. J. Taylor, and K. Keil, Zagami: Product of a two-stage magmatic history, *Geochim. Cosmochim. Acta*, 56, 3571-3582, 1992.

McFadden, L. A., Spectral reflectance of SNC meteorites: Relationships to Martian surface composition, *Lunar Planet. Inst. Tech. Rept.*, 88-05, 88-90, 1987.

McGetchin, T. R., M. Settle, and J. W. Head, Radial thickness variation in impact crater ejecta: Implications for lunar basin deposits, *Earth Planet. Sci. Lett.*, 20, 226-236, 1973.

McSween, H. Y. Jr., What we have learned about Mars from SNC meteorites, *Meteoritics*, 29, 757-779, 1994.

McSween, H. Y. Jr. and E. Jarosewich, Petrogenesis of the Elephant Moraine A79001 meteorite: Multiple magma pulses on the shergottite parent body, *Geochim. Cosmochim. Acta*, 47, 1501-15113, 1983.

McSween, H. Y. Jr. D. D. Eisenhour, L. A. Taylor, M. Wadhwa, and G. Crozaz, QUE94201 shergottite: Crystallization of a Martian basaltic magma, *Geochim. Cosmochim. Acta*, 60, 4563-4569, 1997.

Moore, H. J., C. A. Hodges, and D. H. Scott, Multiringed basins - illustrated by Orientale and associated features, *Proc. 5th Lunar Sci. Conf., Geochim. Cosmochim. Acta*, suppl. 1, 71-100, 1974.

Moore, H. J., D. W. G. Arthur, and G. G. Schaber, Yield strengths of flows on the Earth, Mars, and Moon, *Proc. 9th Lunar Planet. Sci. Conf.*, 3351-3378, 1978.

Morris, R. V., and H. V. Lauer, Jr., Matrix effects for reflectivity spectra of dispersed nanophase (superparamagnetic) hematite with application to martian spectral data, *J. Geophys. Res.*, 95, 5101-5109, 1990.

Morris, R., H. Lauer, C. Lawson, E. Gibson, G. Nace, and C. Stewart, Spectral and other physiochemical properties of submicron powders of hematite (α-Fe_2O_3), maghemite (γ-Fe_2O_3), magnetite (Fe_3O_4), goethite (α-FeOOH), and lepidocroicite (γ-FeOOH), *J. Geophys. Res.*, 90, 3126-3144, 1985.

Morris, R. V., J. J. Gooding, H. V. Lauer, Jr., and R. B. Singer, Origins of Marslike spectral and magnetic properties of a Hawaiian palagonitic soil, *J. Geophys. Res.*, 95, 14,427-14,434, 1990.

Morris, R. V., D. C. Golden, J. F. Bell III, H. V. Lauer, Jr., and J. B. Adams,

Pigmenting agents in martian soils: Inferences from spectral, Mössbauer, and magnetic properties of nanophase and other iron oxides in Hawaiian palagonitic soil PN-9, *Geochim. Cosmochim. Acta*, 57, 4597-4609, 1993.

Morris, R. V., D. C. Golden, J. F. Bell III, and H. V. Lauer, Jr., Hematite, pyroxene, and phyllosilcates on Mars: Implications from oxidized impact melt rocks from Manicouagan Crater, Quebec, Canada, *J. Geophys. Res.*, 100, 5319-5328, 1995.

Morris, R. V., D. C. Golden, J. F. Bell III, T. D. Shelfer, S. Mertzmann, D. W. Ming, J. Bishop, C. C. Allen, and D. L. Britt, Possible hydrolytic, hydrochloric, and sulfuric weathering products at the Mars Pathfinder landing site: Evidencefrom multispectral, elemental, and magnetic data on analog samples, *J. Geophys. Res.*, this volume.

Mustard, J. F., and J. F. Bell III, New composite reflectance spectra of Mars from 0.4 to 3.14 μm, *Geophys. Res. Lett.*, 21, 353-356, 1994.

Mustard, J. F., and J. E. Hays, Effects of hyperfine particles on reflectance spectra from 0.3 to 25 micrometers, *Icarus*, 125, 145-163, 1997.

Mustard, J. F., and J. M. Sunshine, Seeing through the dust: Martian crustal heterogeneity and links to the SNC meteorites, *Science*, 267, 1623-1626, 1995.

Mustard, J. F., S. Erard, M.-P. Bibring, J. W. Head, S. Hurtrez, Y. Langevin, C. M. Pieters, and C. J. Sotin, The surface of Syrtis Major: Composition of the volcanic substrate and mixing with altered dust and soil, *J. Geophys. Res.*, 98, E2, 3387-3400, 1993.

Mustard, J. F., S. Murchie, S. Erard, and J. M. Sunshine, In situ compositions of Martian volcanics: Implications for the mantle, *J. Geophys. Res.*, 102, E11, 25,605-25,615, 1997.

Mysen, B. O., I. Kushiro, I. A. Nicholls, and A. E. Ringwood, A possible mantle origin for andesite magmas: Discussion and replies, *Earth Planet. Sci. Lett.*, 21, 221-229, 1974.

Nicholls, I. A., and A. E. Ringwood, Effects of water on olivine stability in tholeiite and the production of silica-saturated magas in the island-arc environment, *J. Geol.*, 81, 285-300, 1973.

Parker, T. J., "Super resolution" of the Mars Pathfinder landing site, using manual techniques, *Lunar Planet. Sci.*, 29, 1817, 1998.

Parker, T. J., and J. W. Rice, Jr., Sedimentary geomorphology of the Mars Pathfinder landing site, *J. Geophys. Res.*, 102, E11, 25,641-25,656, 1997.

Reid, R. J., A. Dummel, R. B. Singer, J. R. Johnson, J. F. Bell III, and T. Daley, Imager for Mars Pathfinder calibration, *EOS*, 78, F402, 1997.

Rieder, R., T. Economou, H. Wänke, A. Turkevich, J. Crisp, J. Brückner, G. Dreibus, and H. Y. McSween, Jr., The chemical composition of Martian soil and rocks returned by the mobile alpha proton X-ray spectrometer: Preliminary results from the X-ray mode, *Science*, 278, 1771-1774, 1997a.

Rieder, R., H. Wänke, T. Economou, and A. Turkevich, Determination of the chemical composition of Martian soil and rocks: The alpha proton X-ray spectrometer, *J. Geophys. Res.*, 102, E2, 4027-4044, 1997b.

Rotto, S., and K. L. Tanaka, Geologic/geomorphic map of the Chryse Planitia region of Mars, *U. S. Geol. Surv. Misc. Invest. Series, Map I-2441*, 1995.

Rover Team, Characterization of the Martian surface deposits by the Mars Pathfinder Rover, Sojourner, *Science*, 278, 1765-1768, 1997.

Rutherford, M. J., and P. C. Hess, Granite genesis: Processes and variables for Mars, *Lunar Planet. Sci.*, 12, 915-917, 1981.

Schultz, P. H., and J. F. Mustard, Martain impact glass: Generation and evidence, *Lunar Planet. Sci.*, 29, 1847, 1998.

Self, S., T. Thordarson, and L. Keszthelyi, Emplacement of continental flood basalt lava flows, in *AGU Geophysical Series Monograph on Large Igneous Provinces: Continental, Oceanic, and Planetary Flood Volcanism*, edited by J J. Mahoney and M. F. Coffin, pp. 381-410, 1997.

Sharp, R. P., and M. C. Malin, Surface geology from Viking landers on Mars: A second look, *Geol. Soc. Am. Bull.*, 95, 1398-1412, 1984.

Shaw, H. R., Viscosities of magmatic silicate liquids - an empirical method of prediction, *Amer. J. Sci.*, 272, 870-893, 1972.

Shelfer, T. D., and R. V. Morris, Effect of a ferric weathering rind on the optical and Mössbauer spectra of a basaltic rock, *Lunar Planet. Sci. XXIX*, in press.

Sherman, D., R. Burns, and V. Burns, Spectral characteristics of the iron oxides with application to the Martian bright region mineralogy, *J. Geophys. Res.*, 87, 10,169-10,180, 1982.

Singer, R. B., The dark materials on Mars: I. New information from reflectance spectroscopy on the extent and mode of oxidation, *Lunar Planet. Sci. Conf.*,11, 1045-1047, 1980.

Singer, R. B., Spectral evidence for the mineralogy of high-albedo soils and dust on Mars, *J. Geophys. Res.*, 87, 10,159-10,168, 1982.

Singer, R. B., and T. B. McCord, Large scale mixing of bright and dark materials and implications for analysis of spectral reflectance, *Proc. Lunar Planet. Sci. Conf.*, 20, 1835-1848, 1979.

Singer, R. B., and H. Y. McSween, Jr., The igneous crust of Mars: Compositional evidence from remote sensing and the SNC meteorites, in *Resources of Near-Earth Space*, edited by J. Lewis, M. S. Matthews, and M. L. Guerrieri, pp. 709-736, Univ. of Arizona Press, Tucson, 1993.

Singer, R. B., and T. Roush, Spectral reflectance properties of particulate weathered coatings on rocks: Laboratory modeling and applicability to Mars, *Lunar Planet. Sci. XIV*, 708-709, 1983.

Sisson, T. W., and T. L. Grove, Experimental investigations of the role of H_2O in calc-alkaline differentiation and subduction zone magmatism, *Contrib. Mineral. Petrol.*, 113, 143-166, 1993.

Smith, P. H., J. F. Bell III, N. T. Bridges, D. T. Britt, L. Gaddis, R. Greeley, H. U. Keller, K. E. Herkenhoff, R. Jaumann, J. R. Johnson, R. L. Kirk, M. Lemmon, J. N. Maki, M. C. Malin, S. L. Murchie, J. Oberst, T. J. Parker, R. J. Reid, R. Sablotny, L. A. Soderblom, C. Stoker, R. Sullivan, N. Thomas, M. G. Tomasko, W. Ward, E. Wegryn, Results from the Mars Pathfinder camera, *Science*, 278, 1758-1765, 1997a.

Smith, P. H., M. G. Tomasko, D. Britt, D. G. Crowe, R. Reid, H. U. Keller, N. Thomas, F. Gliem, P. Rueffer, R. Sullivan, R. Greeley, J. M. Knudsen, M. B. Madsen, H. P. Gunnlaugsson, S. F. Hviid, W. Goetz, L. A. Soderblom, L. Gaddis, and R. Kirk, The imager for Mars Pathfinder experiment, *J. Geophys. Res.*, 102, E2, 4003-4025, 1997b.

Soderblom, L. A., The composition and mineralogy of the Martian surface from spectroscopic observations: 0.3 μm to 50 μm, in *Mars*, edited by H. H. Kieffer, B. M. Jakosky, C. W. Snyder, and M. S. Matthews, pp. 557-597, Univ. of Arizona Press, Tucson, 1992.

Stöffler, D., R. Ostertag, C. Jammes, G. Pfannschmidt, P. R. Sen Gupta, S. B. Simon, J. J. Papike, and R. H. Beauchamp, Shock metamorphism and petrography of the Shergotty achondrite, *Geochim. Cosmochim. Acta*, 50, 889-913, 1986.

Sunshine, J. M., L. A. McFadden, and C. M. Pieters, Reflectance spectra of the Elephant Moraine A79001 meteorites: Implications for remote sensing of planetary bodies, *Icarus*, 105, 79-91, 1993.

Tanaka, K. L., Sedimentary history and mass flow structures of Chryse and

Acidalia Planitiae, Mars, *J. Geophys. Res.*, xx, 4131-4149, 1997.

Thordarson, T., and S. Self, Sulfur, chlorine, and fluorine degassing and atmospheric loading by the Roza eruption, Columbia River Basalt Group, Washington, USA, *J. Volcanol. Geotherm. Res.*, 74, 49-73, 1996.

Toramaru, A., A. Ishiwatari, M. Matsuzawa, N. Nakamura, and S. Arai, Vesicle layering in solidified intrusive magma bodies: A newly recognized type of igneous structure, *Bull. Volcanol.*, 58, 393-400, 1996.

Treiman, A. H., The parent magma of the Nakhla (SNC) meteorite, inferred from magmatic inclusions, *Geochim. Cosmochim. Acta*, 57, 4753-4767, 1993.

Treiman, A. H., A petrographic history of Martian meteorite ALH84001: Two shocks and an ancient age, *Meteoritics*, 30, 294-302.

Wänke, H., and G. Dreibus, Chemical composition and accretional history of terrestrial planets, *Phil. Trans. Roy. Soc. London*, A235, 545-557, 1988.

Warren, P. H., P. Claeys, and E. Cedillo-Pardo, Mega-impact melt petrology (Chicxulub, Sudbury, and the Moon): Effects of scale and other factors on potential for fractional crystallization and development of cumulates, *Geol. Soc. Amer. Spec. Paper*, 307, 105-124, 1996.

Warren, P. H., and G. W. Kallemeyn, Yamato-793605, EET79001, and other presumed Martian meteorites: Compositional clues to their origins, *Antarctic Meteorite Research*, 10, 61-81, 1997.

Wendlandt, W. W., and H. G. Hecht, *Reflectance Spectroscopy*, Interscience Pub., New York, 298 pp, 1966.

Whitney, M. I., and R. V. Dietrich, Ventifact sculpture by windblown dust, *Geol. Soc. Am. Bull.*, 84, 2561-2582, 1973.

Yang, H.-J., R. J. Kinzler, and T. L. Grove, Experiments and models of anhydrous, basaltic olivine-plagioclase-augite saturated melts from 0.001 to 10 kbar, *Contrib. Mineral. Petrol.*, 124, 1-18, 1996.

Zimbelman, J. R., Estimates of rheological properties for flows on the Martian volcano Ascraeus Mons, *J. Geophys. Res.*, 90 suppl., D157-D162, 1985.

Figure Captions

Figure 1. Sketch map of the Pathfinder landing site showing the approximate locations of rocks and other features described or referenced in the text. Eight rocks which were analyzed by the APXS are colored black, and six soil APXS analysis sites are indicated by small boxes. APXS chemical analysis numbers are also given. Off the map in the direction indicated by the arrow are Bakers Bench and Seal, which are 8 and 37.5 m from the center of the lander, respectively. The rover traverse, spanning 105 m, is also illustrated; fine lines connecting some traverse segments indicate repositioning of the rover's internal guidance system based on end-of-day IMP images.

Figure 2. Rover camera image mosaic of Stimpy (25 cm tall), with pits 1-3 cm in diameter. Mosaic is composed of the image frames with these Planetary Data System PRODUCT IDs:
RVR_EDR-1252885649-S070104-LEFT,
RVR_EDR-1252886142-S070105-LEFT, and
RVR_EDR-1252886657-S070106-LEFT.

Figure 3. Monochrome rover camera image of Squash (11 cm tall). The lobe on left side of the rock juts out ~12 cm. Mosaic is composed of two image frames:
RVR_EDR-1249070145-N027093-RIGHT and
RVR_EDR-1249070974-N027094-RIGHT.

Figure 4. Stereo image of Chimp (39 cm tall) produced by combining two right-eye mosaics (two frames mosaiced together for the red, and two for the cyan), taken before and after commanding the rover to rotate 18^{o} in place, while 25 cm away from Chimp. The frame showing more of the left side of Chimp was assigned to the red color plane of the anaglyph and the other frame assigned to the green and blue color planes (cyan), to produce a stereo anaglyph. This image can be viewed in 3-D by wearing red-blue glasses. The texture in the upper left resembles exfoliation. Prominent banding is roughly horizontal around the lower 2/3 of the rock, wrapping around the rounded nose closest to the camera, and continues around the left side of the rock. These image frames were converted to linear coordinates before combining them into the anaglyph image:
RVR_EDR-1253231644-S074032-RIGHT,
RVR_EDR-1253232878-S074033-RIGHT,
RVR_EDR-1253233245-S074044-RIGHT, and

RVR_EDR-1253233615-S074045-RIGHT.

Figure 5. Super-resolution IMP image of Wedge (30 cm tall), produced by combining 25 red-filter left-eye frames. The individual frames were enlarged by 1000%, sharpened, manually co-registered at 1/10 pixel scale, and then co-added, giving equal weight to each frame. This produces, in effect, a super-resolution image that is sharper than any individual frame. Soil or dust appears to be plastered upon the rock face, more heavily on the left side of the rock than the right. Image frames used as input:
IMP_EDR-1248443296-REGULAR-0199020004,
IMP_EDR-1248443332-REGULAR-0199020008,
IMP_EDR-1248443380-REGULAR-0199020012,
IMP_EDR-1248443428-REGULAR-0199020016,
IMP_EDR-1248443476-REGULAR-0199020020,
IMP_EDR-1248443525-REGULAR-0199020024,
IMP_EDR-1248443573-REGULAR-0199020028,
IMP_EDR-1248443621-REGULAR-0199020032,
IMP_EDR-1248443669-REGULAR-0199020036,
IMP_EDR-1248443717-REGULAR-0199020040,
IMP_EDR-1248443765-REGULAR-0199020044,
IMP_EDR-1248443812-REGULAR-0199020048,
IMP_EDR-1248443860-REGULAR-0199020052,
IMP_EDR-1248443908-REGULAR-0199020056,
IMP_EDR-1248443957-REGULAR-0199020060,
IMP_EDR-1248444004-REGULAR-0199020064,
IMP_EDR-1248444052-REGULAR-0199020068,
IMP_EDR-1248444100-REGULAR-0199020072,
IMP_EDR-1248444148-REGULAR-0199020076,
IMP_EDR-1248444196-REGULAR-0199020080,
IMP_EDR-1248444244-REGULAR-0199020084,
IMP_EDR-1248444292-REGULAR-0199020088,
IMP_EDR-1248444340-REGULAR-0199020092,
IMP_EDR-1248444388-REGULAR-0199020096, and
IMP_EDR-1248444436-REGULAR-0199020100.

Figure 6. Super-resolution stereo image (see caption for Figure 5) of Barnacle Bill (22 cm tall), produced by combining 7 right-eye frames and 8 left-eye frames from the "super panorama" taken by the IMP camera. The left-eye super-resolution image was assigned to the red color plane of the analglyph and the right-eye image to the green and blue planes (cyan), to produce a stereo analglyph. Two

sets of images were processed in this manner and mosaiced to cover the full extent of the rock. The pits on Barnacle Bill are 0.25 to 1 cm in diameter. Dark notches or tiny ledges on the left side of the rock constitute one subtle set of lineations. Other sets of very faint lineations are oriented at 45° clockwise from vertical on the top middle and top right of the rock and at 140° clockwise from vertical on the front and upper left rock faces. These image frames were used as input:
IMP_EDR-1248281345-REGULAR-0182010120,
IMP_EDR-1248281345-REGULAR-0182010121,
IMP_EDR-1248281367-REGULAR-0182010122,
IMP_EDR-1248281367-REGULAR-0182010123,
IMP_EDR-1248281393-REGULAR-0182010124,
IMP_EDR-1248281393-REGULAR-0182010125,
IMP_EDR-1248281454-REGULAR-0182010126,
IMP_EDR-1248281454-REGULAR-0182010127,
IMP_EDR-1248281504-REGULAR-0182010128,
IMP_EDR-1248281504-REGULAR-0182010129,
IMP_EDR-1248281554-REGULAR-0182010130,
IMP_EDR-1248281554-REGULAR-0182010131,
IMP_EDR-1248281607-REGULAR-0182010132,
IMP_EDR-1248281607-REGULAR-0182010133,
IMP_EDR-1248281660-REGULAR-0182010134,
IMP_EDR-1248281694-REGULAR-0182010136,
IMP_EDR-1248281694-REGULAR-0182010137,
IMP_EDR-1248281716-REGULAR-0182010138,
IMP_EDR-1248281716-REGULAR-0182010139,
IMP_EDR-1248281734-REGULAR-0182010140,
IMP_EDR-1248281734-REGULAR-0182010141,
IMP_EDR-1248281757-REGULAR-0182010142,
IMP_EDR-1248281757-REGULAR-0182010143,
IMP_EDR-1248281797-REGULAR-0182010144,
IMP_EDR-1248281797-REGULAR-0182010145,
IMP_EDR-1248281848-REGULAR-0182010146,
IMP_EDR-1248281848-REGULAR-0182010147,
IMP_EDR-1248281903-REGULAR-0182010148,
IMP_EDR-1248281903-REGULAR-0182010149, and
IMP_EDR-1248281962-REGULAR-0182010150.

Figure 7. Monochrome rover camera image of Prince Charming (lower right, 20 cm wide), Shark (upper left, 47 cm tall), and Half Dome (upper right, 51 cm tall). The shiny rounded pebble in the soil to the left of Prince Charming is 3 cm in diameter. Prince Charming has a bumpy texture with 0.5-3 cm size hollows (dark tops and bright bases) and 0.5 cm protrusions (bright tops and dark bases). Shark's surface has a similar bumpy texture. Mosaic is composed of six image frames:
RVR_EDR-1252969487-S071070-LEFT,
RVR_EDR-1252969661-S071071-LEFT,
RVR_EDR-1252969833-S071072-LEFT,
RVR_EDR-1252970002-S071073-LEFT,
RVR_EDR-1252970175-S071074-LEFT, and
RVR_EDR-1252970356-S071075-LEFT.

Figure 8. IMP spectrum of brown soil near the rock Mint Julep, showing the principal parameters used to characterize reflectance spectra of rocks and associated soils.

Figure 9. Laboratory spectra of typical ferric minerals which are found in SNC meteorites or may be expected thermodynamically at the Martian surface, resampled into the bandpasses of IMP. Note that hematite, maghemite, and ferrihydrite (all solid lines) exhibit the observed inflection in the three channels used to calculate the 530 nm "kink."

Figure 10. Four renditions of color properties of a portion of the quadrant northeast from the lander. Note the variability of the spectral character of downwind rock faces. (*a*) Contrast-enhanced visible color, constructed from 440, 530 and 670 nm image mosaics. Colored arrows show examples of gray rocks (blue arrows), red rocks (bright red arrows), pink rocks (pink arrows), and maroon rocks (dark red arrows). Representative drift is shown with a white arrow for comparison. (*b*) Red/blue (670/440 nm) color ratio, shown in false color where redder hues represent higher red/blue ratios, overlain on 670 nm reflectance. (*c*) Depth of the 530 nm kink, shown in false color where redder hues represent a stronger absorption, overlain on 670 nm reflectance. (*d*) 440 nm reflectance in units of R^*. Note the blandness of the scene, save for atypically dark large boulders (dark red arrows) and atypically bright, tabular, rock-like masses in the foreground (pink arrows).

Figure 11. Spectral heterogeneity not related to wind direction. (a) Little Flat Top, a tabular boulder in the Rock Garden. Arrows denote the brightening and reddening of the upper surface due to accumulated drift, and the redder band along the lowermost several centimeters of the front face. (b) Ginger, a 15-cm cobble southeast of the lander. (c) Boris, a 20-cm cobble southeast of the lander.

Figure 12. Representative spectra of the three major rock spectral classes (gray, red, pink) at the Pathfinder landing site. (a) Reflectance in units of R^*. (b) Ratioed to an average of typical drifts at the site ("mean bright red drift"), highlighting spectral differences.

Figure 13. Representative spectra of maroon rocks at the Pathfinder landing site, compared with pink rock. (a) Reflectance in units of R^*. (b) Ratioed to an average of typical drifts at the site, highlighting spectral differences.

Figure 14. Comparison of spectra of subtly distinct drift materials. Bright red drift (solid lines) has its reflectance peak at 750 nm and lacks an obvious infrared absorption. Brown soil has a peak at 800 nm and exhibits a weak infrared absorption centered near 900 nm.

Figure 15. Comparison of parameterized spectral properties of the four spectral classes of rocks, bright red drift, and brown soil. (*a*) Red/blue (670/440 nm) ratio and depth of the 530 nm absorption, or kink. The close correlation shows that the reddening phase or phases exhibits this feature, which is characteristic of a subset of ferric minerals including hematite, maghemite, and ferrihydrite. (*b*) Red (670 nm) reflectance and red/blue ratio. Two trends are evident in the data: "primary trend" gray, red, and pink rocks, and a "secondary trend" consisting of maroon rocks and brown soils. (*c*) Strengths of the 530 and 900 nm absorptions. In primary trend rocks, calculated absorption strengths are inversely related, whereas in secondary trend rocks and in drift the strength of the 900 nm absorption varies without a corresponding change in strength of the kink. Secondary trend rocks and soils further from the intersection of the two trends exhibit a reflectance maximum at 800 nm. (*d*) Red/blue ratio and strength of the 900 nm absorption. The primary and secondary spectral trends appear as in (c). The linear fit of the two variables for primary trend rocks is shown, and boundaries of unit classifications in Figure 16 are indicated.

Figure 16. Association of the primary and secondary spectral trends with different rock and soil environments in the quadrant northwest of the lander, containing Yogi and several other large, round boulders. (*a*) Contrast-enhanced visible color, constructed from 440, 530 and 670 nm image mosaics. Red arrows show the largest boulders partly or completely covered with maroon surfaces. (*b*) False color representation of depth of the "residual" 900 nm absorption. For the primary spectral trend, a linear fit between red/blue and 900 nm band depth was determined. Using this relationship, a "predicted" band depth was calculated for the red/blue ratio of each pixel, and subtracted from the observed 900 nm band depth. Low residuals are shown in bluer hues, and the highest residuals in redder hues. Materials on the primary spectral trend appear in shades of blue and green, and materials on the secondary spectral trend in shades of red. The image base is 670 nm reflectance. (*c*) Red/blue (670/440 nm) color ratio, shown in false color where redder hues represent higher red/blue ratios, overlain on 670 nm reflectance. (d) Spectral groupings of rocks and spectrally similar soils, derived by thresholding red/blue ratio as in Table 2. Pink rocks and bright red drift were separated from maroon rocks and associated brown soils based on the latter's residual 900 nm band depth of _0.5%. Gray rocks are colored in blue, red rocks in yellow, pink rocks and bright red drift in gray, and maroon rocks and brown soils in red.

Figure 17. Spectral similarities of primary trend rocks with ferric-coated dark substrates. Both plots show type locations of gray, red, and pink rocks ratioed to bright red drift, and measured or modeled ferric coatings ratioed to uncompacted ferric powder. (a) Variations in thickness of a ferric coating on a dark substrate. (b) Variations in areal coverage by an optically thick ferric coating on a dark substrate.

Figure 18. Most oxide abundances in Pathfinder rocks form approximately linear arrays when plotted against sulfur, with Pathfinder soils plotting consistently at one end of the array. Lines represent linear regressions for the rock data only. All Pathfinder data are normalized to 98% total oxides and Viking XRF soil analyses [*Clark et al.*, 1982] have been normalized to 95.4% oxides (see text).

Figure 19. Additional plots of oxides versus sulfur, illustrating how extrapolation of linear regression lines to zero sulfur gives the composition of the sulfur-free (presumably igneous) rock. Viking soil analyses [*Clark et al.*, 1982] are normalized as described in the text.

Figure 20. C.I.P.W. normative composition of the Pathfinder sulfur-free rock, compared to those of common terrestrial volcanic rocks, adapted from *Irvine and Baragar* [1971] (all norms in these plots are in molecular %, rather than weight % as given in Table 3). (a) Normative feldspar compositions, and (b) normative color index (hypersthene + diopside + magnetite + ilmenite) versus normative plagioclase composition (anorthite/(anorthite + albite). The normative composition of average Pathfinder soil [*Bell et al.*, 1998] is shown for comparison.

Figure 21. Chemical classification of volcanic rocks, after *Le Bas et al.* [1986]. The sulfur-free rock plots within the field of andesite. Shergottites (shown as filled squares), commonly thought to be Martian igneous rocks, fall within the basalt field.

Figure 22. IMP images of the APXS deployed on rocks at the Pathfinder landing site. APXS analysis numbers are keyed to rock names in Figure 1.

Figure 23. Comparison of the SO_3 contents in APXS rock analyses with the red (750 nm)/blue (440 nm) ratios of their spectra. The long regression line was calculated for all data (rocks and soils), whereas the short regression line was determined for rocks only. Rocks with higher sulfur have high red/blue ratios, supporting the conclusion that the rock compositions define a mixing line between a rock end member and adhering dust or soil.

Figure 24. Proposed stratigraphy of spectral heterogeneities on rocks at the Pathfinder landing site.

Figure 25. Pyroxene quadrilateral (En = $MgSiO_3$, Fs = $FeSiO_3$, Wo = $CaSiO_3$), illustrating the analyzed compositions of zoned augite (open squares) in the Nakhla meteorite [*Harvey and McSween*, 1992], pigeonite (filled circles) and augite (filled squares) in the Shergotty meteorite [*Stöffler et al.*, 1986], and calculated compositions of normative diopside and hypersthene in the Pathfinder sulfur-free rock (Table 3). Contours of the "1 μm" band minima for pyroxenes of various compositions are taken from *Cloutis and Gaffey* [1991]. Pyroxene band positions for bulk Nakhla and basaltic shergottites (Shergotty and EETA79001B) are illustrated by shaded boxes) [*McFadden*, 1987; *Sunshine et al.*, 1993]. The downward slope of the contours toward the Fs side of the quadrilaterial suggests that the absorp-

tion band for the iron-rich pyroxenes in the sulfur-free rock might occur at a wavelenth >1000 nm, possibly accounting for its absence in IMP spectra. Alternatively, a high proportion of calcium-rich pyroxene, as in Nakhla, and breakdown of metastable iron-rich pigeonite into fayalite plus silica, would also push the absorption band minimum past the IMP spectral range.

Figure 26. Comparison of tholeiitic and calc-alkaline differentiation trends that lead to andesites, adapted from *Gill* [1981]. The calculated sulfur-free rock and the compositions of Pathfinder rocks fall within the tholeiite field. Orogenic suites are from volcanoes in Tonga, New Britain, and El Salvador (tholeiitic), and in New Britain, New Zealand, and Chile (calc-alkaline); anorogenic icelandites are from Iceland. Also illustrated are the compositions of SNC meteorite melts: intercumulus liquids in basaltic shergottites [EETA79001, *Longhi and Pan*, 1989; Zagami, *McCoy et al.*, 1992; Shergotty, *Hale et al.*, 1997], Chassigny [*Longhi and Pan*, 1989], and Nakhla [*Longhi and Pan*, 1989; *Treiman*, 1993], as well as the bulk composition for the QUE94201 shergottite [*Warren and Kallemeyn*, 1997] which, unlike other SNC meteorites, is thought to represent a liquid composition [*McSween et al.*, 1997].

Figure 27. AFM diagram comparing tholeiitic and calc-alkaline differentiation trends, adapted from *Grove and Kinzler* [1986]. The sulfur-free rock composition, Pathfinder rock analyses, and SNC melts (sources given in caption for Figure 26) plot within the tholeiitic field. Orogenic suites are from volcanoes in the Lesser Antilles and California, and icelandite suites are from Iceland and the Galapagos Spreading Center.

Figure 28. Chemical variations in fractionated lavas from the Galapagos Spreading Center at 85°W and the experimentally determined Galapagos liquid line of descent [*Juster et al.*, 1989] are compared with the Pathfinder sulfur-free rock composition. The Pathfinder rock is a close match to highly evolved icelandite members of this MORB differentiation sequence, except for its lower TiO_2 abundance. Also illustrated are the intercumulus liquid composition for Shergotty [*Hale et al.*, 1997] and the bulk composition of the QUE94201 shergottite [*Warren and Kallemeyn*, 1997], as well as their calculated liquid lines of descent. Fractionation of basaltic shergottite magma at shallow depths apparently cannot generate a melt having the Pathfinder andesite composition.

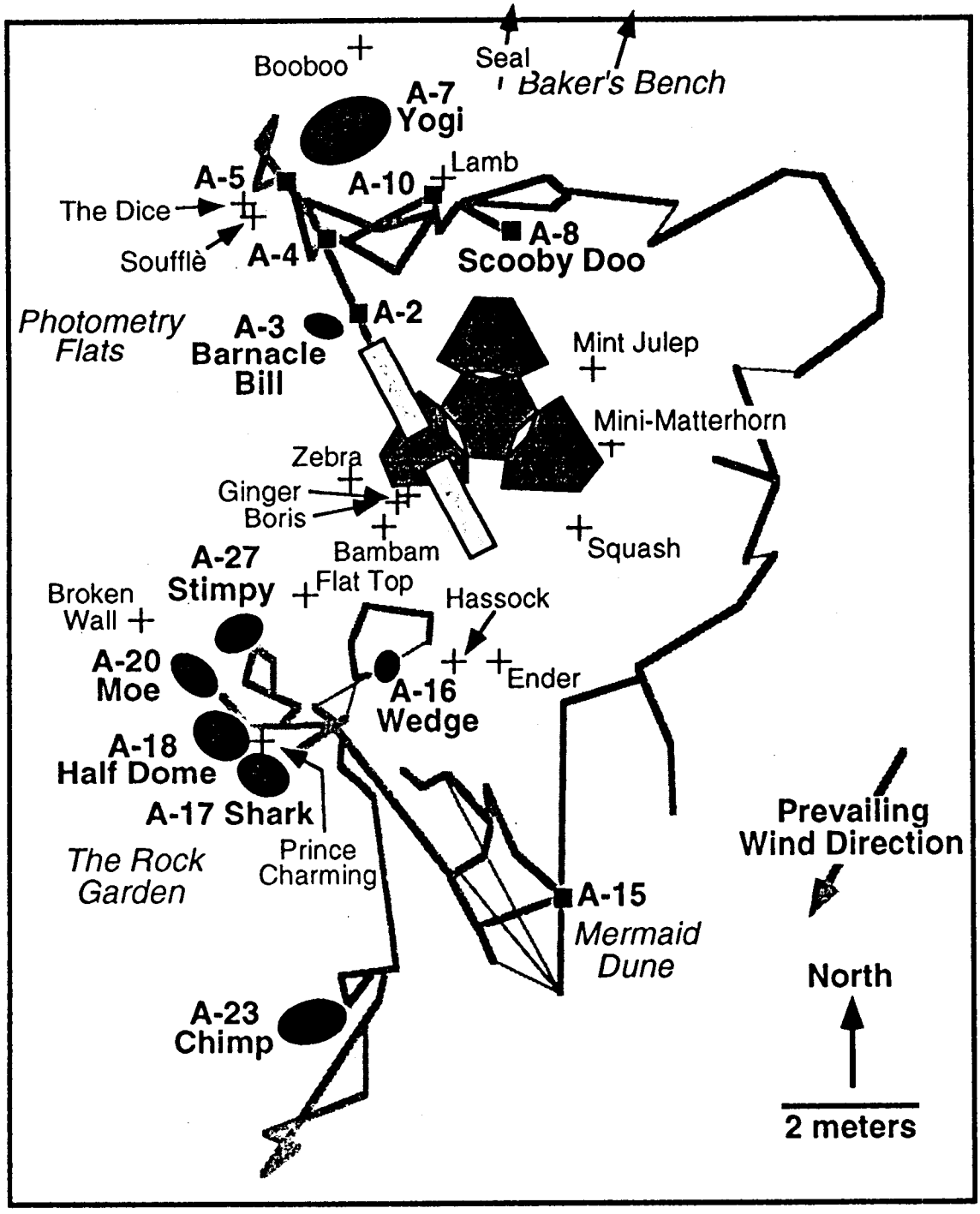
Booboo
Seal
Baker's Bench
A-7
Yogi
A-5
A-10
Lamb
The Dice
Soufflè
A-4
A-8
Scooby Doo
Photometry
Flats
A-3
Barnacle
Bill
A-2
Mint Julep
Mini-Matterhorn
Zebra
Ginger
Boris
Bambam
Squash
A-27
Stimpy
Flat Top
Broken
Wall
Hassock
A-20
Moe
A-16
Wedge
Ender
A-18
Half Dome
A-17 Shark
The Rock
Garden
Prince
Charming
A-15
Mermaid
Dune
Prevailing
Wind Direction
North
A-23
Chimp
2 meters

MRPS 86410

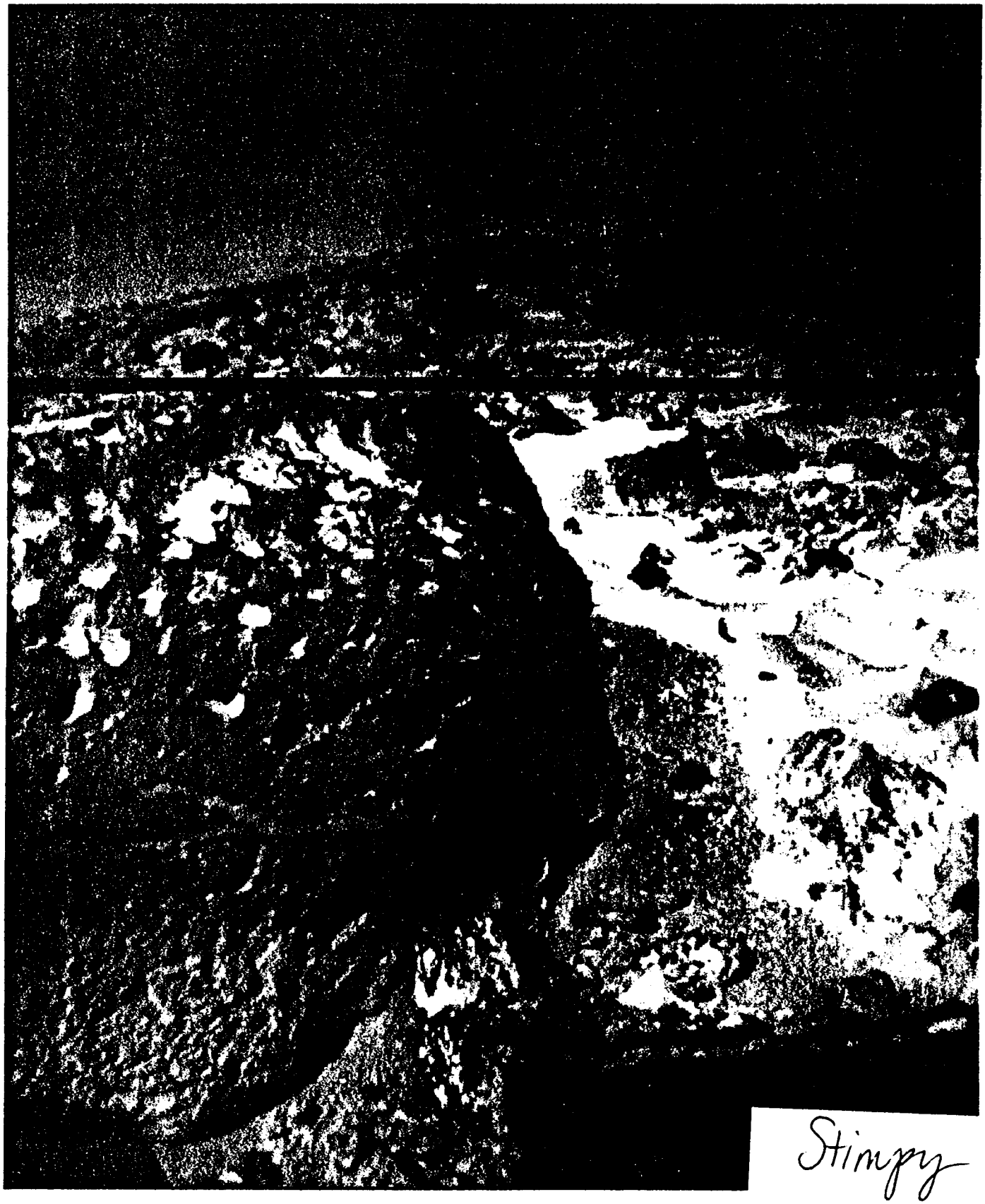

Stimpy

2

MRPS 80411

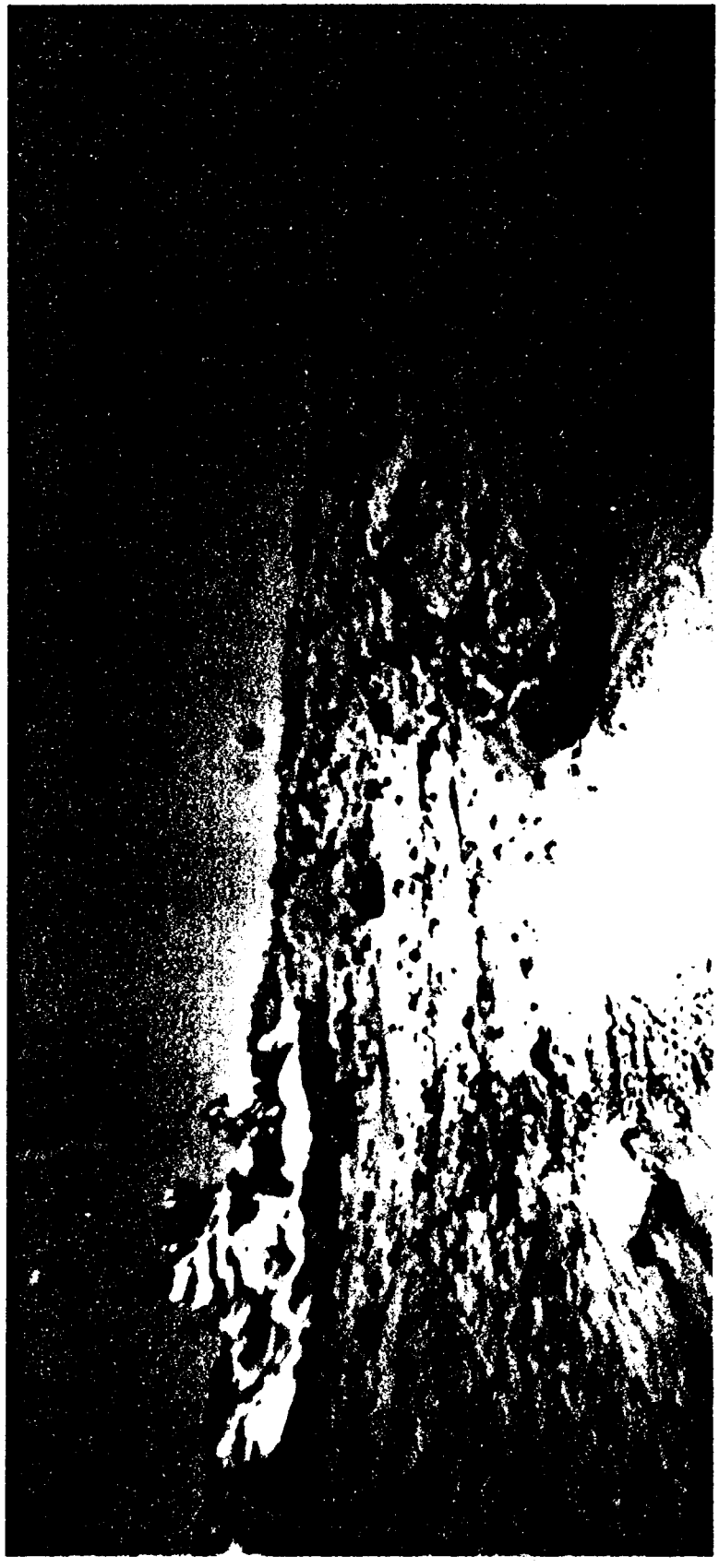

Squash
3

MRP- 8011

Chimp
3-D
4

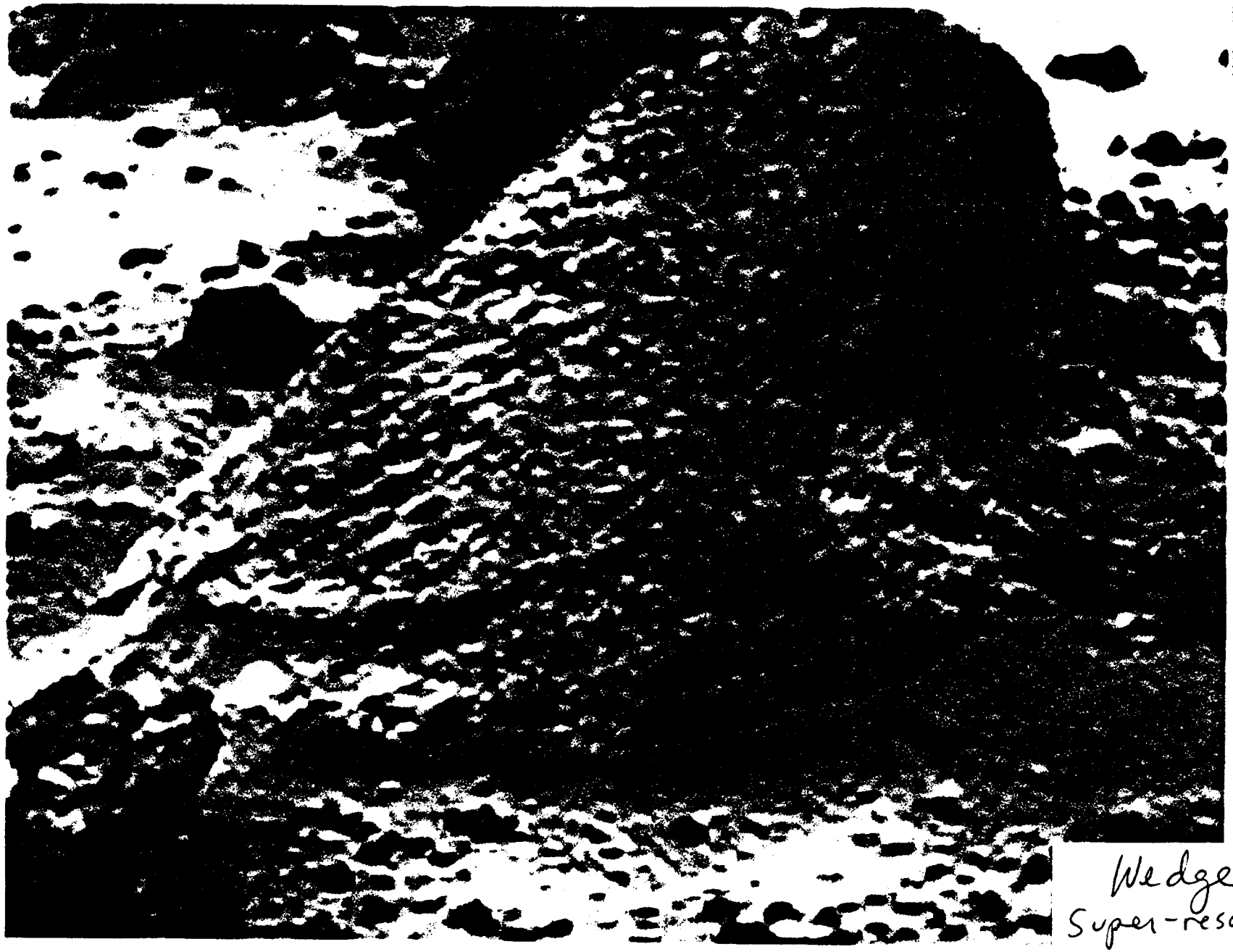

Wedge
Super-resolution

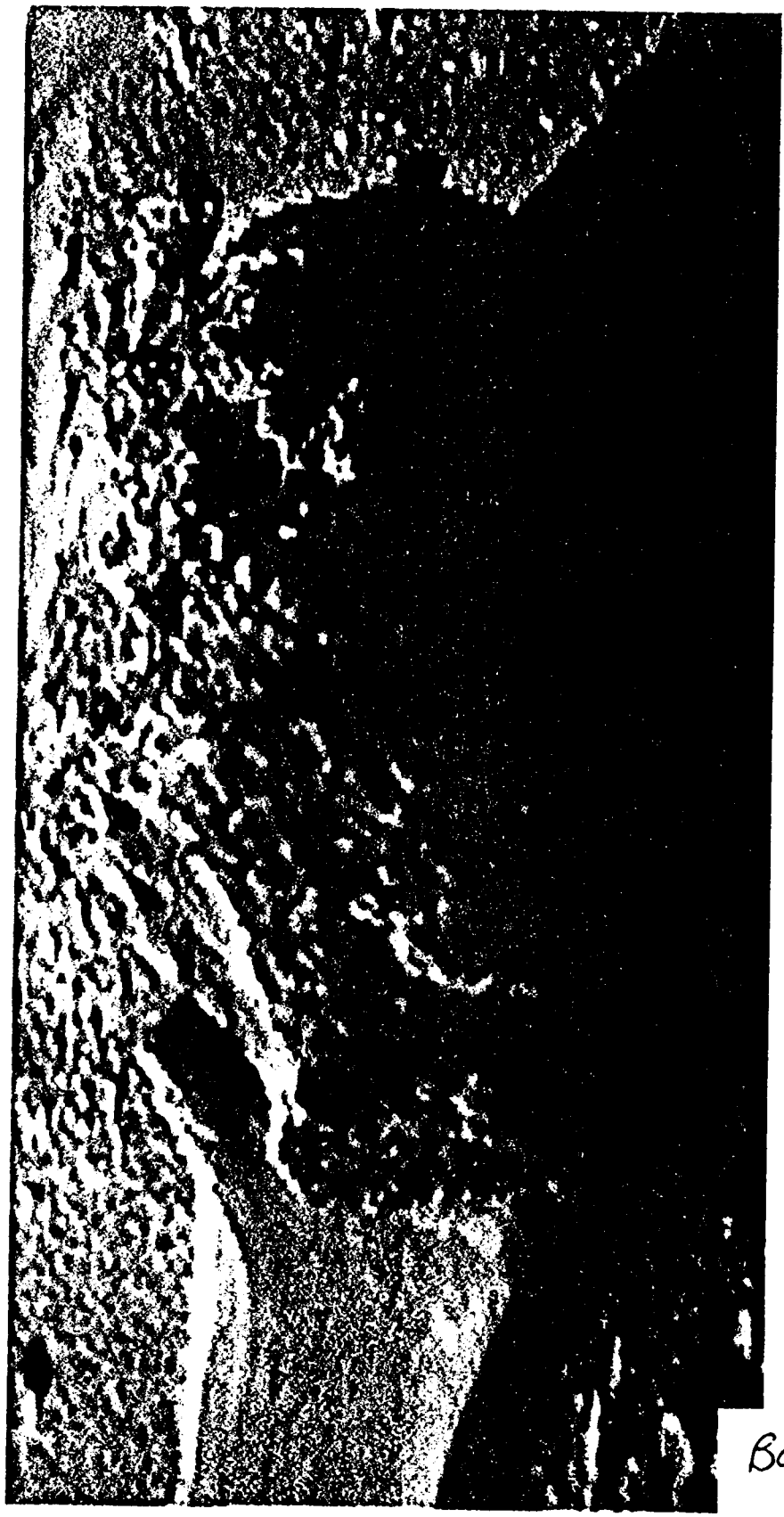

Barnacle Bill

3-D

6

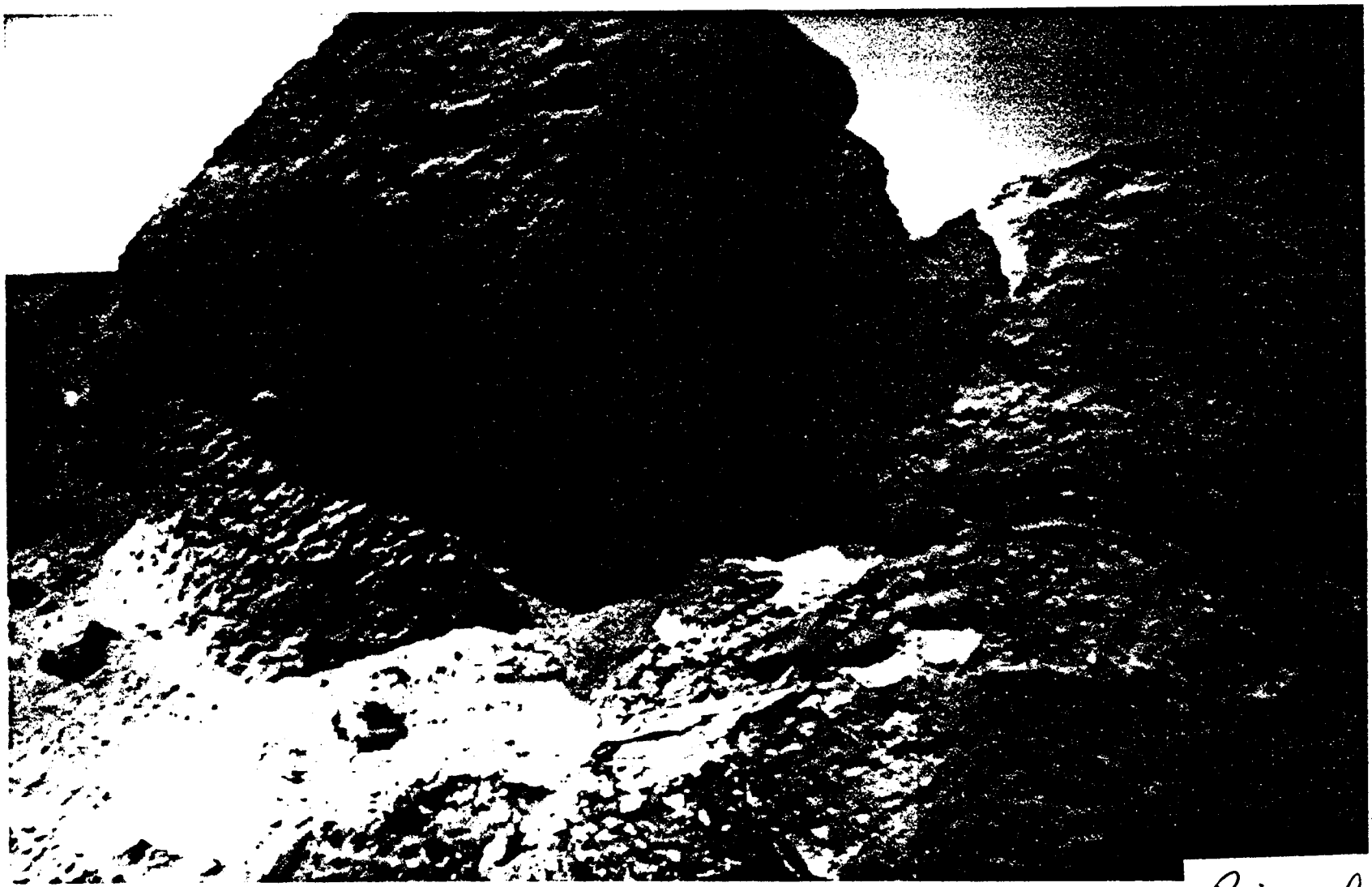

Prince Charmin

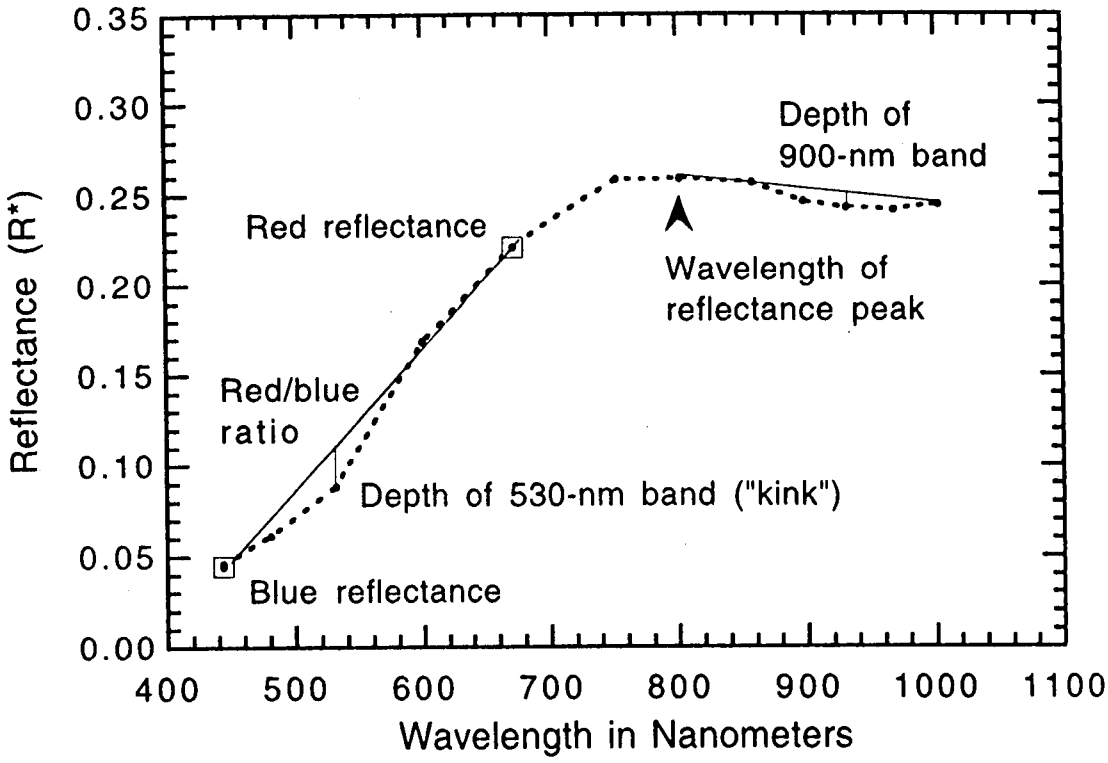
0.35
0.30
0.25
0.20
0.15
0.10
0.05
0.00
Reflectance (R*)
Depth of
900-nm band
Red reflectance
Wavelength of
reflectance peak
Red/blue
ratio
Depth of 530-nm band ("kink")
Blue reflectance
400
500
600
700
800
900
1000
1100
Wavelength in Nanometers

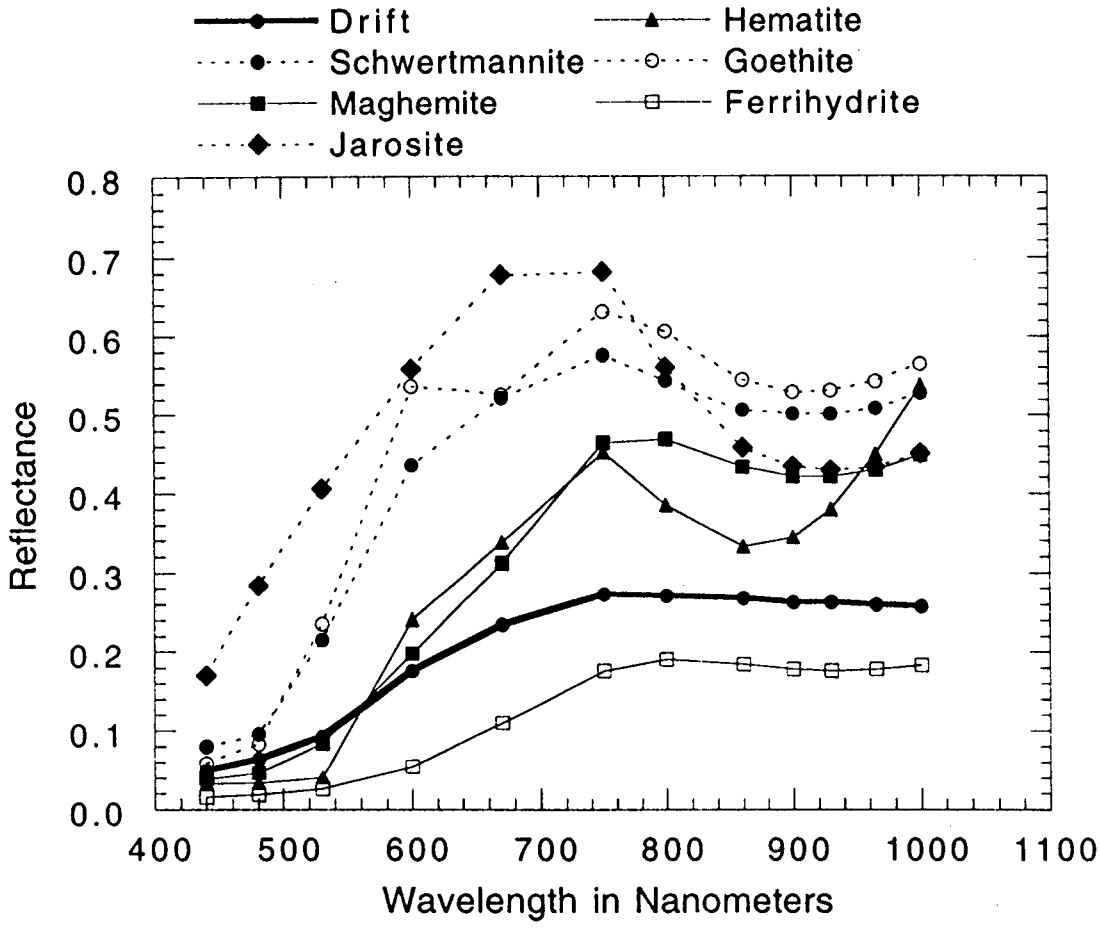
Drift
Hematite
Schwertmannite
Goethite
Maghemite
Ferrihydrite
Jarosite
Reflectance
0.0
0.1
0.2
0.3
0.4
0.5
0.6
0.7
0.8
400
500
600
700
800
900
1000
1100
Wavelength in Nanometers

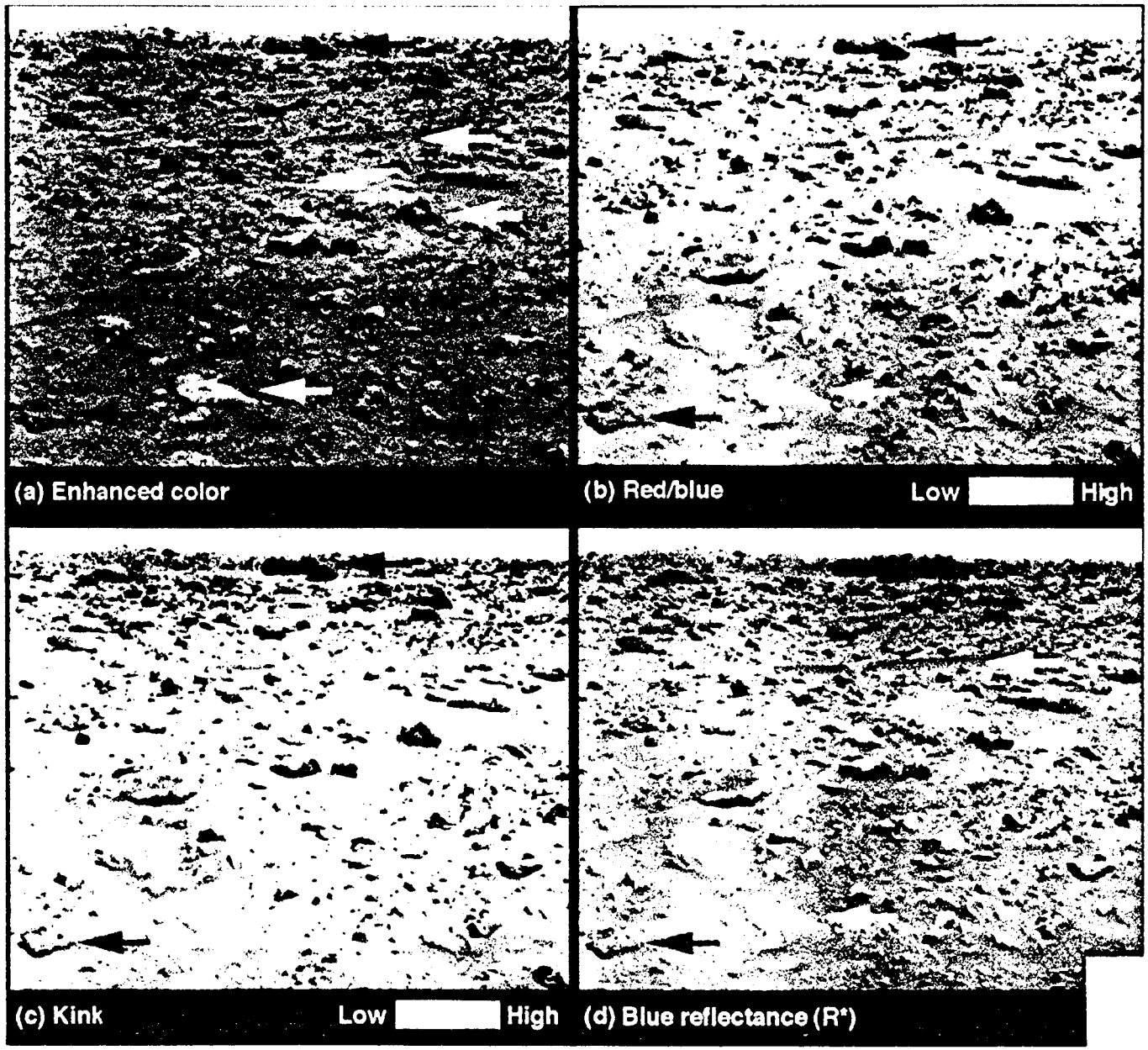
(a) Enhanced color
(b) Red/blue
Low
High
(c) Kink
Low
High
(d) Blue reflectance (R^*)

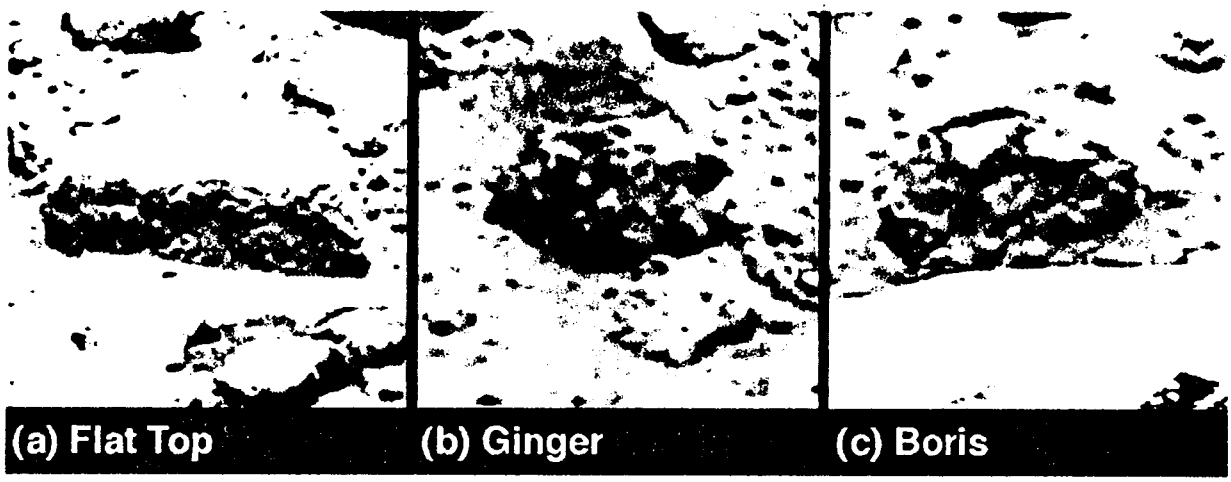
(a) Flat Top
(b) Ginger
(c) Boris

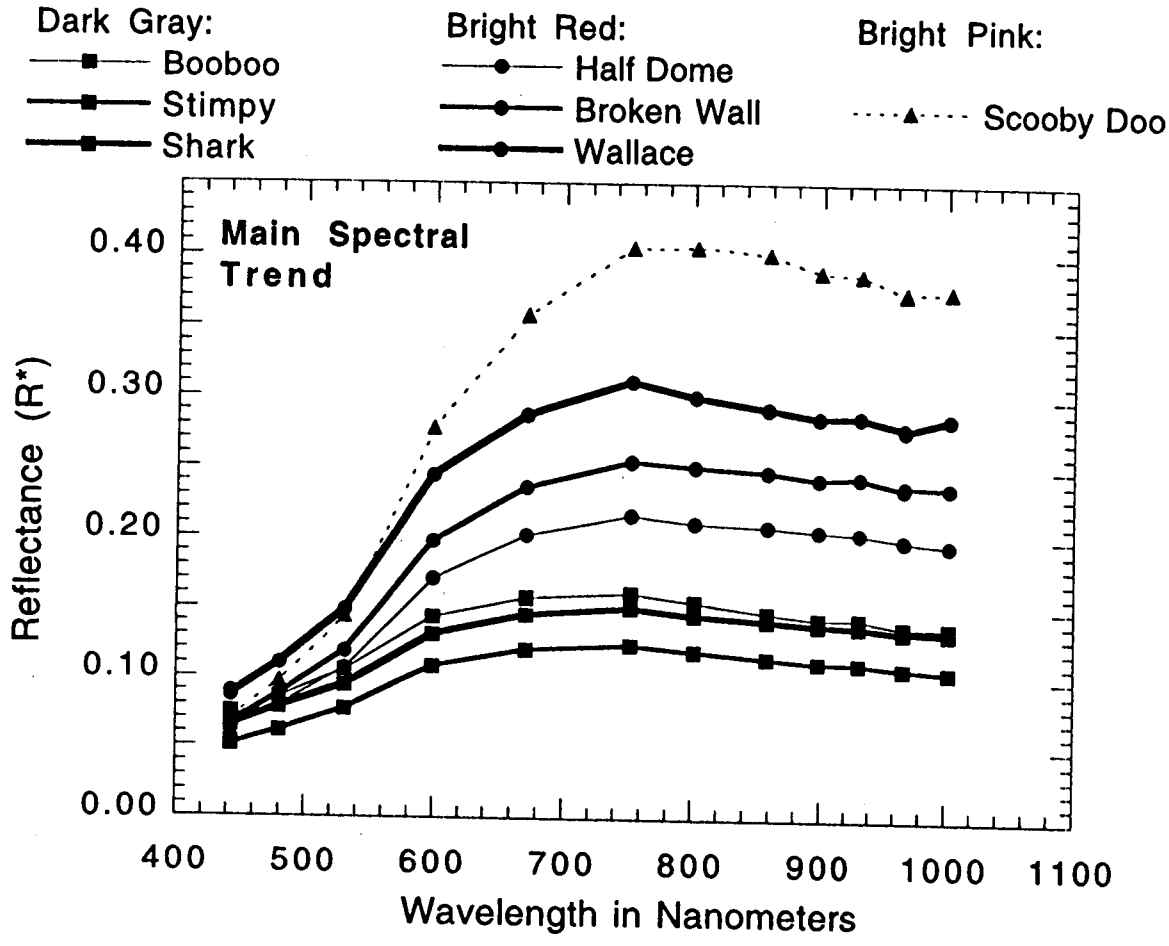
Dark Gray:
Booboo
Stimpy
Shark
Bright Red:
Half Dome
Broken Wall
Wallace
Bright Pink:
Scooby Doo
Main Spectral Trend
Reflectance (R*)
0.40
0.30
0.20
0.10
0.00
400
500
600
700
800
900
1000
1100
Wavelength in Nanometers

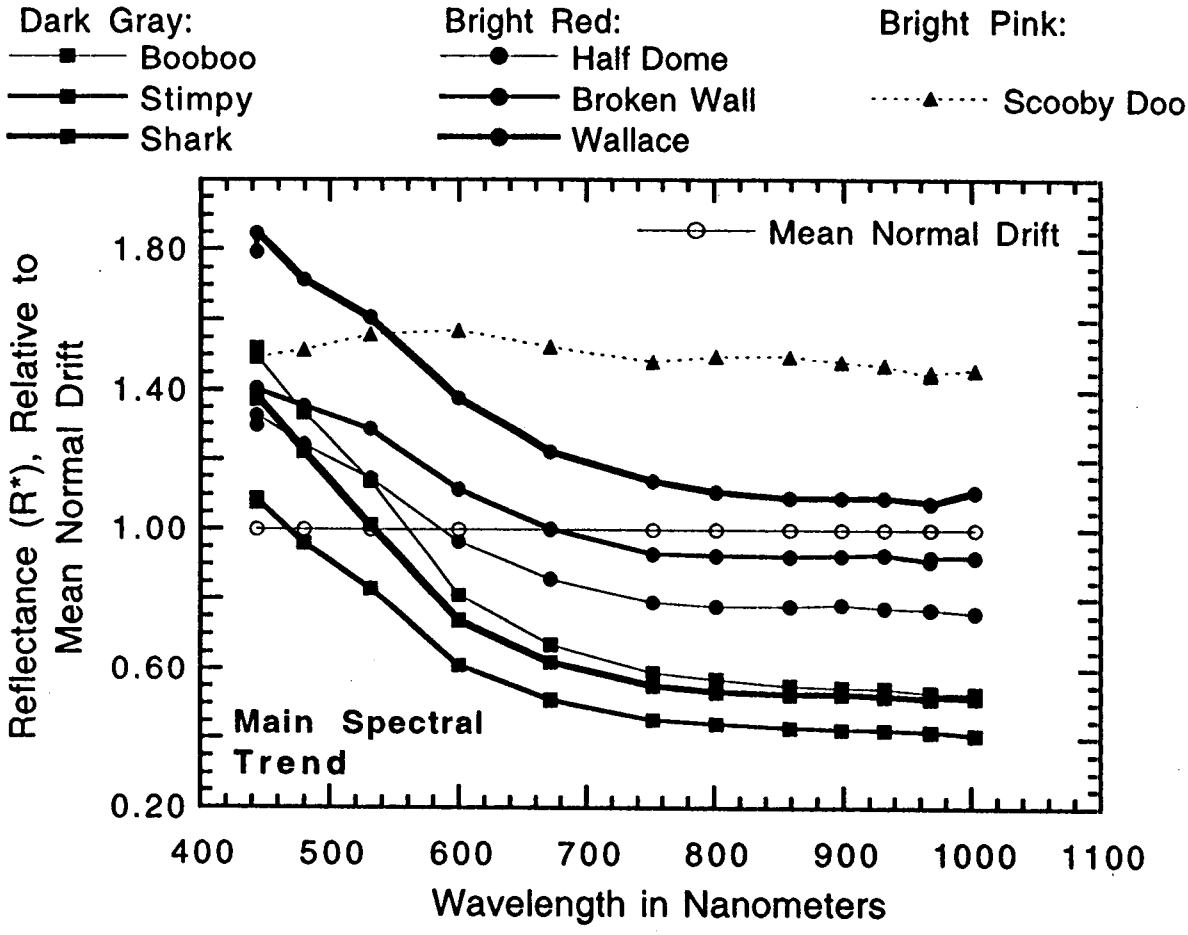
Dark Gray:
Booboo
Stimpy
Shark
Bright Red:
Half Dome
Broken Wall
Wallace
Bright Pink:
Scooby Doo
Mean Normal Drift
Reflectance (R*), Relative to Mean Normal Drift
1.80
1.40
1.00
0.60
0.20
Main Spectral Trend
400
500
600
700
800
900
1000
1100
Wavelength in Nanometers

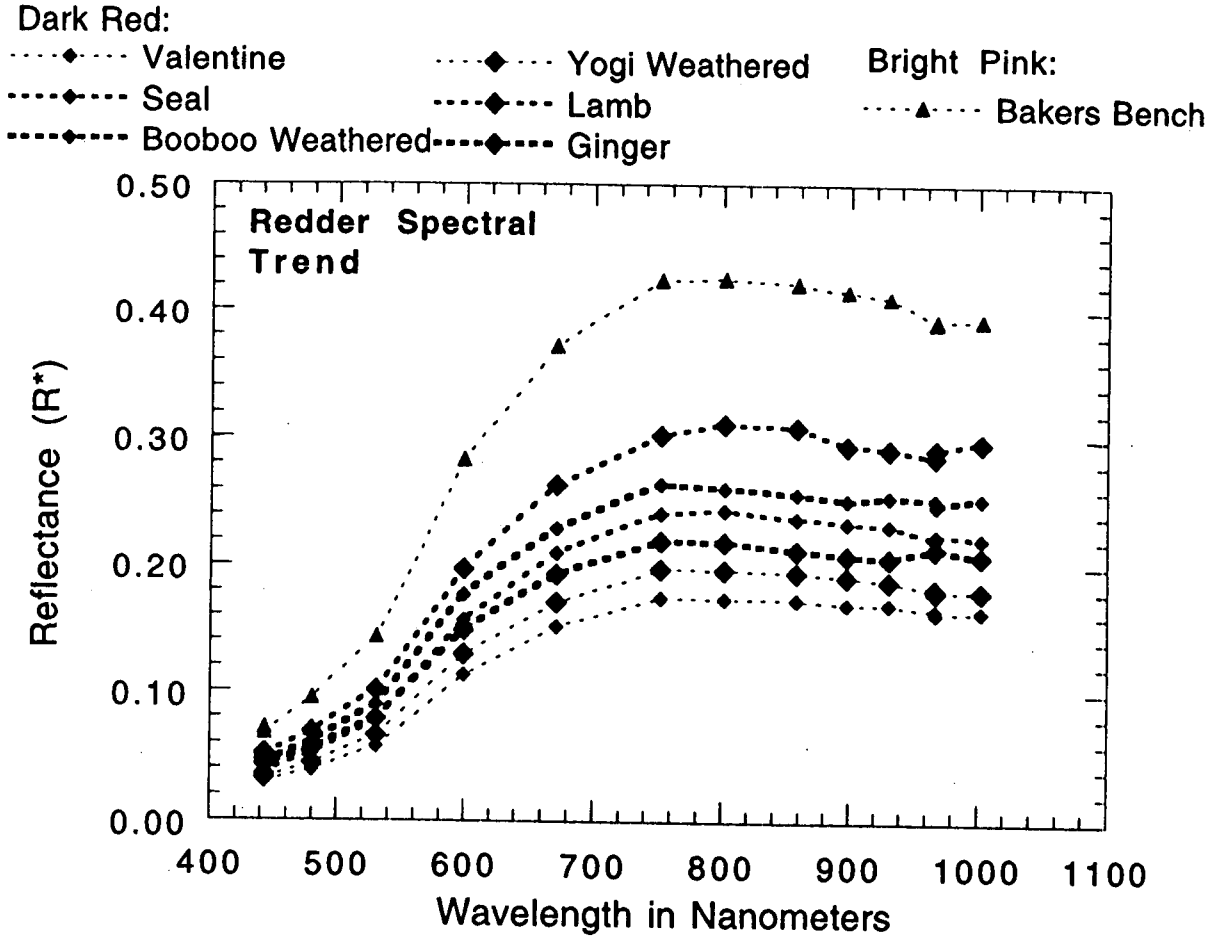
Dark Red:
Valentine
Seal
Booboo Weathered
Yogi Weathered
Lamb
Ginger
Bright Pink:
Bakers Bench
Redder Spectral Trend
Reflectance (R*)
0.50
0.40
0.30
0.20
0.10
0.00
400
500
600
700
800
900
1000
1100
Wavelength in Nanometers

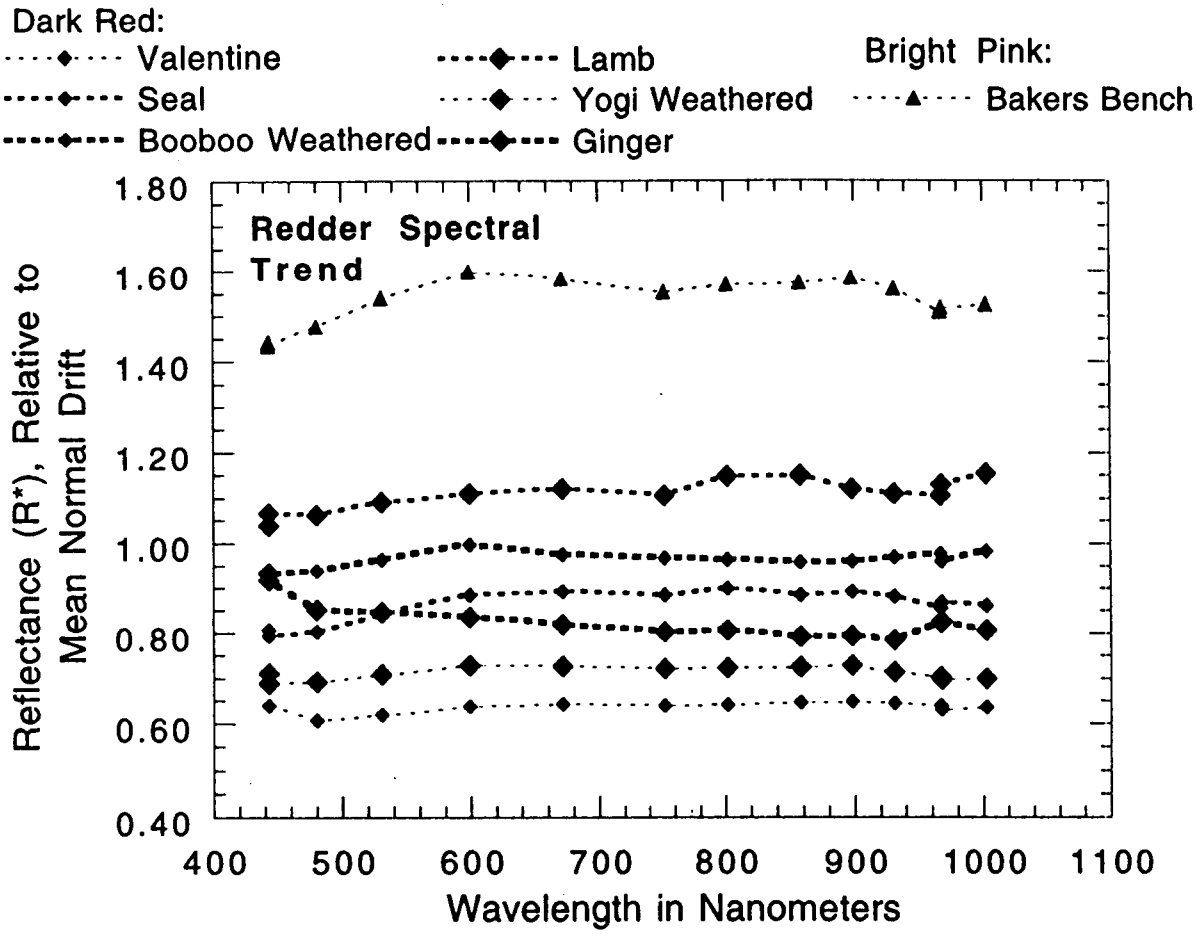
Dark Red:
Valentine
Lamb
Bright Pink:
Seal
Yogi Weathered
Bakers Bench
Booboo Weathered
Ginger
Redder Spectral Trend
Reflectance (R*), Relative to Mean Normal Drift
1.80
1.60
1.40
1.20
1.00
0.80
0.60
0.40
400
500
600
700
800
900
1000
1100
Wavelength in Nanometers

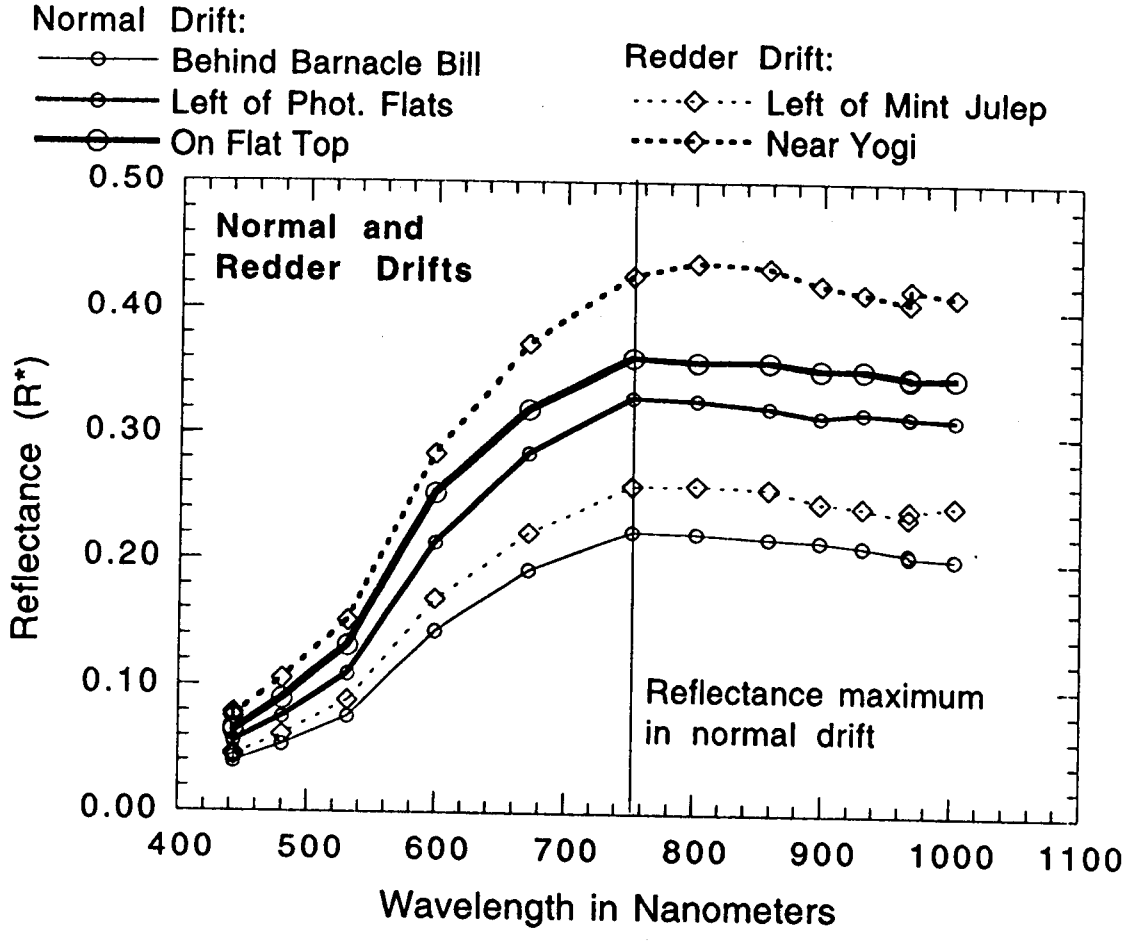
Normal Drift:
Behind Barnacle Bill
Left of Phot. Flats
On Flat Top
Redder Drift:
Left of Mint Julep
Near Yogi
Normal and
Redder Drifts
Reflectance maximum
in normal drift
Reflectance (R*)
0.50
0.40
0.30
0.20
0.10
0.00
400
500
600
700
800
900
1000
1100
Wavelength in Nanometers

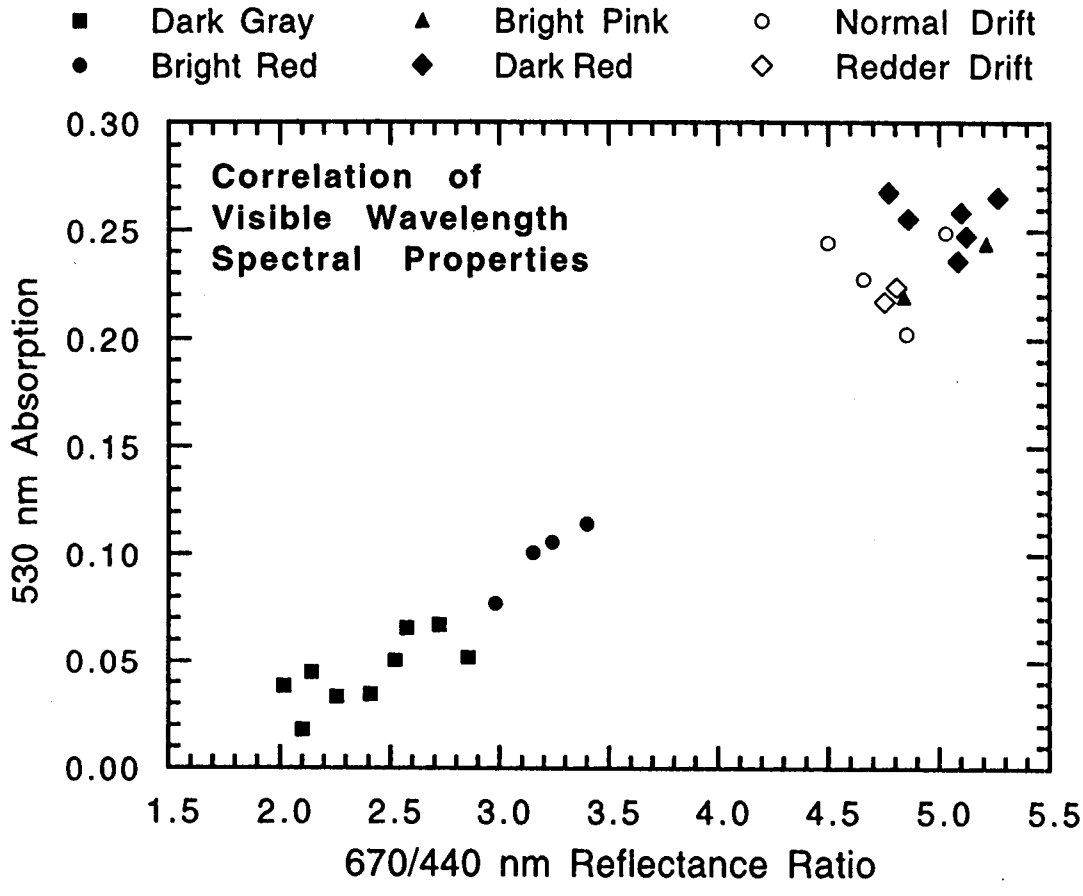
Dark Gray
Bright Pink
Normal Drift
Bright Red
Dark Red
Redder Drift
Correlation of
Visible Wavelength
Spectral Properties
530 nm Absorption
0.30
0.25
0.20
0.15
0.10
0.05
0.00
1.5
2.0
2.5
3.0
3.5
4.0
4.5
5.0
5.5
670/440 nm Reflectance Ratio

15a

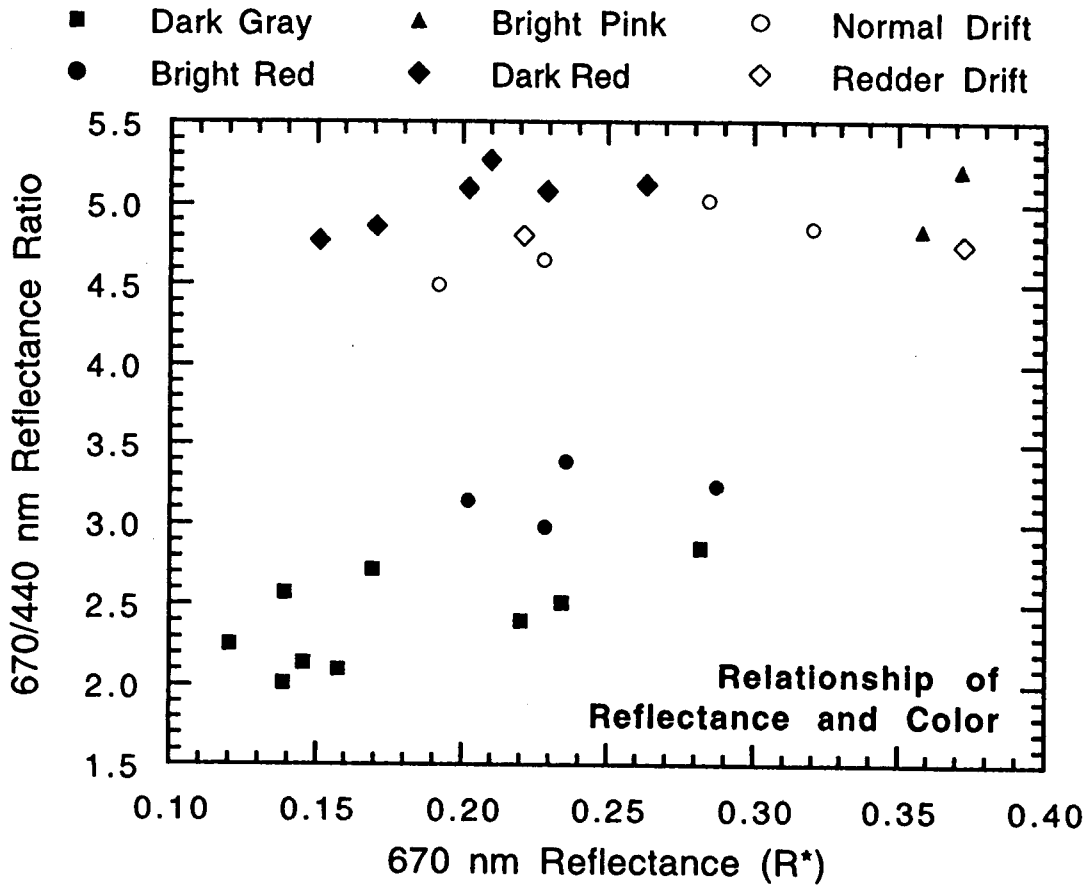
Dark Gray
Bright Pink
Normal Drift
Bright Red
Dark Red
Redder Drift
670/440 nm Reflectance Ratio
5.5
5.0
4.5
4.0
3.5
3.0
2.5
2.0
1.5
0.10
0.15
0.20
0.25
0.30
0.35
0.40
670 nm Reflectance (R*)
Relationship of
Reflectance and Color

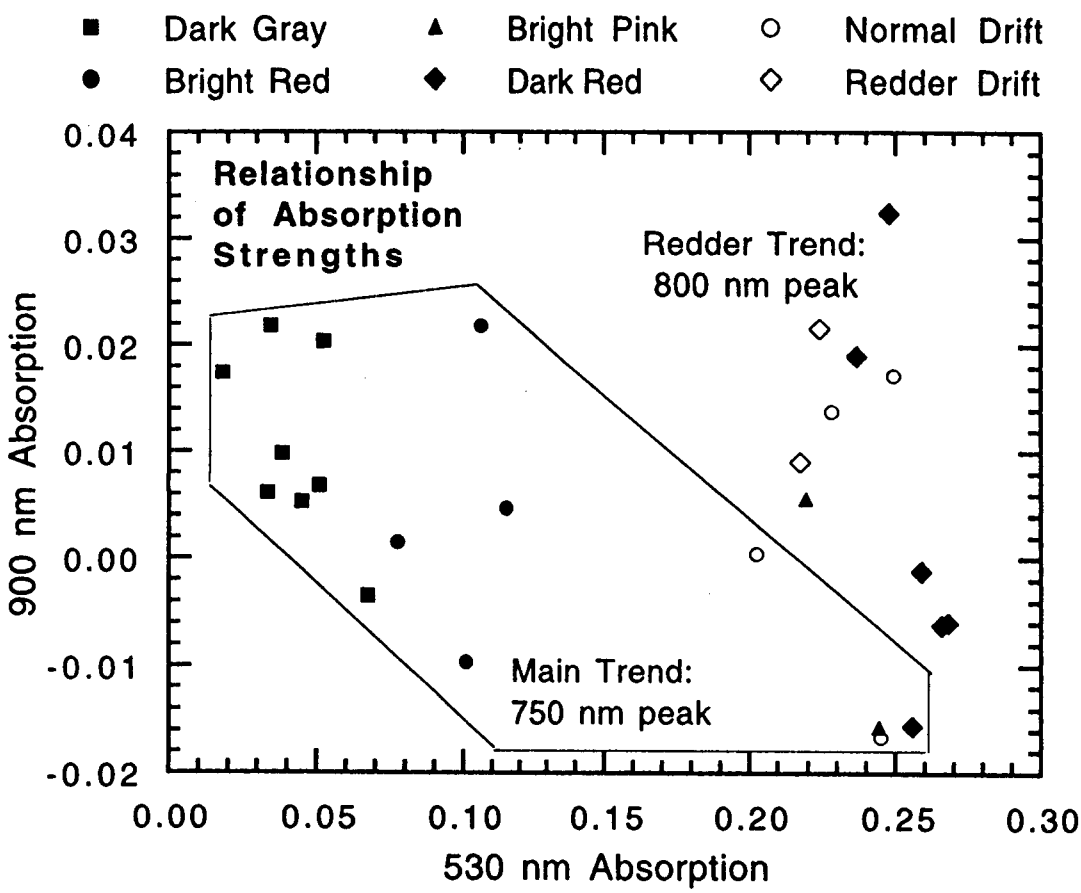
Dark Gray
Bright Pink
Normal Drift
Bright Red
Dark Red
Redder Drift
Relationship of Absorption Strengths
Redder Trend: 800 nm peak
Main Trend: 750 nm peak
900 nm Absorption
530 nm Absorption
0.04
0.03
0.02
0.01
0.00
-0.01
-0.02
0.00
0.05
0.10
0.15
0.20
0.25
0.30

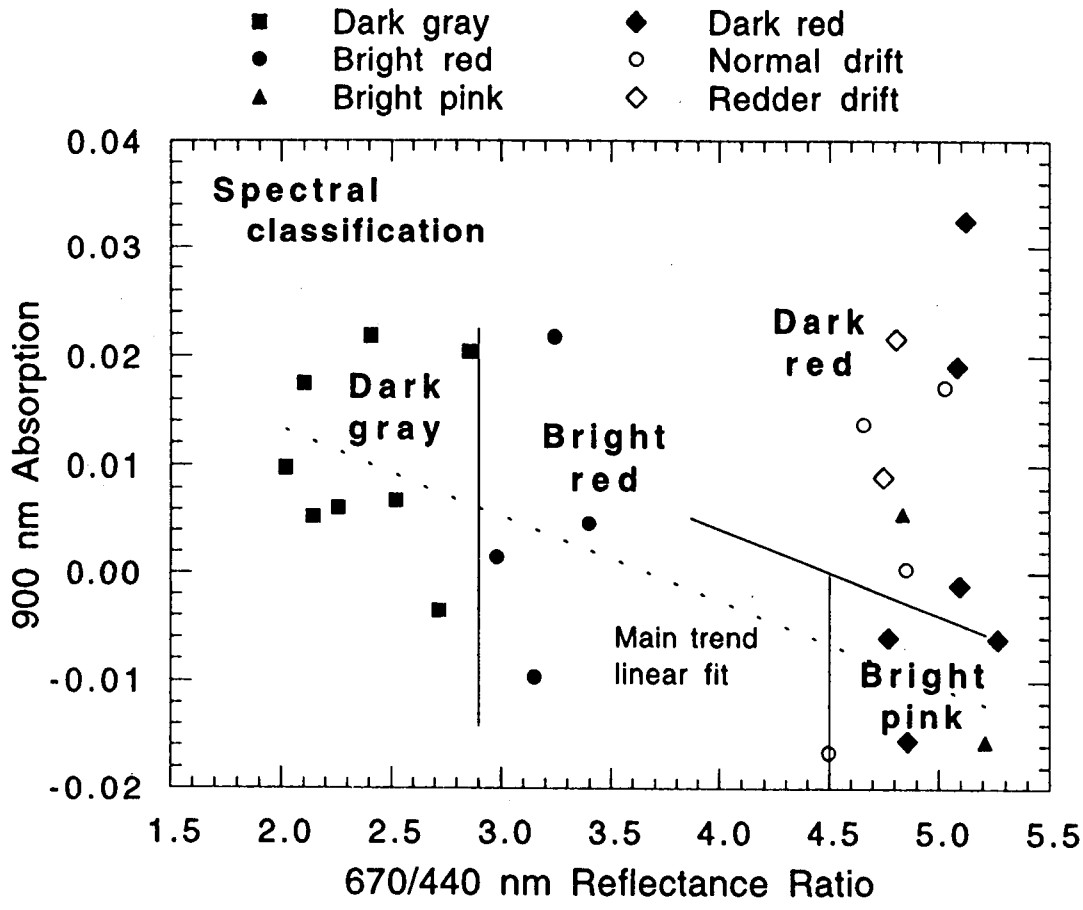
Dark gray
Bright red
Bright pink
Dark red
Normal drift
Redder drift
Spectral classification
Dark gray
Bright red
Dark red
Main trend linear fit
Bright pink
900 nm Absorption
0.04
0.03
0.02
0.01
0.00
-0.01
-0.02
1.5
2.0
2.5
3.0
3.5
4.0
4.5
5.0
5.5
670/440 nm Reflectance Ratio

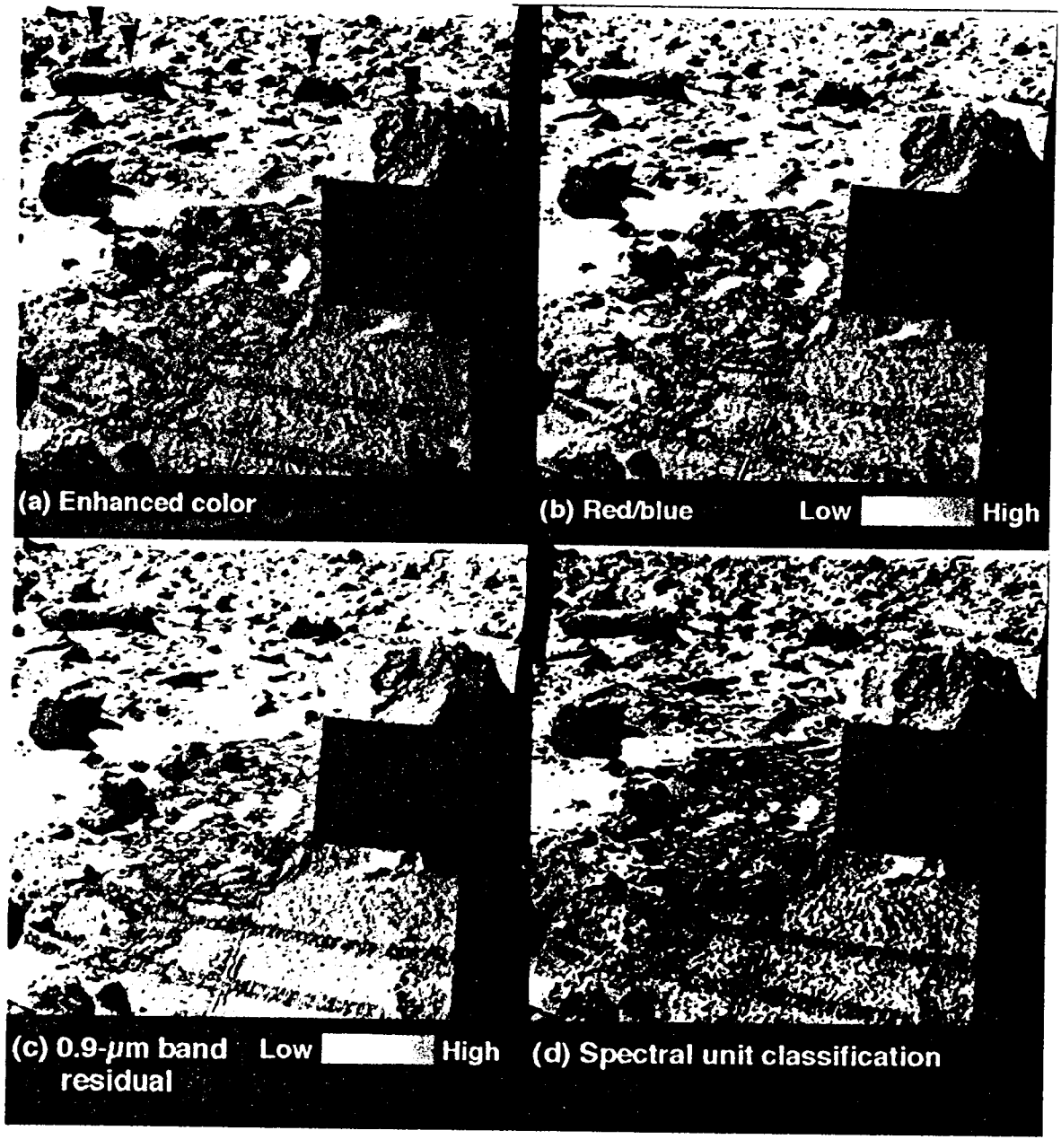
(a) Enhanced color
(b) Red/blue
Low
High
(c) 0.9-μm band residual
Low
High
(d) Spectral unit classification

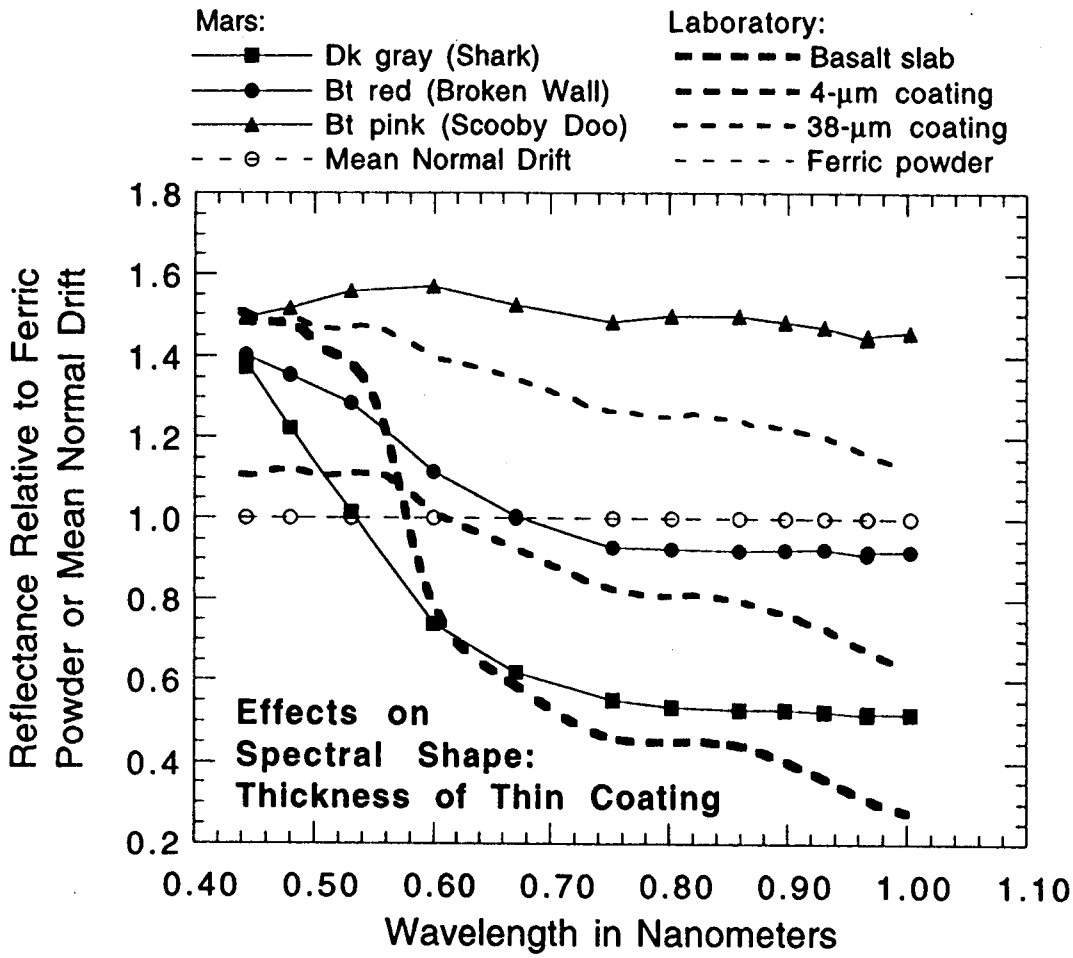
Mars:
Dk gray (Shark)
Bt red (Broken Wall)
Bt pink (Scooby Doo)
Mean Normal Drift
Laboratory:
Basalt slab
4-µm coating
38-µm coating
Ferric powder
Reflectance Relative to Ferric Powder or Mean Normal Drift
1.8
1.6
1.4
1.2
1.0
0.8
0.6
0.4
0.2
Effects on Spectral Shape: Thickness of Thin Coating
0.40
0.50
0.60
0.70
0.80
0.90
1.00
1.10
Wavelength in Nanometers

17a

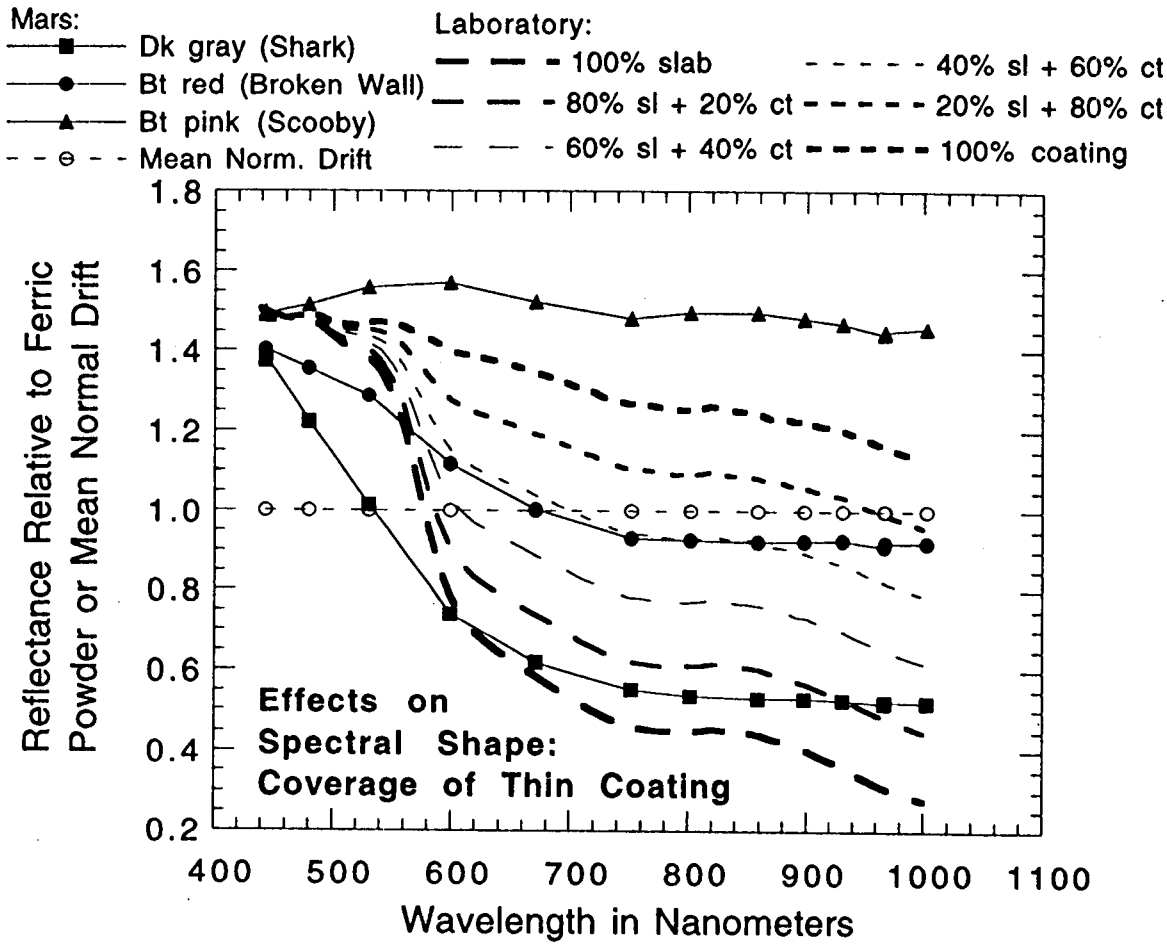
Mars:
Dk gray (Shark)
Bt red (Broken Wall)
Bt pink (Scooby)
Mean Norm. Drift
Laboratory:
100% slab
80% sl + 20% ct
60% sl + 40% ct
40% sl + 60% ct
20% sl + 80% ct
100% coating
Reflectance Relative to Ferric Powder or Mean Normal Drift
1.8
1.6
1.4
1.2
1.0
0.8
0.6
0.4
0.2
Effects on Spectral Shape: Coverage of Thin Coating
400
500
600
700
800
900
1000
1100
Wavelength in Nanometers

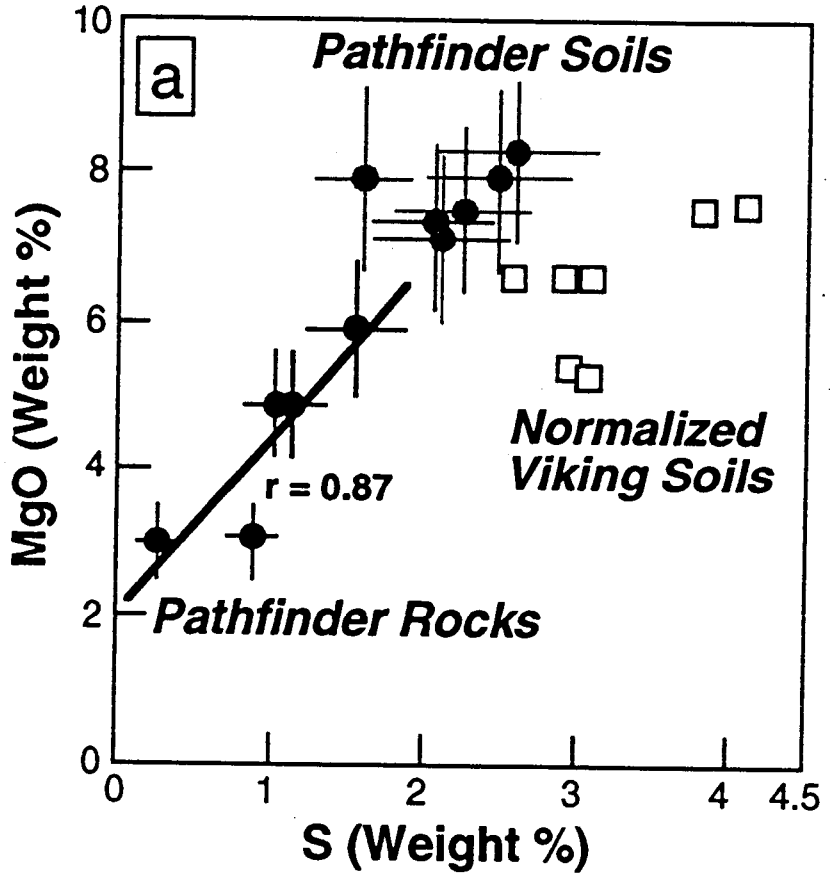
a
Pathfinder Soils
Normalized
Viking Soils
r = 0.87
Pathfinder Rocks
MgO (Weight %)
S (Weight %)
0
2
4
6
8
10
0
1
2
3
4
4.5

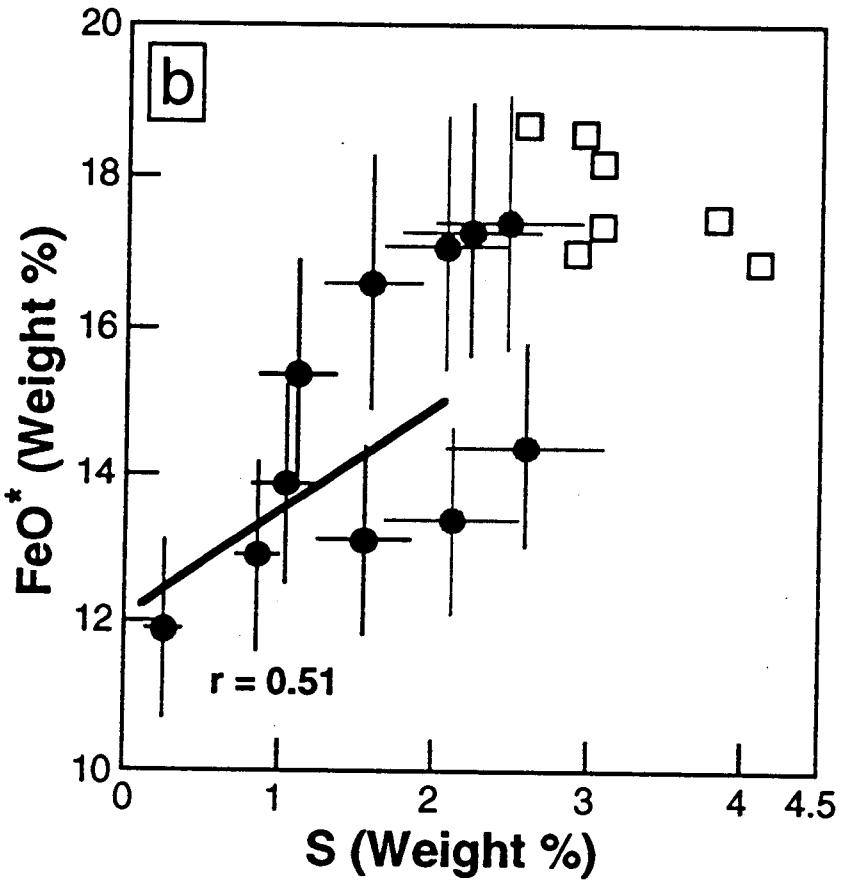
b
r = 0.51
FeO* (Weight %)
S (Weight %)
10
12
14
16
18
20
0
1
2
3
4
4.5

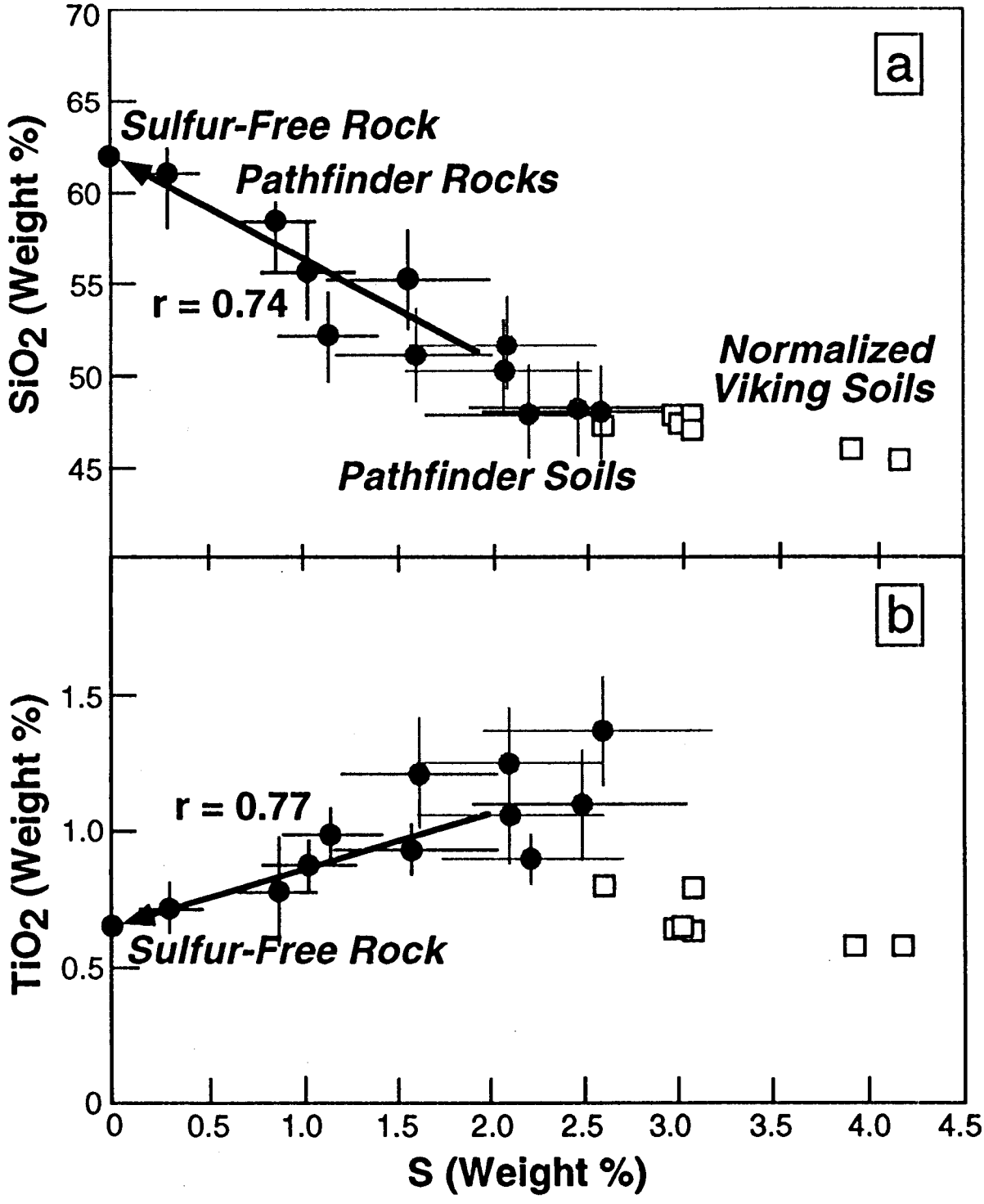
a
b
Sulfur-Free Rock
Pathfinder Rocks
r = 0.74
Normalized
Viking Soils
Pathfinder Soils
r = 0.77
Sulfur-Free Rock
SiO2 (Weight %)
TiO2 (Weight %)
S (Weight %)
70
65
60
55
50
45
1.5
1.0
0.5
0
0
0.5
1.0
1.5
2.0
2.5
3.0
3.5
4.0
4.5

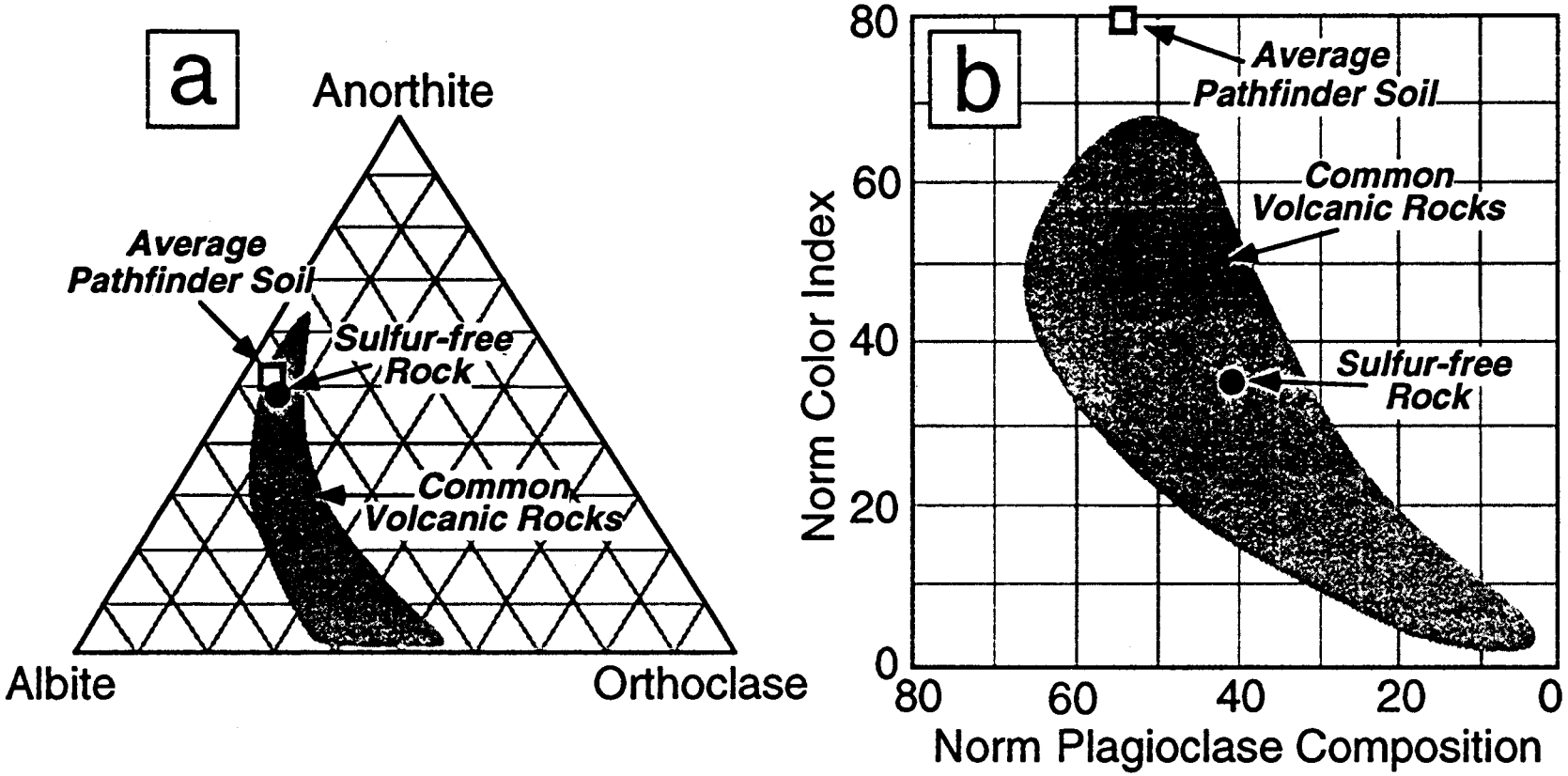
a
Anorthite
Average
Pathfinder Soil
Sulfur-free
Rock
Common
Volcanic Rocks
Albite
Orthoclase
b
Average
Pathfinder Soil
Common
Volcanic Rocks
Sulfur-free
Rock
Norm Color Index
80
60
40
20
0
80
60
40
20
0
Norm Plagioclase Composition

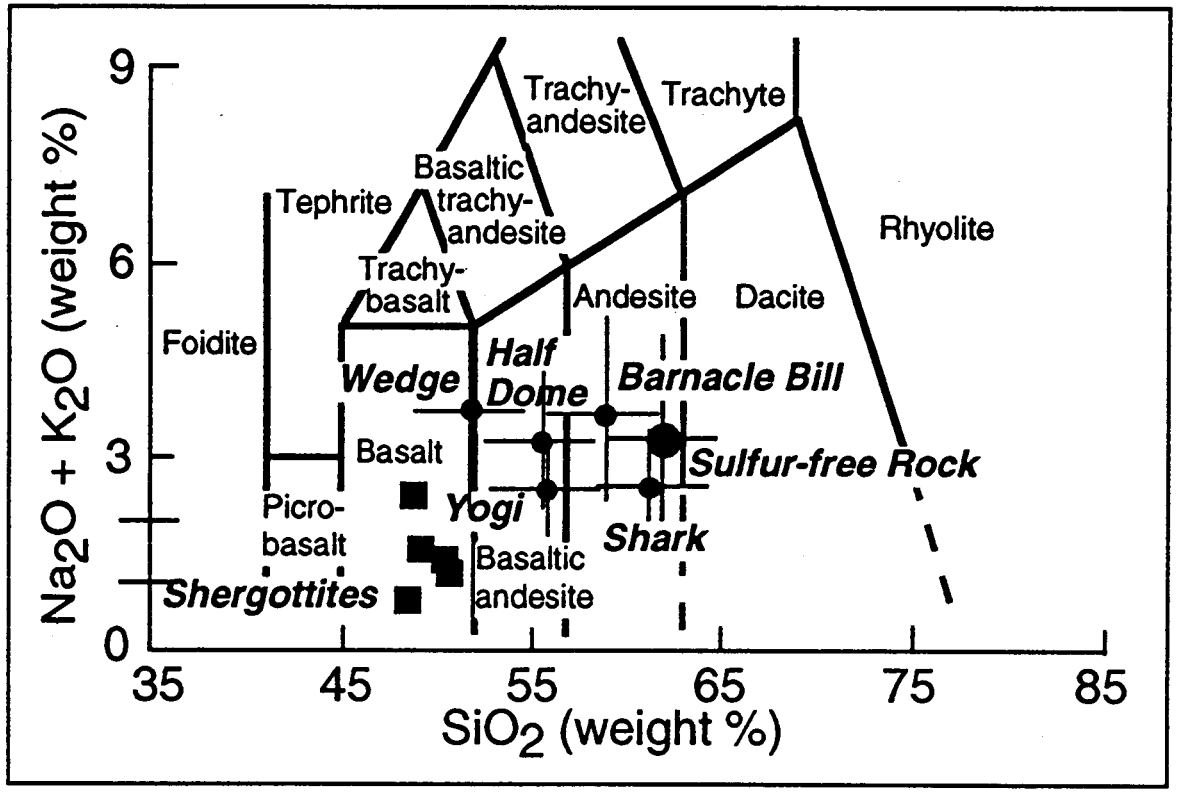
9
6
3
0
35
45
55
65
75
85
$Na_2O + K_2O$ (weight %)
SiO_2 (weight %)
Trachy-
andesite
Trachyte
Basaltic
trachy-
andesite
Tephrite
Rhyolite
Trachy-
basalt
Andesite
Dacite
Foidite
Wedge
Half
Dome
Barnacle Bill
Basalt
Sulfur-free Rock
Yogi
Picro-
basalt
Shark
Basaltic
andesite
Shergottites

A-3

A-7

A-16

A-17

A-18

A-19

A-20

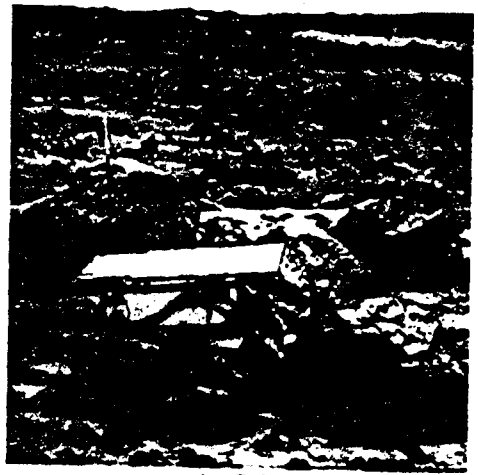

A-23

A-27

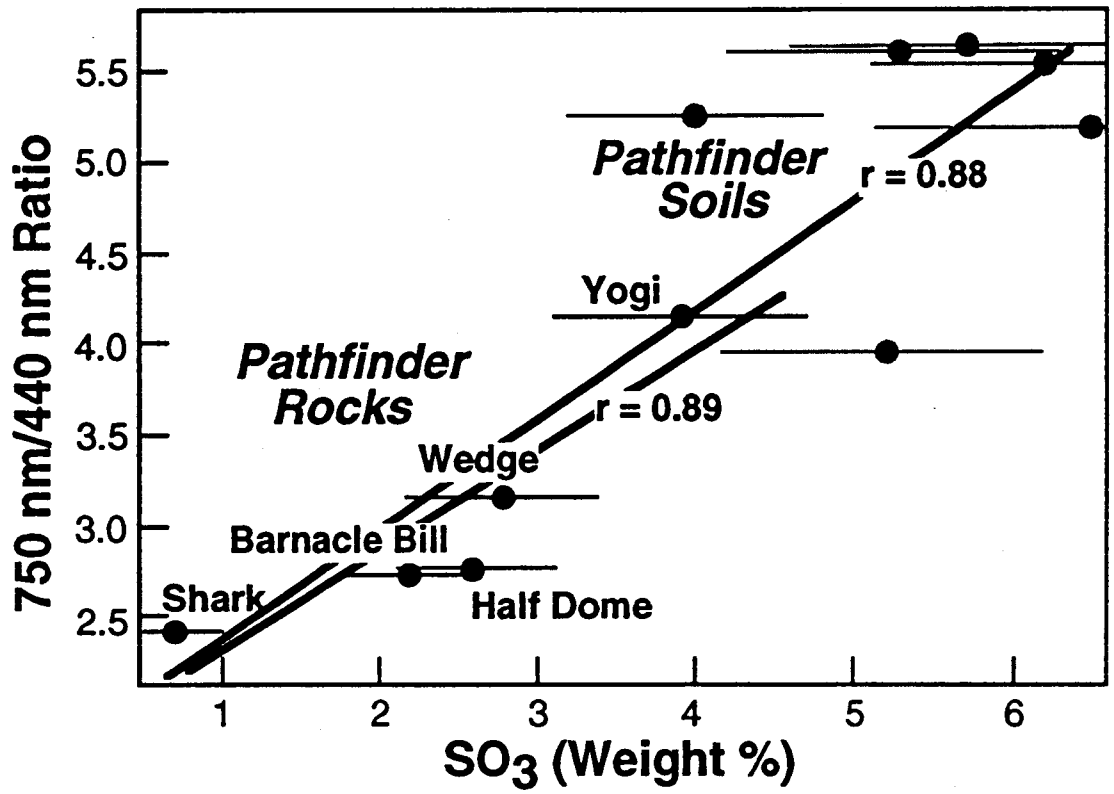
750 nm/440 nm Ratio
5.5
5.0
4.5
4.0
3.5
3.0
2.5
1
2
3
4
5
6
SO3 (Weight %)
Pathfinder Soils
r = 0.88
Yogi
Pathfinder Rocks
r = 0.89
Wedge
Barnacle Bill
Shark
Half Dome

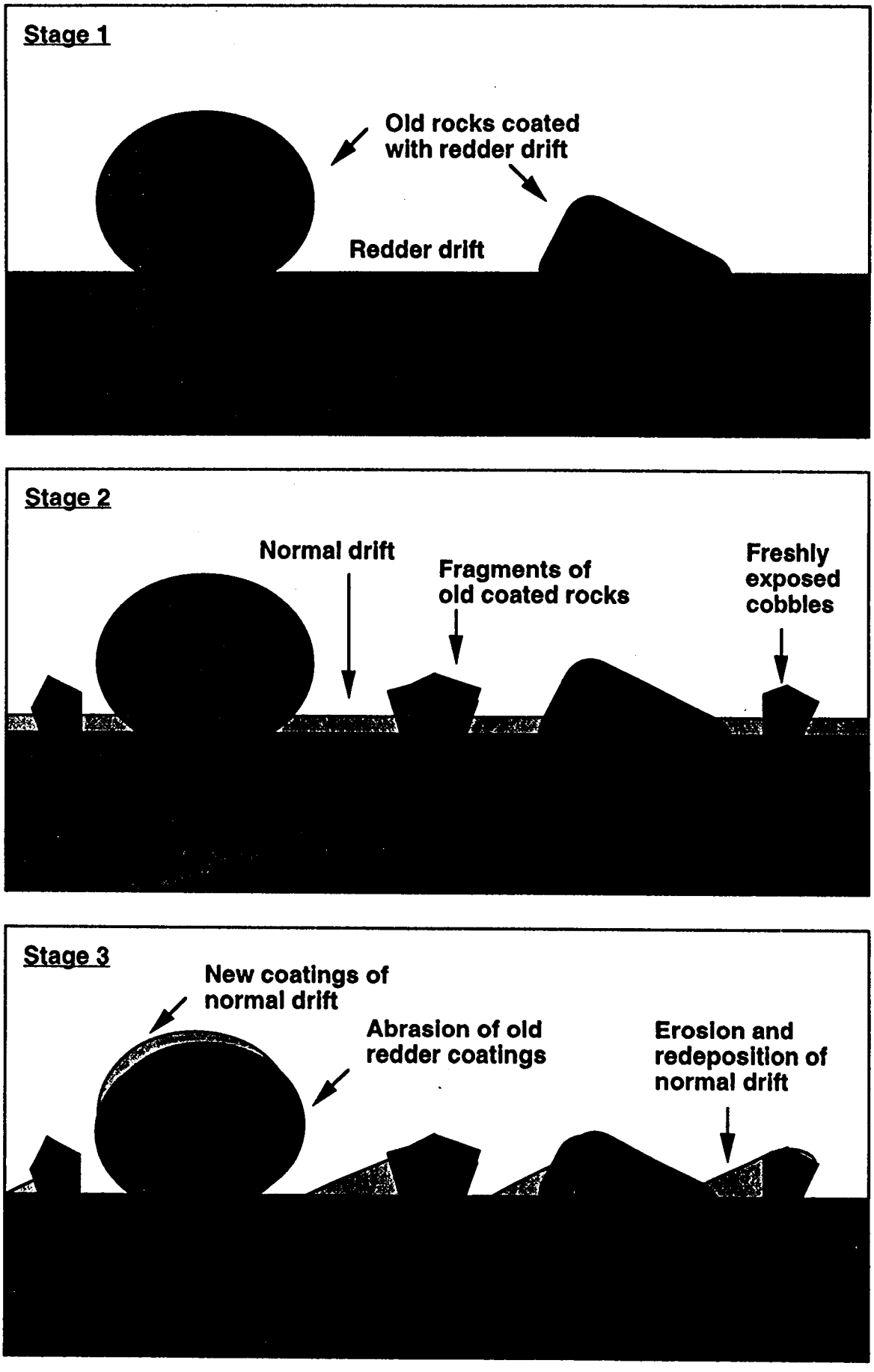
Stage 1
Old rocks coated with redder drift
Redder drift
Stage 2
Normal drift
Fragments of old coated rocks
Freshly exposed cobbles
Stage 3
New coatings of normal drift
Abrasion of old redder coatings
Erosion and redeposition of normal drift

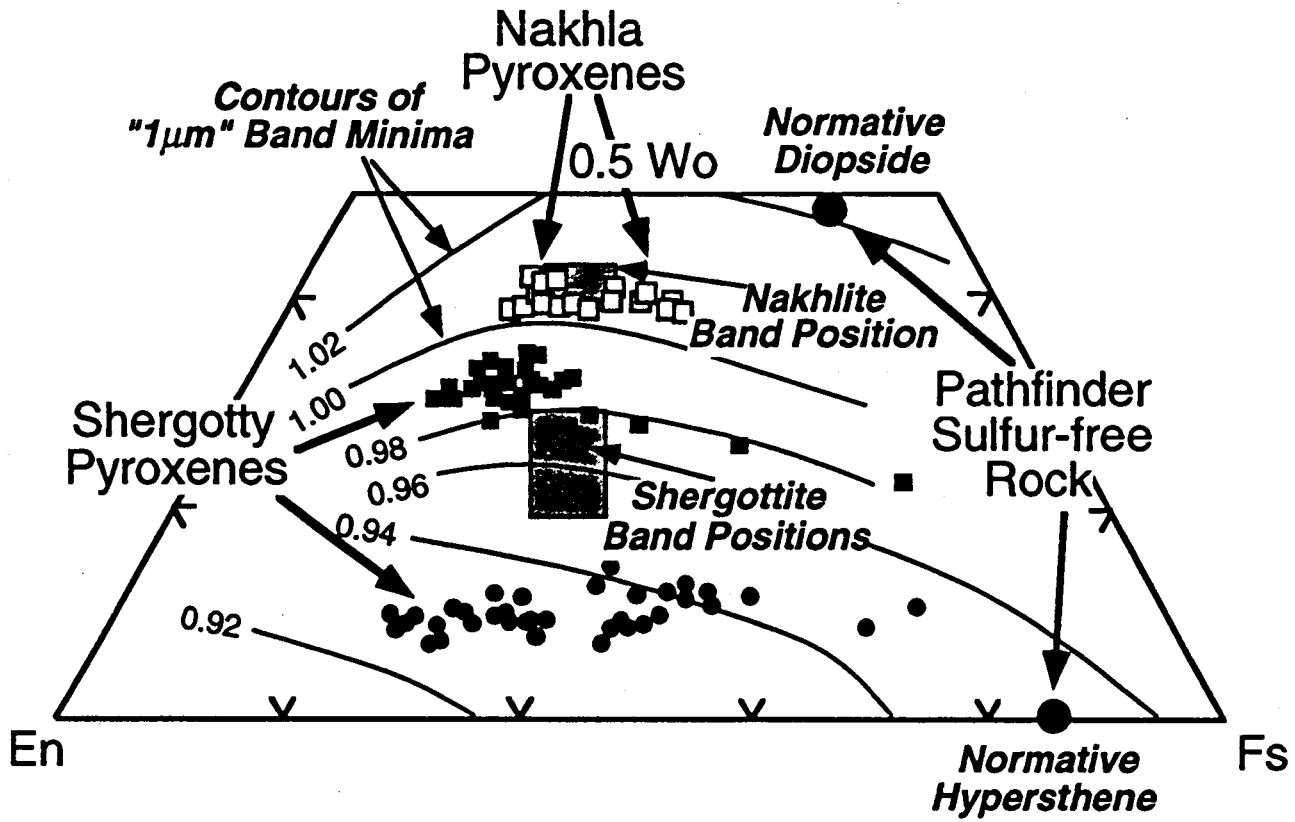
Nakhla
Pyroxenes
Contours of
"1μm" Band Minima
0.5 Wo
Normative
Diopside
Nakhlite
Band Position
1.02
1.00
0.98
0.96
0.94
0.92
Shergotty
Pyroxenes
Pathfinder
Sulfur-free
Rock
Shergottite
Band Positions
En
Fs
Normative
Hypersthene

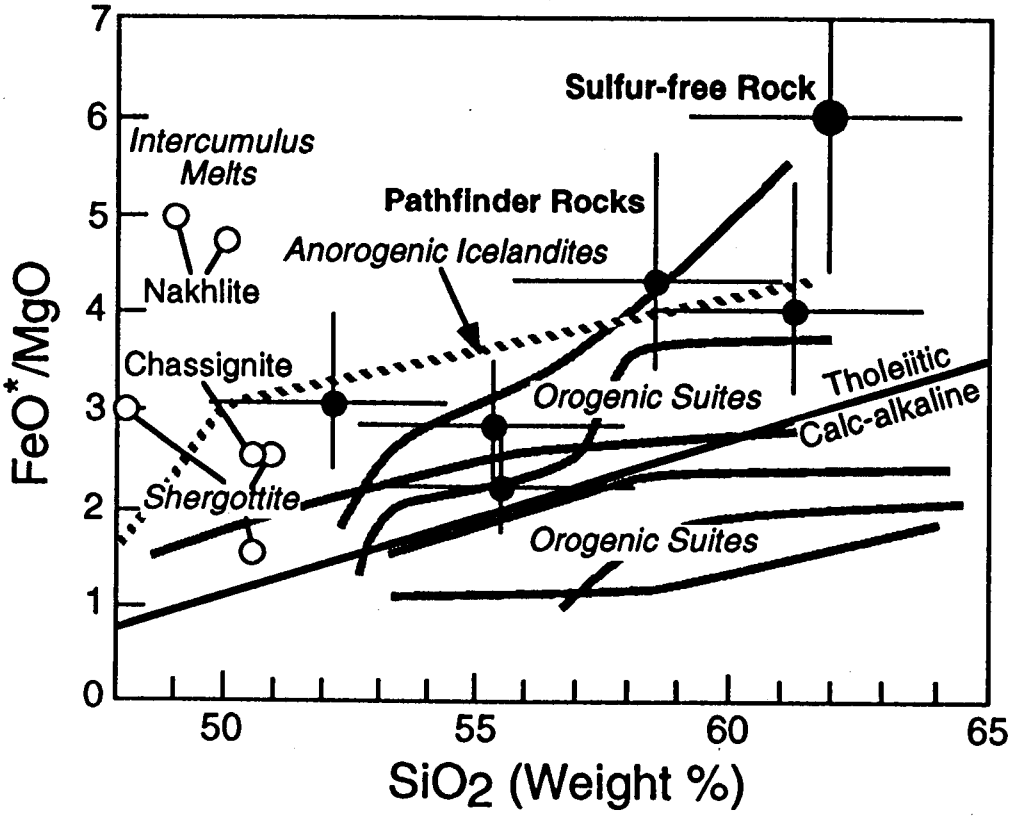
Sulfur-free Rock
Intercumulus Melts
Pathfinder Rocks
Anorogenic Icelandites
Nakhlite
Chassignite
Orogenic Suites
Tholeiitic
Calc-alkaline
Shergottite
Orogenic Suites
FeO*/MgO
SiO2 (Weight %)
0
1
2
3
4
5
6
7
50
55
60
65

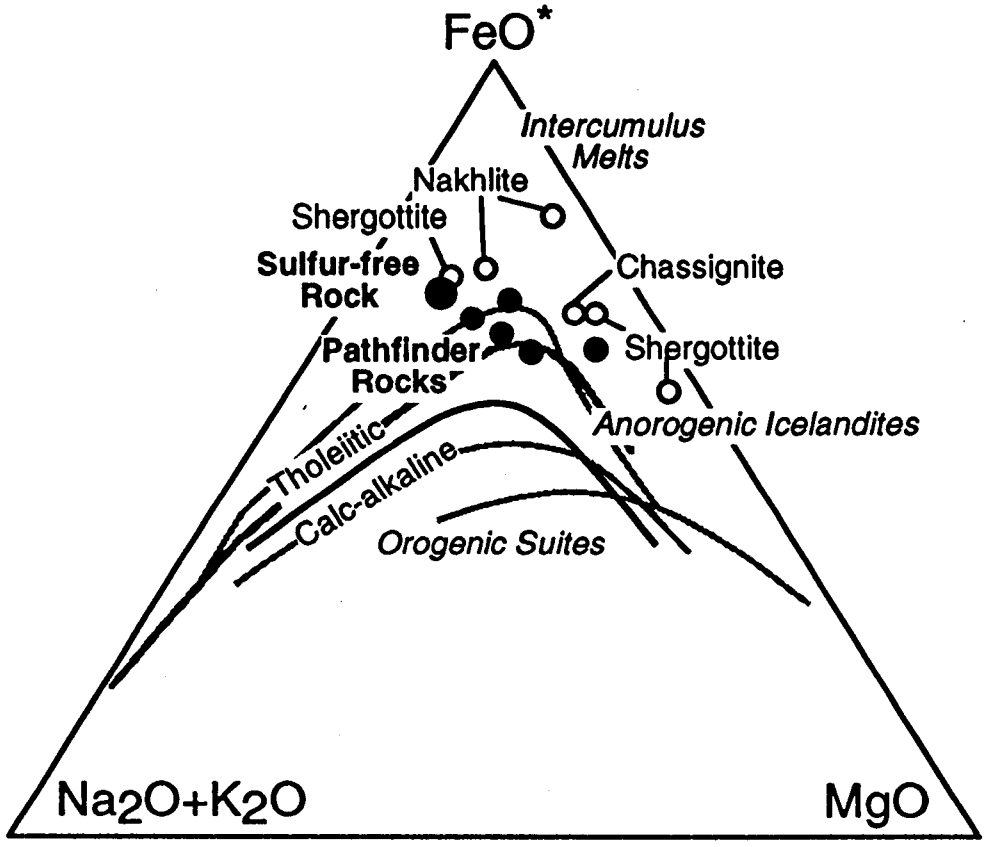
FeO*
Intercumulus Melts
Nakhlite
Shergottite
Sulfur-free Rock
Chassignite
Pathfinder Rocks
Shergottite
Anorogenic Icelandites
Tholeiitic
Calc-alkaline
Orogenic Suites
Na2O+K2O
MgO

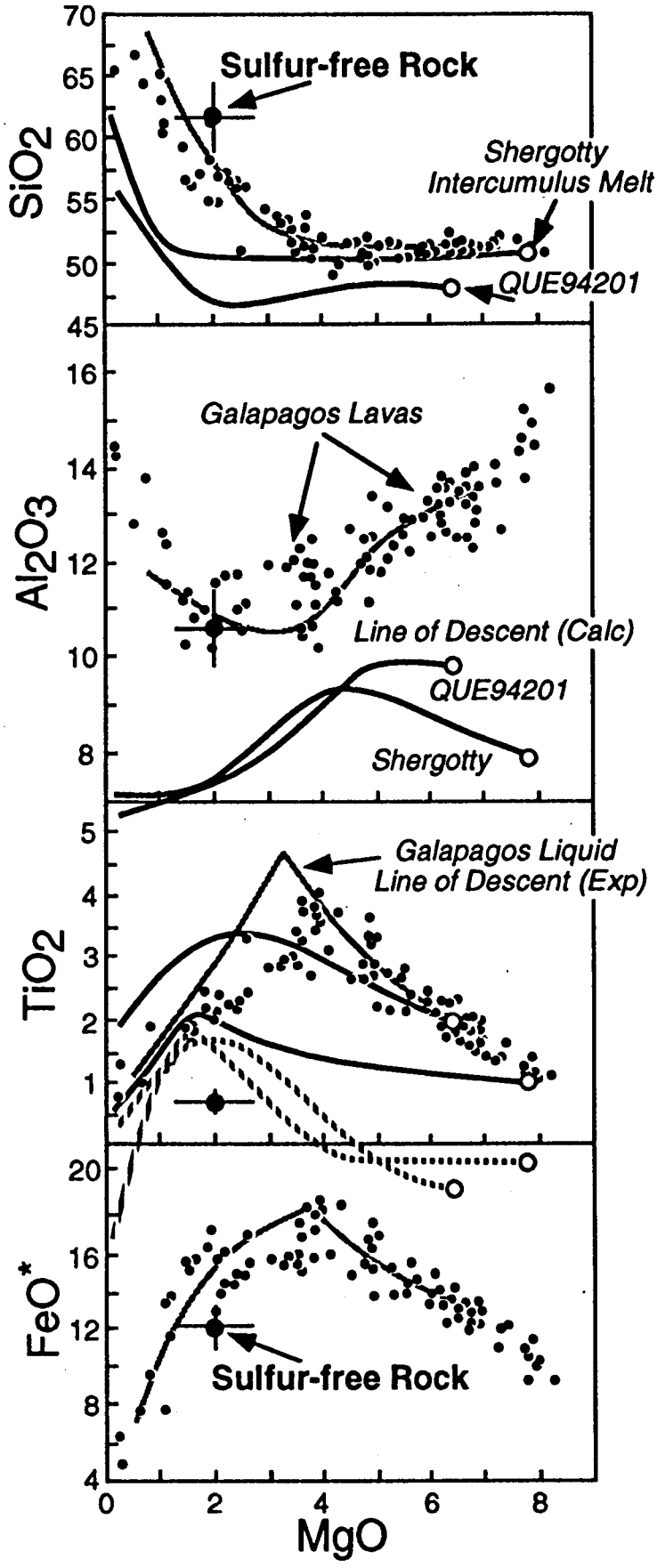
Sulfur-free Rock
Shergotty
Intercumulus Melt
QUE94201
Galapagos Lavas
Line of Descent (Calc)
QUE94201
Shergotty
Galapagos Liquid
Line of Descent (Exp)
Sulfur-free Rock
SiO2
Al2O3
TiO2
FeO*
MgO

Table 1. Observed surface textures for rocks analyzed by APXS

Rock Name	Pits	Smooth Flutes	Lineations	Bumps
Barnacle Bill	**X**		*x*	*x*
Yogi	?		**X**	**X**
Wedge	**X**	*x*		**X**
Shark	*x*			**X**
Half Dome	**X**	**X**	*x*	**X**
Moe	?	**X**		
Stimpy	**X**	**X**	?	
Chimp	**X**	*x*	**X**	**X**

X = strongly developed, *x* = weakly developed, ? = subtle or inconclusive

Table 2. Parameterized properties of rock spectral classes

Rock Spectral Class	0.75 μm Reflectance	Red/Blue (0.67/0.44 μm) Ratio ("Kink")	0.53 μm Absorption	Residual Depth of 0.9-μm Absorption[1]	Occurrence
Gray	10-20%	≤2.9	0-7%	≤0.5%	Pebbles, small cobbles, upwind faces of boulders
Red	15-30%	2.9-4.5	7-18%	≤0.5%	Pebbles, small cobbles, downwind faces of boulders
Pink	≥35%	≥4.5	18-28%]	≤0.5%	Tabular rock-like masses, crust on pebbles and cobbles in soil
Maroon	15-30%	≥2.9	~15-28% (not used for classification)	>0.5%	Upwind faces of large rounded boulders, rare on cobbles

[1]Difference between observed absorption depth and that predicted from linear fit between red/blue and absorption depth in main spectral trend.

Table 3. Preliminary APXS analyses (weight % oxides[1] from *Rieder et al.*, 1997a), and calculated composition and normative mineralogy of sulfur-free rock

APXS Site	Na_2O	MgO	Al_2O_3	SiO_2	SO_3	Cl	K_2O	CaO	TiO_2	FeO*
Barnacle Bill A-3	3.2±1.3	3.0±0.5	10.8±1.1	58.5±2.9	2.2±0.4	0.5±0.1	0.7±0.1	5.3±0.8	0.8±0.2	12.9±1.3
Yogi A-7	1.7±0.7	5.9±0.9	9.1±0.9	55.5±2.8	3.9±0.8	0.6±0.2	0.5±0.1	6.6±1.0	0.9±0.1	13.1±1.3
Wedge A-16	3.1±1.2	4.9±0.7	10.0±1.0	52.2±2.6	2.8±0.6	0.5±0.2	0.7±0.1	7.4±1.1	1.0±0.1	15.4±1.5
Shark A-17	2.0±0.8	3.0±0.5	9.9±1.0	61.2±3.1	0.7±0.3	0.3±0.2	0.5±0.1	7.8±1.2	0.7±0.1	11.9±1.2
Half Dome A-18	2.4±1.0	4.9±0.7	10.6±1.1	55.3±2.8	2.6±0.5	0.6±0.2	0.8±0.1	6.0±0.9	0.9±0.1	13.9±1.4
Calculated Sulfur-free Rock										
	2.6±1.5	2.0±0.7	10.6±0.7	62.0±2.7	0	0.2±0.2	0.7±0.2	7.3±1.1	0.7±0.1	12.0±1.3

Provisional C.I.P.W. Norm (weight %)[2]							
quartz	orthoclase	albite	anorthite	diopside	hypersthene	ilmenite	magnetite
21.0	4.1	22.0	15.2	18.2	15.6	1.3	0.5

[1]APXS analyses are normalized to 98 % oxides, to allow for unreported P_2O_5, MnO, and Cr_2O_3.

[2]Calculated norm assumes a molar Fe_2O_3/FeO ratio of 0.026 (average basaltic shergottite value of *McSween and Jarosewich*, 1983).

Table 4. Coefficients for linear correlations between oxide abundances in Pathfinder rock analyses

	Na_2O	MgO	Al_2O_3	SiO_2	SO_3	Cl	K_2O	CaO	TiO_2	FeO*
Na_2O	1									
MgO	-0.36	1								
Al_2O_3	0.72	-0.58	1							
SiO_2	-0.28	-0.77	0.15	1						
SO_3	-0.09	0.87	-0.40	-0.75	1					
Cl	0.03	0.76	-0.03	-0.69	0.89	1				
K_2O	0.69	0.02	0.79	-0.46	0.12	0.46	1			
CaO	-0.36	0.05	-0.56	0.01	-0.34	-0.60	-0.54	1		
TiO_2	0.29	0.78	-0.14	-1.00	0.77	0.72	0.46	-0.06	1	
FeO*	0.52	0.54	0.09	-0.95	0.51	0.50	0.60	0.03	0.94	1

Table 5. Spectral reflectance data used to calculate red (750 nm)/blue (440 nm) ratios for selected Pathfinder rocks

APXS Site	Local Solar Time of Measurement	Reflectance 440 nm	Reflectance 750 nm	Red/Blue Ratio
A-3	10:42 am	0.0458	0.1248	2.725
A-7	3:31 pm	0.0743	0.3075	3.140
A-16	9:30 am	0.0708	0.2236	3.158
A-16	9:48 am	0.0645	0.2016	3.124
A-17	10:09 am	0.0329	0.0848	2.568
A-17	9:32 am	0.0422	0.0950	2.250
A-18	10:12 am	0.0636	0.1711	2.692
A-18	9:36 am	0.0626	0.1740	2.779